DESIGN AND SIMULATION OF DIELECTRIC NANOPARTICLES AND GRATING EMBEDDED MULTILAYER STRUCTURES FOR ORGANIC LIGHT EMITTING DIODES AND SOLAR CELLS

Ph.D. THESIS

by

VIDHI MANN

DEPARTMENT OF PHYSICS
INDIAN INSTITUTE OF TECHNOLOGY ROORKEE
ROORKEE - 247 667 (INDIA)
FEBRUARY, 2020

DESIGN AND SIMULATION OF DIELECTRIC NANOPARTICLES AND GRATING EMBEDDED MULTILAYER STRUCTURES FOR ORGANIC LIGHT EMITTING DIODES AND SOLAR CELLS

A THESIS

Submitted in partial fulfilment of the requirements for the award of the degree

of

DOCTOR OF PHILOSOPHY

in

PHYSICS

by

VIDHI MANN

DEPARTMENT OF PHYSICS
INDIAN INSTITUTE OF TECHNOLOGY ROORKEE
ROORKEE - 247667 (INDIA)
FEBRUARY, 2020

INDIAN INSTITUTE OF TECHNOLOGY ROORKEE
ROORKEE

STUDENT'S DECLARATION

I hereby certify that the work presented in the thesis entitled **"DESIGN AND SIMULATION OF DIELECTRIC NANOPARTICLES AND GRATING EMBEDDED MULTILAYER STRUCTURES FOR ORGANIC LIGHT EMITTING DIODES AND SOLAR CELLS"** is my own work carried out during a period from July, 2013 to February, 2020 under the supervision of Dr. Vipul Rastogi, Professor, Department of Physics, Indian Institute of Technology Roorkee, Roorkee.

The matter presented in this thesis has not been submitted for the award of any other degree of this or any other Institute.

Dated: **(VIDHI MANN)**

SUPERVISOR'S DECLARATION

This is to certify that the above mentioned work is carried out under my supervision.

Dated: **(VIPUL RASTOGI)**

ABSTRACT

Optoelectronics is the field that deals with devices based on light matter interaction. A device which converts electrical energy into light or vice-versa is usually referred to as an optoelectronic device. Major optoelectronics devices which show direct conversion between photons and electrons include light emitting diodes, laser diodes, photodiodes and solar cells. Light emitting diodes and laser diodes convert the electricity into light energy whereas photodiodes and solar cells convert light energy into electrical energy.
In this thesis, we have mainly focused on light emitting diodes and solar cells due to their significant contribution in general purpose lighting and sustainable renewable green energy.

Organic light emitting diodes (OLEDs) have drawn much interest than that of inorganic or semiconductor LEDs due to their advantage such as low power consumption, high internal quantum efficiency, high contrast, high brightness, and low cost. Despite achieving almost 100% internal quantum efficiency, the external quantum efficiency of OLED is limited to 20% in conventional cases. A large fraction of light (~80%) is lost due to the different mechanisms that take place inside the device. Use of various techniques such as microlens array, textured surface, gratings, nanoparticles, nanostructures has been reported in the literature to increase the light extraction efficiency of OLEDs.

Organic solar cells (OSCs) have been of great significance over the past several years because of their low-cost roll-to-roll manufacturing, suitability with flexible substrates and high absorption coefficient. However, when compared with silicon based conventional solar cells, the power conversion efficiency of OSCs is still low. Due to the low diffusion length of the charge carriers in organic materials, regarding the choice of the thickness of the organic active layer there has always been a trade-off between light absorption and charge carrier extraction. The optimal thickness for the active layer of bulk heterojunction solar cells based on polymer and fullerene derivative is found to be in the range of 100 nm to 200 nm by taking into account the recombination losses. Many photons are left unharvested due to the thin active layer. To overcome the issue of light absorption in the active layer of the device to improve its efficiency, interest has been aroused in light trapping techniques and optical designs of the organic solar cells. Light trapping

techniques are designed to redirect the incoming light. These techniques help in increasing the optical path length or photon absorption in the active layer of the cell. Initially these light trapping techniques were developed for thick active layer silicon solar cells but now they have attracted attention for thin film solar cells. Various techniques such as textured grooves, anti reflection coating, photonic crystals, diffraction gratings, and nanostructures have been numerically and experimentally studied to enhance the light absorption in active layer and hence the efficiency of the organic solar cells.

This thesis presents designs and simulations of novel multilayer structures for organic light emitting diodes and organic solar cells. In particular, we have used dielectric nanoparticles and dielectric diffraction grating as light trapping techniques to reduce the optical losses and to increase the efficiency of the devices. Nanoparticles will act as scattering medium and diffraction gratings will split and diffracts the light into different directions.

In organic light emitting diodes, we have proposed two multilayer designs based on dielectric nanoparticles. In first design, the dielectric nanoparticles layer is placed at glass substrate and in second design; the nanoparticles layer is incorporated at anode layer. Optical properties of single nanoparticle have been studied by Mie theory and the full OLED structure has been simulated and analyzed using Lumerical software based on finite difference time domain (FDTD) method. We have optimized the size, interparticle separation and refractive index of the nanoparticles. Enhancement of 1.7 times in light extraction efficiency is achieved with optimized parameters in both the OLED designs.

We have further investigated the role of dielectric nanoparticles and diffraction grating in the enhancement of light absorption in the active layer and short circuit current density of OSC. Optical properties of single nanoparticle have been studied by Mie theory and the full OSC structure has been designed and studied by Full Wave Utility based on FDTD method. In the first design, the dielectric nanoparticles are placed at the glass substrate of the OSC structure. Optimization of diameter and interparticle separation has been carried out to achieve the maximum enhancement. Using this design, enhancement of 20.4% in light absorption and 19.8 % in short circuit current density (J_{sc}) with SiC nanoparticles has been achieved. Using TiO_2 nanoparticles, absorption could be enhanced by 19% and J_{sc} by 18.5%.

In the next design, the periodic dielectric diffraction grating has been placed at the glass substrate. We have examined the effects and optimized the width, period and height of the grating. Improvement in the light absorption by 24.2% and short circuit current density by 18.6% is obtained with optimized parameters.

Further, the dielectric nanoparticles are introduced at anode (ITO) layer. By considering this design we were able to achieve enhancement of 40% in absorption and 33.9% in J_{sc} using SiC nanoparticles. Also, the light absorption improved by 29% and J_{sc} by 20.2% with ZrO_2 material whereas for TiO_2 material, the absorption improved by 37% and J_{sc} by 32.7%.

The proposed studies will be useful for developing high efficiency OLEDs and OSCs. We have also discussed in brief the future scopes coming out of this thesis.

LIST OF RESEARCH PUBLICATIONS

Journal articles:

1. **V. Mann**, and V. Rastogi, "Dielectric nanoparticles for the enhancement of OLED light extraction efficiency", *Opt. Commun.*, vol. 387, pp. 202-207, 2017.
2. **V. Mann**, B. Hooda and V. Rastogi, "Improvement of light extraction efficiency of organic light emitting diodes using dielectric nanoparticles", *J. Nanophotonics*, vol. 11, pp. 036010-1-036010-11, 2017.
3. **V. Mann** and V. Rastogi, "FDTD simulation studies on improvement of Light Absorption in Organic Solar Cells by dielectric Nanoparticles", *Opt. Quant. Electron.* (Revision submitted).
4. **V. Mann**, and V. Rastogi, "Enhancement in light absorption and short circuit current density by the use of dielectric nanoparticles in an organic solar cell" (To be communicated).

Conference contributions:

1. **V. Mann** and V. Rastogi, "Effect of Dielectric Nanoparticles on Light Extraction Efficiency of OLED", *Workshop on Recent Advances in Photonics (WRAP)*, Indian Institute of Science, Bangalore, India, December 16-17, 2015, IEEE proceeding (978-1-5090-3921-0).
2. **V. Mann**, B. Hooda and V. Rastogi, "Light Extraction Efficiency enhancement in OLED by Dielectric Nanoparticles", *77th JSAP Autumn Meeting*, Nagoya Congress Center, Japan, September 13-16, 2016.
3. **V. Mann** and V. Rastogi, "Efficiency Enhancement in Organic Solar Cell using Dielectric Nanoparticles", *Frontiers in Optics/Laser Science Conference (FiO/LS)*, Rochester Riverside Convention Center, Rochester, USA, October 17-21, 2016, OSA proceeding (FF5B.7).
4. **V. Mann** and V. Rastogi, "Role of Dielectric Nanoparticles in the enhancement of Organic Solar Cell Efficiency", *Fiber Optics and Photonics–PHOTONICS*, IIT Kanpur, Uttar Pradesh, India, December 5-8, 2016, OSA proceeding (Th4B.2).

5. **V. Mann** and V. Rastogi “Increasing the efficiency of organic solar cell using dielectric grating”, *Progress in Electromagnetic Research Symposium (PIERS)*, Nanyang Technological University, Singapore, November 19-22, 2017.

Dedicated to My Parents

For their endless love, support and encouragement

ACKNOWLEDGEMENTS

Firstly, I would like to express my deep sense of gratitude and respect to my research supervisor Prof. Vipul Rastogi for his guidance, patience and continuous encouragements during my entire research work. Without his advice, the dream of writing "Dr." before my name would not have fulfilled. His constructive suggestions and valuable discussions have made this work a successful one. I have learnt various skills under his supervision. I am also thankful to his wife Mrs. Kopal Rastogi for valuable personal advices and his kids Divish and Ishi.

I am also grateful to the members of my Student Research Committee, Prof. Davinder Kaur, Prof. Sudeb Dasgupta, and Dr. Ajay Wasan for their valuable time and useful suggestions during each and every presentation of this work. I am also thankful to Prof. R. Srivastava and Prof. K. L. Yadav, former and present Head of Department of Physics, for providing the basic infrastructure to carry out the entire research work in a better manner. I would also like to extend my thanks to Prof. Joby Joseph, Department of Physics, Indian Institute of Technology Delhi, for his help with the FDTD software.

I would like to acknowledge my lab seniors Dr. Ashok Nandam, Dr. Babita Hooda, Dr. Gyanendra Kumar, Dr. Bipin, and Dr. Ankita Gaur for all their support and motivation during the initial days of my stay in the lab. My heartfelt thanks to my fellow labmates, Ashish Bijalwan, Rehan, Savita, Aashish Kumar and Uwais for always being there with me during my wonderful days of Ph.D.

I would also like to express my gratitude to my friends Pragati, Renu, Priti Gagandeep, Naini, Shailesh, Karunava, Atin, Avijeet Dewasi, Mayank and Mansi who made my time more enjoyable during the stay at IITR. I appreciate their support, cooperation and motivation, which drives me to give my best. I find myself lucky to have friends like them in my life. I am also thankful to Mrs. Meena Kothyari for her motherly love and care. I would like to acknowledge Himalaya explorer club, IIT Roorkee and their members for giving wonderful and adventurous experiences.

I would also like to acknowledge Ministry of Human Resource Development, India for the financial support during the period of research. I am also thankful to Optical Society of America, USA, Department of Science and Technology, India and IITR Alumni Fund

Committee, Roorkee for providing me the travel grant to attend the various international/national conferences.

I would like to extend my respect and gratitude to my parents for their faith, moral support, timely encouragement and impeccable patience. I don't imagine a life without their love and blessings. I deeply thank my brother Vipin for his love and care. I am also grateful to my husband Sachin for his care, affection and support which enabled me to complete my thesis successfully. I am indebted to my in-laws for all their support and patience. How can I forget to acknowledge my sweet and loving son Ojas. His presence gives me strength and makes me optimistic about my life and dreams.

Above all, I would like to thank almighty God for everything.

(Vidhi Mann)

CONTENTS

LIST OF FIGURES

CHAPTER-1

Introduction

Optoelectronics is the field that deals with devices based on light matter interaction. The light often involved visible and invisible form of radiation like infrared, ultraviolet, X-rays and gamma rays. A device which converts electrical energy into light or vice-versa is usually referred to as an optoelectronic device. Major optoelectronics devices which show direct conversion between photons and electrons include light emitting diodes, laser diodes, photodiodes and solar cells.

Light emitting diodes (LEDs) are p–n junction diodes in which holes and electrons recombine to form a photon. The radiative recombination process takes place mainly in a direct band gap semiconductor. The diode emits incoherent spectrum light when it is electrically forward biased. This effect is known as electroluminescence (EL). The energy band gap of the material decides the color of the emitted light. LEDs find applications in flat panel displays, general lighting, medical devices, household appliances etc**. Laser diodes (LDs)** operate under the stimulated emission condition and convert electrical energy into light. When a p-n junction is forward biased, the population inversion of electrons is produced and then from semiconductor region laser beam is available. The ends of p-n junction are polished so that emitted photons reflect back to form more electron pairs. LDs find applications in telecommunication, military applications, CD players etc. A **Photodiode** is a light detector which converts light energy into electric current or voltage based on the mode of operation. It consists of

semiconductor material based p-n junction, which operates in reverse bias. Photodiodes may have small or large area surfaces. But they usually suffer low response time as the area increases. They find applications in medical devices, cameras, optical communication devices, bar scanners etc. A **Solar cell or a photovoltaic cell** is a device which directly converts sunlight into electricity through the photovoltaic effect. When sunlight which is composed of photons strikes the cell, a portion of it get absorbed in the active material and generates both voltage and current to produce electric power. Solar cells comprise large surface area. Solar cells are used for remote lighting systems, portable power supplies, satellites, rural electrification in addition to being a major source of electricity in not so distant future.

In this thesis, we have mainly focused on light emitting diodes and solar cells because of their promise for contributing significantly in general purpose lighting and sustainable green electricity.

1.1 Light Emitting Diodes

LEDs have acquired acceptance in the market of lighting and substituting traditional lighting sources (incandescent and halogen lamps) in the display, decorative and public lighting applications [1-3]. LED's increasing popularity is mainly due to these factors: energy saving property, long lifetime, mercury-free design, and color rendering [4-6]. The first light emitting diode was invented by Nick Holonyak in 1962 that emitted light in the visible wavelength range [7]. The LED was red in color. M. George Craford, a graduate student of Holonyak, discovered the first yellow LED in 1972. He also discovered a brighter red LED. The first bright blue LED, using indium gallium nitride as semiconductor material, was demonstrated by Shuji Nakamura of Nichia Corporation in 1993 [8]. He was honored with Nobel Prize in Physics in 2014 along with Hiroshi Amano and Isamu Akasaki for discovering blue LEDs [9]. Now days, LEDs can be made in one or more colors. White light LEDs can be generated by use of yellow phosphorous together with short wavelength range LEDs such as blue light LEDs or by suitably combining the light from red, green and blue LEDs.

Most of the basic lighting objectives such as color rendering, long life, high reliability and environment friendly have been achieved by LED. But the performance of LED

also depends on the ambient temperature which could lead to failure of device if there is no heat sink and outside temperature is high. Beside this, LED's capital cost (high price per lumen) is another disadvantage. Its cost is considered high as compared to other lighting devices like fluorescent and incandescent light bulbs. So, to overcome the issues faced by semiconductor based LEDs, another lighting source technology which has highly developed over the past two decades and has more improvement prediction is organic light emitting diode (OLED). An OLED is made of very thin layer of organic material, which makes it more flexible and lighter than an LED. Unlike conventional inorganic semiconductor LEDs which are point sources, organic light emitting diodes (OLEDs) is a surface emitting light source as the light is distributed all over the surface area. Another advantage of OLEDs is that the emitted wavelength can be tuned due to the presence of various emissive materials [10, 11]. So, OLED is a promising technology due to its potential applications in flat panel displays, illumination, and solid state lighting [12, 13].

1.1.1 Organic Light Emitting Diodes

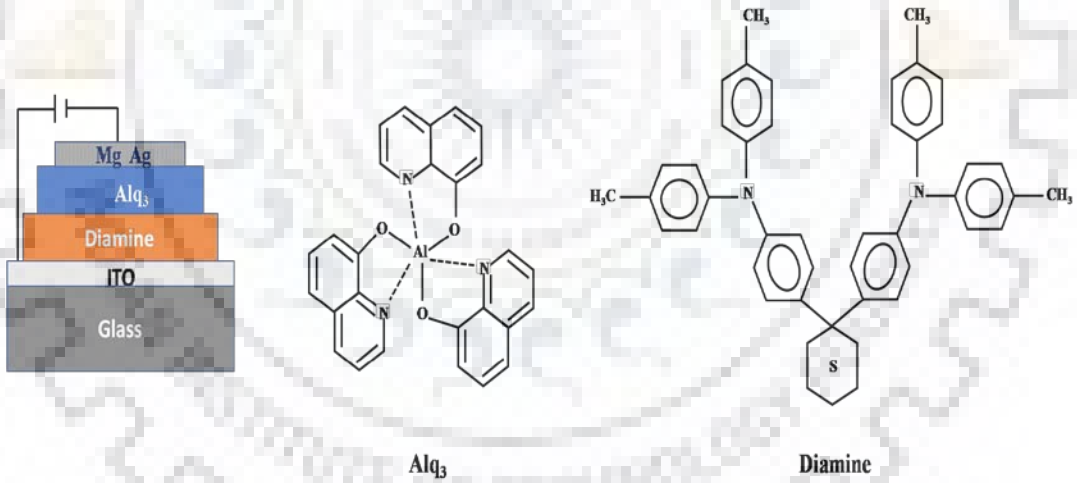

Figure 1.1 *Schematic structure of first efficient OLED and chemical structure of Alq_3 and diamine*

OLEDs have been of much interest due to their advantages of low cost, high contrast ratio, low power consumption, high brightness and large emitting area [14, 15]. OLED is a type of light emitting diode in which the light emitting layer is made up of organic material. When an OLED is biased, it emits the visible light. The first electroluminescence in organic materials was detected at National Research Council in

1965 by Helfrich and Schneider from crystals of anthracene, which consists of polycyclic benzene rings [16]. Due to its high operating voltage no practical application was seen. In 1987, Tang et al. in Kodak reported the first low voltage organic light emitting diode using small organic molecules as shown in Fig. 1.1 [17]. This invention was considered as the significant step for practical applications of OLEDs.

Typically, an OLED consists of a substrate, anode, organic emissive layer and a cathode. The organic emissive layer is sandwiched between a metal layer (cathode) and transparent conducting oxide layer (anode) commonly comprised of electron transport layer (ETL), light emitting layer, and hole transport layer (HTL). The device structure is systematically shown in Fig. 1.2.

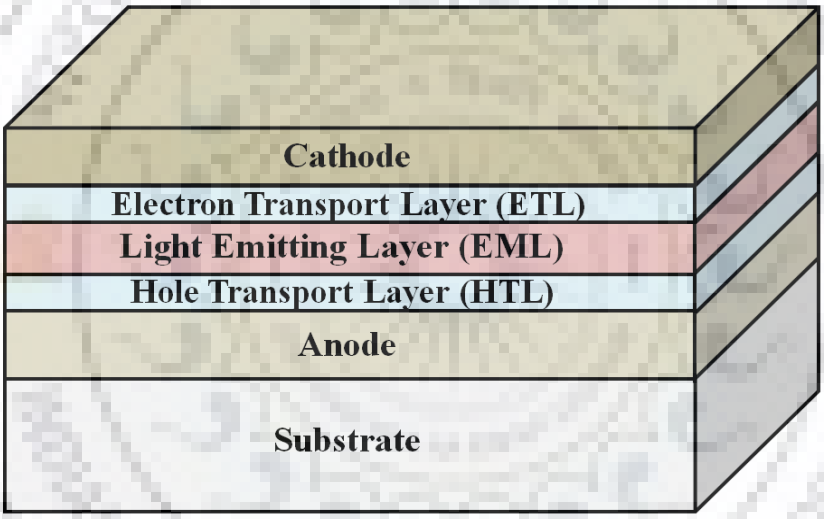

Figure 1.2 *Pictorial representation of OLED components.*

The main purpose of using several layers or multilayers in an OLED is to improve the light extraction efficiency of the device and to prevent charge carriers to reach opposite electrodes. The substrate which is usually made of glass, foil or plastic is used to support OLED. The commonly used anode is Indium Tin Oxide (ITO). This material is highly conductive and is transparent to visible light. The anode has high work function which helps in transportation of holes into the highest occupied molecular orbital (HOMO) level of organic layer. Other materials which can be used as anode are poly(3,4-ethylenedioxythiophene) poly(styrenesulfonate) (PEDOT:PSS) polymer, and graphene [18, 19]. HTL provides a pathway for holes to migrate from anode to the light

emitting layer. Commonly used materials for HTL are N,N-diphenyl-N,N-bis(3-methylphenyl)-1,1-biphenyl-4,4-diamine (TPD), and N,N-Di(naphthalene-1-yl)-N,N′-diphenyl-benzidine (α-NPD). ETL helps in transporting the electrons from cathode layer to light emitting layer. Commonly used materials for ETL are 2-(4-biphenyl)-5-(4-t-butylphenyl)-1,3,4-oxadiazole (PBD), and 1,3,5-tris(N-phenylbenzimidizol-2-yl)benzene (TPBI). The emitting layer can be based on small molecules or polymers. Small molecules based materials used for emitting layer are Tris(8-hydroxyquinolinato)aluminium (Alq_3) (fluorescent dyes), Tris[2-(p-tolyl)pyridine]-iridium(III) (Ir(mppy)3) (phosphorescent dyes), and polyfluorene (polymer). Usually metals like calcium, magnesium, aluminium and barium are used as a cathode as they have low work function which helps in injecting electrons into the lowest unoccupied molecular orbitals (LUMO) level of organic layer [20]. Now days, commonly used cathode in OLED devices is made of LiF/Al bi-layer material [21].

In organic semiconductors, LUMO and HOMO are similar to conduction and valence bands of inorganic semiconductors. When voltage is applied across the OLED such that anode is made positive with respect to cathode, electrons and holes are injected from respective electrodes, passes through HTL and ETL and recombine in the organic light emitting layer through the intermediate formation of emissive excitons (a bound state of hole and electron). It generates light in the visible region through the radiative decay of molecular excited states. The emitted wavelength depends on the band gap of the material. In case of OLED, the bang gap is the energy difference between HOMO and LUMO. The charge transport and light generation in an OLED is shown in Fig. 1.3.

The quantum efficiency (*QE*) of the OLED device is defined by the internal quantum efficiency (*IQE*) and light extraction efficiency (*LEE*) as [22]:

$$QE = LEE \times IQE \tag{1.1}$$

Light extraction efficiency is defined as the ratio of photons coming out of the device to the photons generated inside the device whereas the ratio of total number of photons generated in the light emitting layer (or emissive layer) to the number of injected electrons defines the internal quantum efficiency. *IQE* is only 25% for fluorescent materials because for light generation only radiative decay of singlet excitons takes place in the emissive layer. In contrast, by utilizing electro phosphorescent materials

which harvest radiative decay of both singlet and triplet excitons, the *IQE* can be achieved to 100% [22].

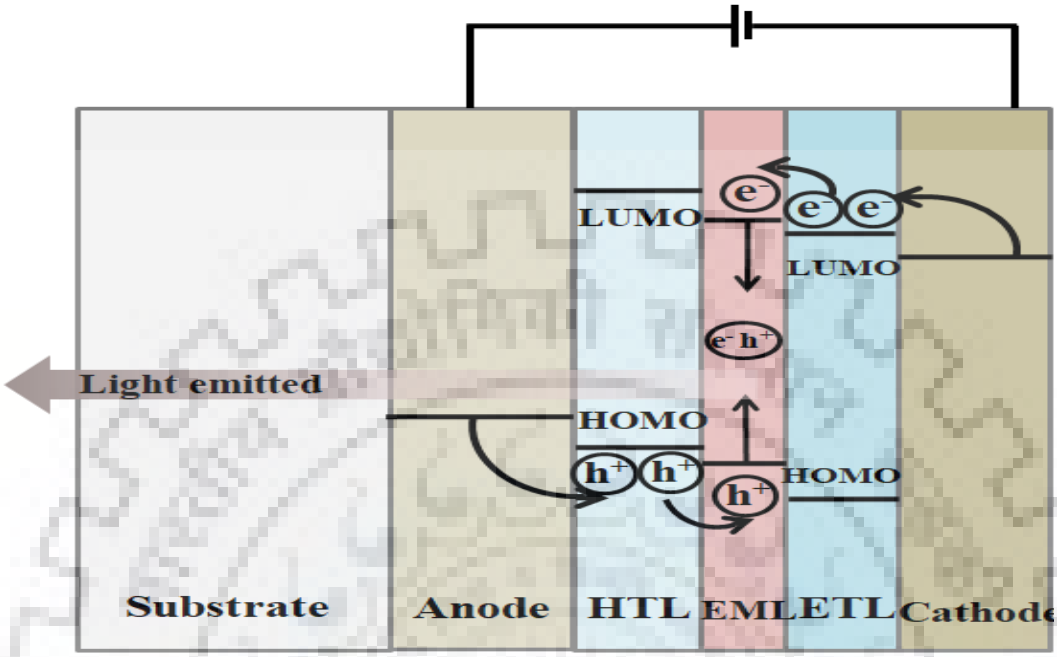

Figure 1.3 *Schematic of charge transport and light generation in an OLED.*

1.1.2 Losses in OLED

Although the *IQE* has been achieved 100% still the quantum efficiency is limited to 20% in conventional structure of OLEDs. Due to the different mechanisms occurring inside the device, nearly 80% of generated light is lost, which implies that most of the light is either emitted from the edges of the device or trapped inside the glass substrate and device [23, 24]. Generation of light takes place from organic light emitting layer spontaneously in all the directions and propagates vis various modes. Radiative losses consist of waveguided losses, surface plasmons losses, absorption losses and loss due to the substrate. Absorption losses arise mainly due to the extinction coefficient of metallic materials. Substrate losses are due to the total internal reflection (TIR) taking place at substrate and air interface. Almost 30% of the generated light is lost in substrate modes [25]. Waveguided losses occur due to ITO/ organic waveguided modes. In these modes, light comes out through the sides of the device. Approximately 20% of light is lost in waveguided modes [26]. Surface plasmons are the collective oscillations of free

electrons confined to the surface (interface between metal and dielectric). When these plasmons interact with light then they form polaritons. In the OLED structure, surface plasmons occur at cathode and organic interface. In this case also light will come out from the sides of the device. Due to surface plasmons modes 30% of generated light is lost [25, 26]. Fig. 1.4 shows the different mechanisms of losses in an OLED device.

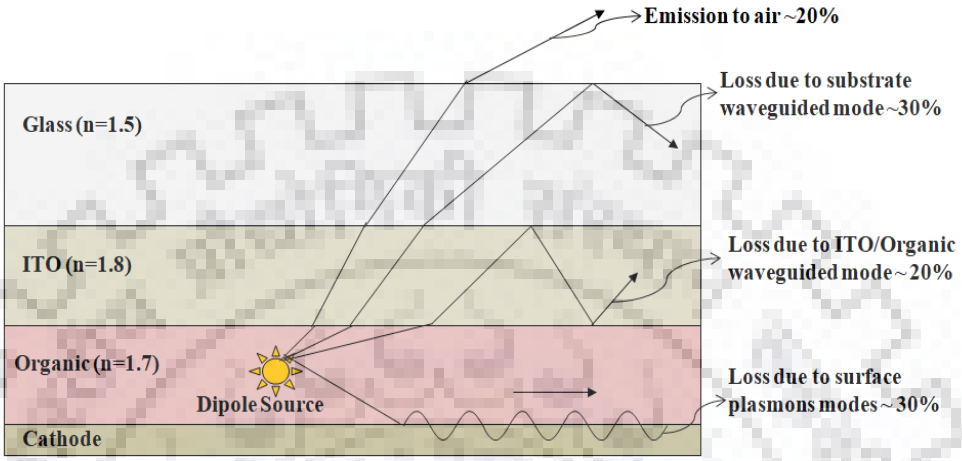

Figure 1.4 *A simplified OLED showing different light trapping modes.*

Various light extraction approaches have been described in literature to reduce these light losses in the device and thereby increase OLED's light extraction efficiency.

1.1.3 Methods to improve light extraction efficiency in an OLED

The basic approach of light extraction techniques is to add an optical structure in the device to minimize the refractive indices difference between the layers. These techniques may use internal and external modification in the device. To avoid the light propagation in substrate mode, back texturing of the glass substrate can be done to increase the light extraction efficiency [27, 28]. Also, enhancement in LEE can be attained by using the texturing of meshed substrate surfaces [29, 30]. Use of Micro lenses and macro lenses at the back side of the glass substrate is another powerful technique for power extraction from substrate modes [31-34]. LEE has been significantly improved by using ordered micro lens arrays [32]. However, the fabrication of micro lens arrays is difficult and expensive. Another technique which can be applied to suppress the substrate modes loss is the use of anti reflecting coating (ARC) at the glass substrate [35]. About two fold enhancement in the luminance can be achieved with the use of MgF_2 ARC [35]. Insertion of silica aerogel layer or low index

layer between ITO and glass substrate can avoid the formation of substrate modes and results in enhancement in LEE [36]. The formation of waveguided modes can be reduced by using high index substrate [37]. However, the high index contrast will take place between substrate and air by the use of high index substrate. Use of low index grid between ITO and organic layers is helpful in extracting out the power from the waveguided modes [38, 39]. These grids can be embedded at ITO/organic interface by the standard photolithographic method. Photonic crystals (PCs) are being widely used for extraction of light in OLEDs [40-44]. Fujita et al. used two dimensional (2D) PC layer between ITO and organic light emitting layer which results in enhancement of 50% in the luminance efficiency [40]. In another study, Ishihara et al. fabricated the 2D-PC between the ITO layer and glass substrate and the device showed the enhancement in luminance by a factor of 1.5 [42]. These PCs can be fabricated by the nano imprint lithography technique. Use of nanostructures, microstructures, diffraction gratings and scattering structures has also been studied to extract out the power from the device [45-53].

In this thesis, we have proposed to enhance the light extraction efficiency of OLED by the insertion of dielectric nanoparticles layer. These nanoparticles will act as scattering medium for the light trapped in the OLED device and help in light extraction.

1.2 Solar Cells

The energy demand by the world is constantly increasing. A lot of pressure has been put on conventional energy sources. The conventional energy sources are non renewable which are based on fossil fuels such as coal, oil, petroleum, natural gases. Consumption of energy sources release green house gases in the atmosphere which creates a bad effect on environment. Another kind of energy source is renewable energy which includes solar energy, biomass, wind energy, geothermal energy. Presently, to maintain the lifestyle of world population, we need 13 terawatts (TW) of energy. An additional 10 TW of clean energy will be needed by 2050 [54]. So, there is need for some sustainable energy source which can meet our energy demand.

Out of all the renewable energy sources, the sun is a clean energy source, the energy from which is in abundance and can provide security for our energy demand. The sun

can provide us with 3×10^{24} joule (J) energy in a year which is thousand times the global power consumption [55]. The sun's energy can be harnessed in different ways such as solar thermal technology (to heat water or steam and run turbines), passive solar heating, and photovoltaics. Solar thermal or water heating technology has been widely accepted. The photovoltaics technology has attracted a lot of attention in the last few years. Photovoltaics are also known as solar cells, converts sunlight directly into electricity using semiconductor materials. When sunlight is incident on the cell, a portion of it is absorbed by these materials, the solar energy knocks electrons loose, allowing them to flow to an external circuit and produce electricity in the form of direct current (DC). The DC can be converted to alternating current (AC) by means of inverter as the standard power used for residential purposes is AC.

The physical phenomenon on which solar cell's working principle is based is known as photovoltaic effect, first discovered by a French physicist, Alexandre E. Becquerel in 1839 in electrolytic cells [56]. The first solar cell based on silicon material was invented in 1954 by three researchers G. Pearson, C. Fuller and D. Chapin at The Bell Laboratories, USA [57]. At that time the efficiency achieved was 4% and after more research it reached upto 6% [57]. Solar cells are mainly divided into three generations. The first generation is made of pure silicon which includes single and poly crystalline silicon solar cells. These are based on silicon wafer and their contribution to the commercial market is more than 85%. The efficiencies of these solar cells are quite good (approx 27%) [58]. But, first generation solar cells are very expensive as the production cost to achieve the pure silicon is quite high. So, many developments have been made to reduce the cost of solar cells. This lead to the birth of second generation solar cells which are based on thin films of materials such as amorphous silicon, nanocrystalline silicon, copper indium gallium diselenide (CIGS), or cadmium telluride (CdTe). The efficiency achieved for CdTe and CIGS solar cells is around 22% and for amorphous silicon it is 14% [58]. But these solar cells are less expensive compared to first generation solar cells. The main issue with this technology is the use of cadmium because of its toxicity. Another issue is that there is scarcity of these materials. Third generation solar cells are mainly focused for high efficiency and less expensive [59]. These includes multijunction concentrator solar cells, organic cells, dye sensitized cells, nanostructured cells like quantum dot cells, tandem solar cells [60, 61]. These cells are very cheap as their fabrication process is easier relative to first and second generation

cells. The efficiency of these cells is very less except the multijunction concentrator solar cells. Various technologies of solar cells with their efficiencies are shown in Fig. 1.5.

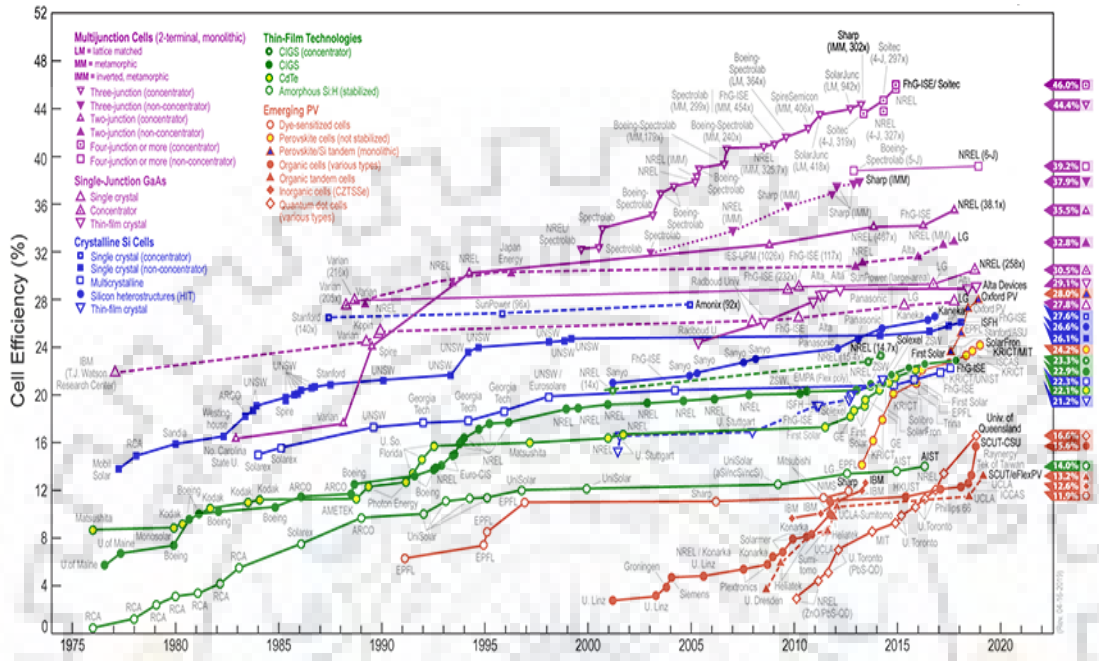

Figure 1.5 *Timeline of cell efficiency for various photovoltaic technologies. (Adapted from Ref. [58]).*

There are some basic characteristics common to all the solar cells. When measurements are done in the dark, the solar cells current versus voltage (*I-V*) characteristics seems similar to the exponential response of a diode with small current in reverse bias and high current in forward bias. When the device is illuminated under the light, it generates a photocurrent or light-generated current in the cell. So, *I-V* characteristic of the solar cell is basically the superposition of the photocurrent and dark characteristic. Therefore, Shockley equation can describe the *I-V* characteristics of the ideal solar cell with an additional light-generated current term, I_L as [62]

$$I = I_0[\exp(qV / nkT) - 1] - I_L \qquad (1.2)$$

where I is the current, I_0 is the diode's reverse saturation current, V is the applied voltage, q is the elementary charge, n is the ideality factor, T is the temperature, and k is Boltzmann constant. The equation can also be written in terms of current density (J) with $J = I / A$; A being the solar cell's area.

Fig. 1.6 depicts typical I-V characteristics of the ideal solar cell [62]. The curve shows that the current is negative and voltage is positive which results in the negative power. The negative power indicates the generation of power from the device. Solar cells are characterized with the four parameters namely short circuit current (I_{sc}), open circuit voltage (V_{oc}), fill factor (FF) and efficiency (η).

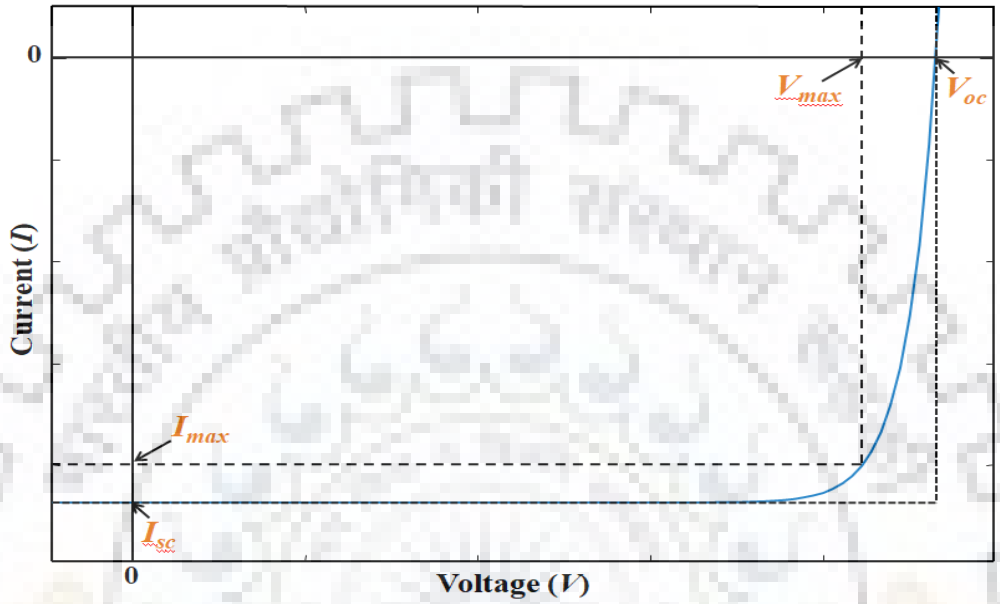

Figure 1.6 *I-V characteristics of a solar cell with its parameters*

Short circuit current (I_{sc}) is defined as the maximum current that passes through the solar cell when the two electrodes are shorted to each other i.e. V=0. This current is due to the generation and collection of light-generated charge-carriers. So, I_{sc} will be similar to the light-generated current I_L i.e. $I_{sc} = -I_L$. As power is the product of voltage and current, power will not be produced at this current. **Open circuit voltage (V_{oc})** is the maximum voltage across the terminals of the solar cell when they are kept open i.e. I=0. By substituting I=0 in equation (1.2), we get

$$V_{oc} = \frac{nkT}{q} \ln\left(\frac{I_L}{I_0} + 1\right) \tag{1.3}$$

This shows that the V_{oc} depends on the reverse saturation current, light generated current and the temperature. No power will be generated at V_{oc}. **Fill factor (FF)** is defined as the ratio of maximum power $p_{\max} = I_{\max} \times V_{\max}$ that can be obtained from the cell to the ideal power $p_0 = I_{sc} \times V_{oc}$ i.e.

$$FF = \frac{p_{\max}}{p_0} = \frac{I_{\max} V_{\max}}{I_{sc} V_{oc}} \tag{1.4}$$

Because of the diode performance and additional resistance and recombination losses, p_{max} is always less than p_0. *FF* also represents the sharpness or squareness of I-V curve of the solar cell. **Efficiency (η)** is the most important and discussed parameter of the solar cell. It is defined as the output power to the input power. The maximum power (p_{max}) is the output power and the power of solar radiation (p_{rad}) is input power. Efficiency in the percentage form can be written as

$$\eta = \frac{p_{\max}}{p_{rad}} = \frac{V_{\max} \times I_{\max}}{p_{rad}} = \frac{FF \times V_{oc} \times I_{sc}}{p_{rad}} \tag{1.5}$$

The efficiency of the solar cell is highly dependent on the solar spectrum and power of the incident light. So, for calculating the efficiency of various solar cells, a standard spectrum should be chosen. Although the solar spectrum at the earth's surface varies with location, cloud coverage and other factors, the AM 1.5G solar spectrum shown in Fig. 1.7 is generally used as the standard spectrum for evaluating the performance of the devices that are designed for outdoor purposes [63].

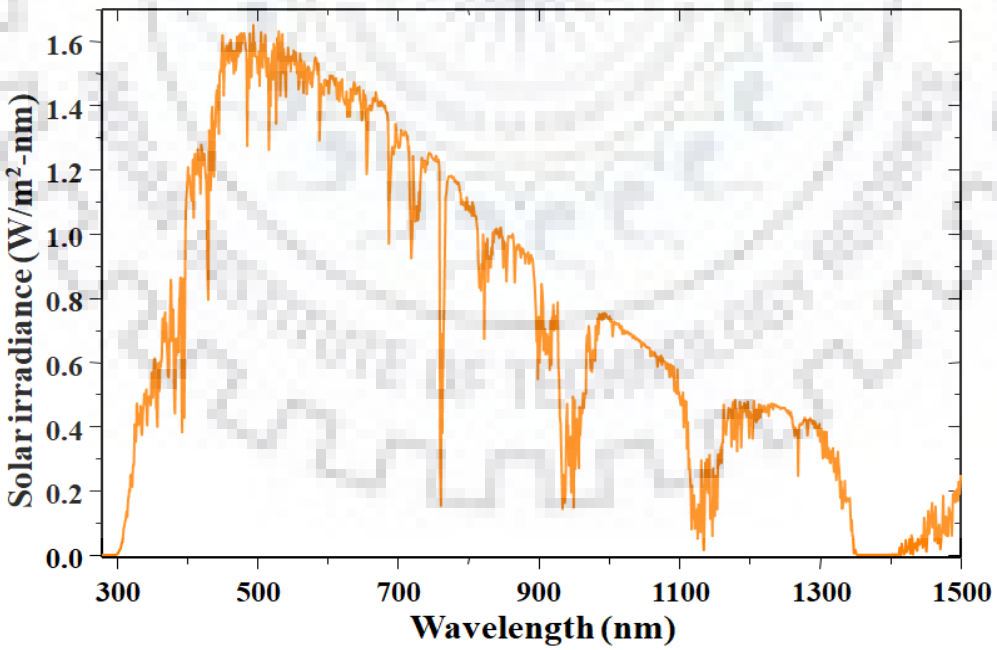

Figure 1.7 *Spectral irradiance of the AM 1.5G solar spectrum.*

1.2.1 Organic Solar Cells (OSCs)

Organic solar cells have been of great significance due to their advantages of low manufacturing cost, mechanical flexibility, affinity for chemical modification, and potential for large scale manufacture [64]. An OSC uses polymers or small organic molecules with semiconductive properties as the photoactive layer for light absorption and charge transport for the production of electricity. The organic materials have high absorption coefficient, a layer of few hundred nanometers is thick enough to absorb a large fraction of the incident light. The first organic solar cell with efficiency of approx 1% was demonstrated by C.W. Tang of Eastman Kodak in 1986 shown in Fig. 1.8 [65

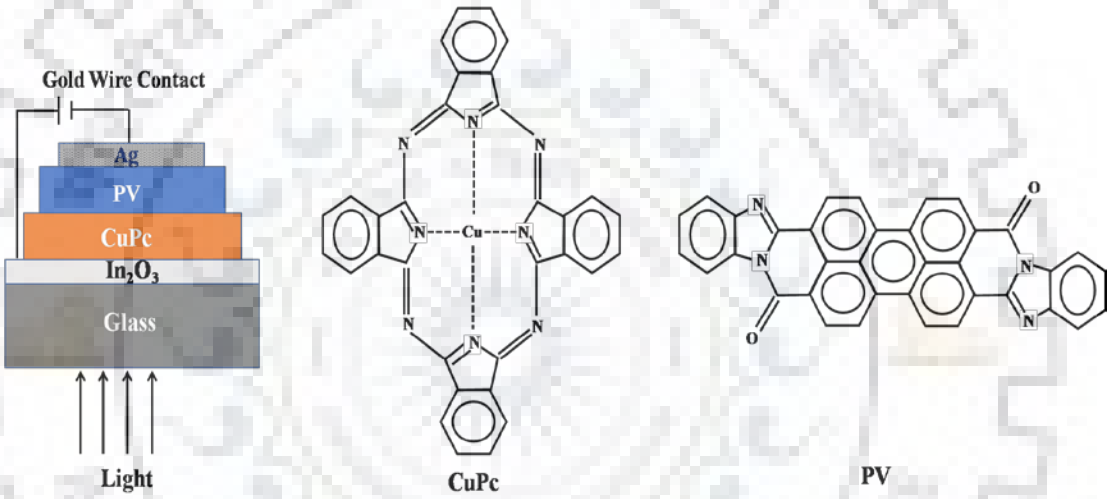

Figure 1.8 *Schematic structure of first OSC and chemical structure of its molecules.*

Typically, in an organic solar cell, a photoactive layer of bilayer planar heterojunction or bulk heterojunction (BHJ) is sandwiched between two electrodes (anode and cathode) with their corresponding interlayers. By replacing the light emitting layer of OLED in Fig. 1.2 with photoactive layer, OSC structure is obtained. Multilayer organic solar cells are used to prevent the charge carriers from reaching the opposite electrodes. In bilayer OSCs, two organic layers with adequate differences in electron ionizations and electron affinities are used whereas in bulk heterojunction based OSCs, an organic blend is formed by the mixing of electron donor and acceptor layers [66]. BHJ is a promising technology compared to bilayer as it increases the acceptor-donor interface area and offers a good environment for the electron movement. The first demonstration on bulk heterojunction structures with phthalocyamine as donor and perylene tertracarboxylic

derivatives as acceptor was made in 1991 [67]. Generally, ITO is used as anode due to its high conductivity and transparency. Another materials used as anode are PEDOT:PSS and graphene. The cathode should be of low work function and mostly used materials are aluminium, magnesium and calcium. The materials used for electron donor are p-type materials such as copper phthalocyanine (CuPc), polyphenylene vinylene (PPV), poly-3-hexythiophene (P3HT), poly[2,6-(4,4-bis-(2-ethylhexyl)-4H-cyclopenta [2,1-b;3,4-b]dithiophene)-alt-4,7(2,1,3-benzothiadiazole)] (PCPDTBT) and for electron acceptor are n-type materials such as fullerene (C60), poly(benzimidazobenzophenanthroline ladder) (BBL), phenyl-C61-butyric acid methyl ester (PCBM), perylene tetracarboxydiimide (PDI).

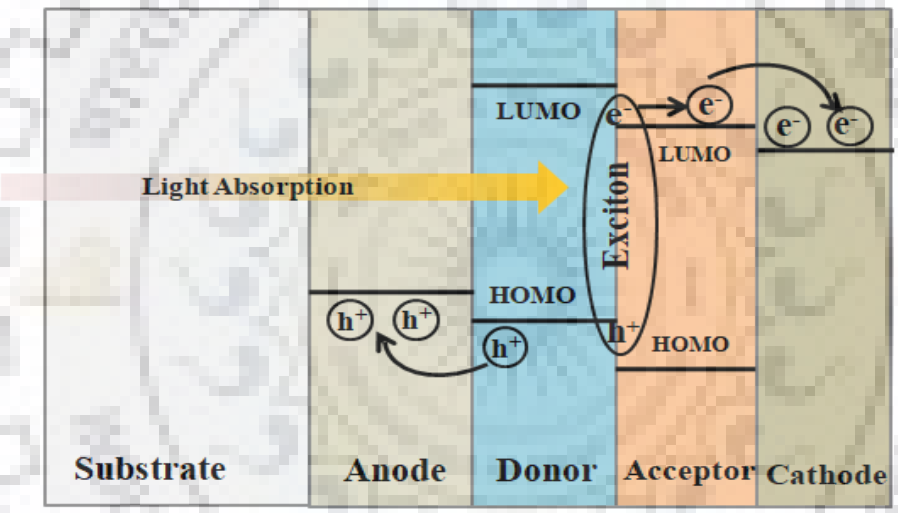

Figure 1.9 *Light absorption and charge separation mechanism in OSC.*

When sunlight strikes the cell, photons get absorbed in the photoactive layer. This results in the excitation of electrons to the LUMO leaving behind holes in the HOMO. Theses charge carriers are not free and remain electrostatically coupled electron hole pairs called excitons. The mobility of excitons is limited to 10 nm and binding energy (B.E.) is the order of 0.2 eV to 0.5 eV. Dissociation of excitons or charge separation occurs at the acceptor donor junctions or interfaces. The dissociation is possible if the difference between the electron affinity of acceptor and ionization potential of acceptor is larger than the B.E. of the excitons. Once the charges are separated, they will move towards the respective electrodes to produce electricity. Light absorption and charge separation mechanism in organic solar cell is shown in Fig. 1.9.

Although OSCs have attracted a lot of attention due to their low cost energy conversion but the power conversion efficiency is still low as compared to inorganic semiconductor based solar cells. Due to the limited mobilities of charge carriers in organic materials, the thickness of photoactive layer is a tradeoff between charge carrier extraction and light absorption [68]. For efficient light absorption and charge carrier extraction, the thickness of active layer is found to be in range of 100 nm – 200 nm [69, 70]. Many photons will be left unharvested due to the thin active layer.

1.2.2 Losses in Solar Cells

Loss in a solar cell indicates the loss of photon energy (full or partial) which, due to some reason, is not able to generate electrons out of the cell. There are basically two types of losses: optical losses and electrical losses. The optical loss refers to the loss of photons which may help in the charge carriers generation. Electrical loss refers to the loss of photons which get absorbed in the cell but do not contribute to the cell output power due to either ohmic or recombination losses. Some of the fundamental losses of the cell include

(a) Transmission Loss: photons that have energy less than the band gap of material (E_g) do not get absorbed and hence do not contribute to the charge carrier generation.

(b) Thermalization Loss: when photon energy (E) is more than the band gap energy then the excessive energy (E-E_g) is released in the form of heat.

(c) Loss arises due to parasitic resistances (series and shunt resistances) of the cell.

There are some other losses also apart from fundamental losses in the cell which includes loss due to the reflection from reflective electrodes and the cell's surface, loss due to the mismatch of indices of different layers, loss due to incomplete absorption because of limited thickness of the cell.

Improvements in the efficiency of organic solar cell can be made by the reduction of these losses.

1.2.3 Methods to improve efficiency of OSC

Numerous approaches have been reported in literature to overcome these losses in the device. The losses can be reduced via the proper choice of electrode's materials [71-73], or interface materials [74], careful designs of device structure [75], or use of optical spacers [76, 77]. The light absorption in the active layer can be improved by the use of

light trapping techniques. These trapping techniques have been broadly studied in inorganic photovoltaics field. They were initially introduced for thick active layer solar cells. For example, the use of anti reflection coating [78, 79], use of textured surface [80, 81] or use of nanostructures [82] can redirect the light and hence trap the light in the device for better absorption. But there is a need for alternative light trapping techniques for thin film solar cells due to the different optical behavior of light in thin films.

Over the past few years, light trapping in inorganic thin films has been an important topic and has gained a lot of attention in the organic solar cells field as well. Loss at the cell's front surface can be reduced via the use of anti-reflection coating (ARC) [83], structured substrate [84, 85], and microlenses [86-88]. It is good to use independently prepared structures to avoid the recombination losses. K. Forberich et al. demonstrated that by the use of nano patterned moth eye ARC, external quantum efficiency (EQE) of the device can be increased by 3.5% [83]. In another demonstration, it has been shown that use of microlenses array on top of metallic mirror with aperture enhances the photocurrent by 20% [86]. With this type of light trapping scheme, enhancement could only be achieved for small set of incident angles. To overcome the issue of weak absorption in OSCs, several other approaches have been reported such as new materials for active layer [89, 90], folded structures [91-93], tandem cell designs [94], diffraction gratings [95-98], nanoparticles [99-104], nanowires [105, 106], nanostructures [107]and photonic crystals [108-110]. By partially substituting the top transparent electrode with periodic silver grating enhances the overall light absorption in the device by 50% [98]. In another case of patterning the silver grating in the active layer increases the light absorption by 23.4% [96]. This type of metal grating structuring is mostly done using soft lithographic imprinting techniques [96]. Use of nanoparticles can enhance the efficiency of OSCs by 17% when deposited on anode and by 10% when incorporated on active layer [101]. Photonic crystal nanostructures introduced in the photoactive bulk heterojunction layer enhances the efficiency of the device by 70% [108].

In this thesis, we have used dielectric nanoparticles and diffraction grating at different interface to enhance the light absorption in the active layer and hence efficiency of the OSC**.**

1.3 Thesis Outline

We have divided the work of this thesis into seven chapters.

This chapter describes the optoelectronics devices mainly the light emitting diodes and solar cells structures. It includes the introduction, applications and literature survey for these structures.

In chapter 2, we have discussed the theoretical methods that are helpful in the study and analysis of OLEDs and OSCs structures. This chapter includes Mie theory which is used to calculate the scattering efficiency of an isolated nanoparticle and finite difference time domain (FDTD) method to calculate the light extraction efficiency of proposed OLED structure and light absorption in the active layer of proposed OSC structure. We have also carried out a brief discussion on commercially available simulation tools (Lumerical's FDTD and R Soft Cad Full Wave) used for analysis of both the structures.

In chapter 3, we have proposed two designs based on dielectric nanoparticles for the enhancement of light extraction efficiency in OLEDs. In design 1, we have incorporated the layer of dielectric nanoparticles at glass substrate. In design 2, the dielectric nanoparticles layer has been incorporated at the anode (indium tin oxide) interface. These nanoparticles act as scattering medium for the light trapped modes inside the device. Scattering properties of nanoparticles have been studied using Mie theory. FDTD method has been used to calculate the LEE of OLED. Optimization of several parameters like diameter, interparticle separation and refractive indices of nanoparticles has been carried out for the maximum enhancement in LEE of OLED. Enhancement of 1.7 times in light extraction efficiency is achieved with optimized parameters in both the OLED designs.

In chapter 4, we have presented the systematic analysis of Organic solar cell structure based on the dielectric nanoparticles. The nanoparticles layer has been incorporated at glass substrate Numerical analysis of the proposed structures has been carried out using the Mie theory and FDTD method has been used to calculate the absorption. No electrical losses have been considered in both the structures. Only the optical effects are taken into account to study the behavior of device performance and an enhancement factor has been evaluated. Diameter, interparticle separation and refractive index of nanoparticles have been optimized. The simulations show the enhancement in light

absorption and short circuit current density of the device. Using this design, increment of 20.4% in light absorption and 19.8 % in short circuit current density (J_{sc}) with SiC nanoparticles is achieved. Using TiO_2 nanoparticles, absorption enhanced by 19% and J_{sc} by 18.5%.

In chapter 5, we have proposed the incorporation of the periodic dielectric diffraction grating between the glass substrate and top transparent anode (ITO) to increase the efficiency of OSCs. Diffraction techniques describe the mechanism of changing the direction of the incident light into different directions and hence can increase the optical absorption in the cell. Optimization of width, period and height of the grating has been done to achieve the maximum enhancement in light absorption. We have used the full wave FDTD simulation method to calculate the optical absorption of the OSC. Improvement in the light absorption by 24.2% is obtained.

In Chapter 6, the proposed structure consists of dielectric nanoparticles layer at anode (indium tin oxide). Mie theory and FDTD based software has been utilized to study the numerical analysis of the proposed structure. Various parameters of nanoparticles have been optimized to obtain the maximum enhancement in light absorption. By considering this design, we were able to obtain enhancement of 40% in absorption and 33.9% in J_{sc} using SiC nanoparticles. Also, light absorption improved by 29% and J_{sc} by 20.2% for ZrO_2 material whereas for TiO_2 material, the absorption improved by 37% and J_{sc} by 32.7%.

Chapter 7 contains the summary and concluding remarks of the thesis. In this thesis, we have presented multilayer organic light emitting diode and organic solar cell designs. Designs have been carried out for the enhancement of efficiency in OLED and OSC. The scope for future work is also discussed in this chapter.

CHAPTER - 2

Modeling

2.1 Introduction

In this thesis, we have carried out the work on multilayer structures for organic light emitting diodes and organic solar cells. We have considered the use of nanoparticles to increase the light extraction efficiency in OLEDs and light absorption in the OSCs. Nanoparticles are commonly considered to be number of molecules or atoms bonded together with radius of <100 nm [111]. Nanoparticles have different properties than those of same bulk materials because the smaller particles have larger surface area compared to bulk materials. When an electromagnetic radiation is incident on these nanoparticles, it can be absorbed and/or scattered. The absorption and scattering of light depends on size, shape and material of the nanoparticles. Metallic nanoparticles exhibit both absorption and scattering of light. The optical properties of metal nanoparticles are strongly influenced by the localized surface plasmon resonance [112, 113]. In case of dielectric nanoparticles, mostly scattering phenomenon takes place as their extinction coefficient is quite low. No plasmon resonance effects can be seen in dielectric nanoparticles. Mie theory includes both the scattering and absorption of plane electromagnetic waves of such nanoparticles [112].

The study of propagation of electromagnetic waves in the multilayer structure is quiet complicated. The behavior of electromagnetic waves in space and materials is described and characterized by the four vector equations of Maxwell's. To study and understand the light propagation in simple structures, analytic methods for solving Maxwell's

equations are useful. For more complex systems like multilayer structures, employment of numerical methods is necessary. Various numerical methods have been considered to study the light propagation in multilayer systems. These consist of finite element method [114], rigorous coupled wave analysis [115], transfer matrix method [116], finite difference time domain method [114], Monte Carlo method [114] etc. Finite difference time domain (FDTD) method has gained a lot of attention amongst other numerical techniques. It provides direct integration of Maxwell's time dependent equations. FDTD method is effective in modeling the complex structures as it is a volume based method. Also, it is a time domain method which implies that it can cover a wide range of frequencies with a single simulation run. FDTD is also an appropriate tool for solving the scattering problems.

In this chapter, we have discussed the Mie theory and FDTD method used for the calculation of proposed OLED and OSC structures. The scattering efficiency of the nanoparticle is calculated by using Mie theory. Light extraction efficiency in OLED and light absorption in the OSC has been evaluated by the FDTD method.

2.2 Mie Theory

Mie theory is named after German physicist Gustav Mie. His famous article on colour of colloidal Gold particles was published in 1908 [117]. Mie theory describes the interaction of spherical, homogenous particles with electromagnetic radiation. This theory provides the exact solution of Maxwell's equations for the calculation of optical properties of metals and dielectrics sphere embedded in a linear, isotropic and homogenous medium [112].

2.2.1 Solutions of Wave Equation

A electromagnetic field ($\vec{E},\vec{H}$) in an linear, isotropic, and homogenous medium satisfies the wave equations [112]

$$\nabla^2\vec{E}+k^2\vec{E}=0 \quad \text{and} \quad \nabla^2\vec{H}+k^2\vec{H}=0 \tag{2.1}$$

where $k=\omega\sqrt{\mu\varepsilon}, k$ is the incident light wave number, ω is the frequency, μ and ε are magnetic permeability and electric permittivity, respectively.

Electric and magnetic fields are divergence free as charge density is zero

$$\nabla.\vec{E} = 0 \qquad \text{and} \qquad \nabla.\vec{H} = 0 \tag{2.2}$$

As $\vec{E}$ and $\vec{H}$ are not independent, therefore, Ampere's and Faraday's laws can be written as follows

$$\nabla \times \vec{E} = i\omega\mu\vec{H}, \qquad \nabla \times \vec{H} = -i\omega\varepsilon\vec{E}, \tag{2.3}$$

The solution to wave equation (2.1) is not simple. Therefore, we introduce an intermediate vector function $\vec{N}$

$$\vec{N} = \nabla \times (\vec{g}\psi) \tag{2.4}$$

ψ represents a scalar function and $\vec{g}$ an arbitrary constant vector.

As the divergence of curl of any vector is zero. Therefore, $\vec{N}$ will become divergence-free. Hence,

$$\nabla.\vec{N} = 0 \tag{2.5}$$

If we apply $\nabla^2 + k^2$ to Eq. (2.4), we get

$$\nabla^2\vec{N} + k^2\vec{N} = \nabla \times [\vec{g}(\nabla^2\psi + k^2\psi) \tag{2.6}$$

From Eqs. (2.6) and (2.1), it is clear that if ψ is a solution to scalar wave equation then $\vec{N}$ will satisfy the vector wave equation

$$\nabla^2\psi + k^2\psi = 0 \tag{2.7}$$

The another divergence free vector function $\vec{M}$ can also be generated which satisfies the vector wave equation

$$\vec{M} = \frac{\nabla \times \vec{N}}{k} \tag{2.8}$$

We also have

$$\nabla \times \vec{M} = k\vec{N} \tag{2.9}$$

Therefore, $\vec{N}$ and $\vec{M}$ known as Vector Spherical Harmonics (VSHs), have all the requirements of an electromagnetic field: they are divergence less, they satisfy the vector wave equation, curl of $\vec{N}$ and curl of $\vec{M}$ are proportional to $\vec{M}$ and $\vec{N}$, respectively.

Therefore, the complex vector wave equation can be reduced to a simpler scalar wave equation with ψ as a generating function for $\vec{M}$ and $\vec{N}$ and $\vec{g}$ the guiding vector.

Geometrical representation of an isolated spherical particle shown in Fig. 2.1 represents the spherical symmetry. Spherical coordinates (r,θ,ϕ) are used to solve the equation (2.7). We choose $\vec{g}=\vec{r}$, where $\vec{r}$ is the radius vector.

The wave equation in spherical coordinates can be written as

$$\frac{1}{r^2}\frac{\partial}{\partial r}\left(r^2\frac{\partial\psi}{\partial r}\right)+\frac{1}{r^2\sin\theta}\frac{\partial}{\partial\theta}\left(\sin\theta\frac{\partial\psi}{\partial\theta}\right)+\frac{1}{r^2\sin\theta}\frac{\partial^2\psi}{\partial\phi^2}+k^2\psi=0 \qquad (2.10)$$

For Eq. (2.10), the solution can be considered in the form mentioned below

$$\psi(r,\theta,\phi)=R(r)\Theta(\theta)\Phi(\phi) \qquad (2.11)$$

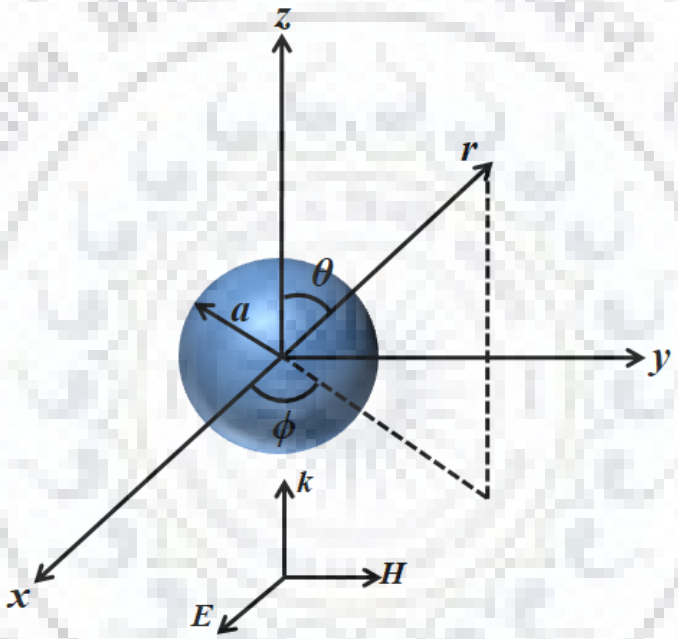

Figure 2.1 *Geometry of the scattering of a spherical particle in spherical polar coordinate system.*

By substituting Eq. (2.11) in scalar wave Eq. (2.10), we obtained three separate equations, one for each coordinate. The conditions of single-valued and linear independence must be satisfied by the solutions of these three equations. Therefore, the complete solution of the scalar wave equation in spherical polar coordinates is given by

$$\psi_{elm}(r,\theta,\phi)=\cos l\phi P_m^l(\cos\theta)z_m(kr) \qquad (2.12)$$

$$\psi_{olm}(r,\theta,\phi)=\sin l\phi P_m^l(\cos\theta)z_m(kr) \qquad (2.13)$$

where *o* and *e* means odd and even, P_m^l is associated first kind Legendre function of order *l* and degree *m* and $z_m(kr)$ represents the spherical Bessel functions from these four kind: $j_m, y_m, h_m^{(1)}, h_m^{(2)}$.

$$h_m^{(1)}(kr) = j_m(kr) + iy_m(kr);\ h_m^{(2)}(kr) = j_m(kr) - iy_m(kr) \tag{2.14}$$

Any function which satisfies the Eq. (2.10) may be expanded as an infinite series of the functions (2.12) and (2.13). The VSHs can be expressed as

$$\vec{N}_{elm} = \nabla \times (\vec{r}\psi_{elm})\ \vec{N}_{olm} = \nabla \times (\vec{r}\psi_{olm}) \tag{2.15}$$

$$\vec{M}_{elm} = \frac{\nabla \times (\vec{r}\psi_{elm})}{k}\ \vec{M}_{olm} = \frac{\nabla \times (\vec{r}\psi_{olm})}{k} \tag{2.16}$$

The component forms of VSHs can be seen from [112].

2.2.2 The incident and Scattered Fields

The incident field is considered to be a plane wave polarized along *x*- direction and propagating along the *z*-direction shown in Fig. 2.1. The incident wave in terms of spherical polar coordinates can be described as:

$$\vec{E}_i = E_0 e^{ikr\cos\theta}\hat{e}_x \tag{2.17}$$

where E_0 is the amplitude of electric field and $\hat{e}_x$ is the unit vector in the polarization direction. Since,

$$\hat{e}_x = \sin\theta\cos\phi\hat{e}_r + \cos\theta\cos\phi\hat{e}_\theta - \sin\theta\hat{e}_\phi \tag{2.18}$$

The incident magnetic field can be obtained by substituting (2.17) in (2.3).

The incident electric field extended as an infinite series of the VSHs is as follows [112]

$$\vec{E}_i = \sum_{l=0}^{\infty}\sum_{m=l}^{\infty}(B_{elm}\vec{N}_{elm} + B_{olm}\vec{N}_{olm} + A_{elm}\vec{M}_{elm} + A_{olm}\vec{M}_{olm}) \tag{2.19}$$

B_{elm}, B_{olm}, A_{elm} and A_{olm} are the expansion coefficients. Using the finiteness of incident field at origin and orthogonality of the VSHs, equation (2.19) can be reduced to

$$\vec{E}_i = \sum_{m=1}^{\infty}(B_{o1m}\vec{N}_{o1m}^{(1)} + A_{e1m}\vec{M}_{e1m}^{(1)}) \tag{2.20}$$

The superscript (1) represents the spherical Bessel function $j_m(kr)$ for the incident field to be finite at the origin.

After doing all the mathematics, the final form of the expansion coefficients is as follows

$$B_{o1m} = i^m E_0 \frac{2m+1}{m(m+1)},\ A_{e1m} = -iE_0 i^m \frac{2m+1}{m(m+1)} \tag{2.21}$$

By substituting Eq. (2.21) in Eq. (2.20), we obtain the expansion of incident electric field as

$$\vec{E}_i = E_0 \sum_{m=1}^{\infty} i^m \frac{2m+1}{m(m+1)} (\vec{N}_{o1m}^{(1)} - i\vec{M}_{e1m}^{(1)}) \tag{2.22}$$

The corresponding magnetic field can also be expressed as

$$\vec{H}_i = \frac{-k}{\omega\mu} E_0 \sum_{m=1}^{\infty} i^m \frac{2m+1}{m(m+1)} (\vec{N}_{e1m}^{(1)} + i\vec{M}_{o1m}^{(1)}) \tag{2.23}$$

For simplification, we will use $E_m = E_0 i^m \frac{2m+1}{m(m+1)}$

By applying the boundary conditions (BCs) between the sphere and the surrounding medium, we can obtain the scattered field $(\vec{E}_s, \vec{H}_s)$

$$(\vec{E}_i + \vec{E}_s - \vec{E}_1) \times \hat{e}_r = (\vec{H}_i + \vec{H}_s - \vec{H}_1) \times \hat{e}_r = 0 \tag{2.24}$$

By using Eq. (2.24), finiteness of the fields and orthogonality of VSHs, the scattered field can be written as

$$\vec{E}_s = \sum_{m=1}^{\infty} E_m (ia_m \vec{M}_{e1m}^{(3)} - b_m \vec{N}_{o1m}^{(3)}), \qquad \vec{H}_s = \frac{k}{\omega\mu} \sum_{m=1}^{\infty} E_m (ib_m \vec{M}_{o1m}^{(3)} + a_m \vec{N}_{e1m}^{(3)}) \tag{2.25}$$

where superscript (3) represents the spherical Hankel function $h_m^{(1)}$. a_m and b_m, are known as the Mie coefficients for the scattered field.

The analytical expressions for Mie coefficients can be achieved from four equations obtained by applying the BCs (in Eq. 2.24) at surface of the sphere (at $r=a$).

$$a_m = \frac{\mu p^2 j_m(p\alpha)[\alpha j_m(\alpha)]' - \mu_1 j_m(\alpha)[p\alpha j_m(p\alpha)]'}{\mu p^2 j_m(p\alpha)[\alpha h_m^{(1)}(\alpha)]' - \mu_1 h_m^{(1)}(\alpha)[p\alpha j_n(p\alpha)]'} \tag{2.26}$$

$$b_m = \frac{\mu_1 j_m(p\alpha)[\alpha j_m(\alpha)]' - \mu j_m(\alpha)[p\alpha j_n(p\alpha)]'}{\mu_1 j_m(p\alpha)[\alpha h_m^{(1)}(\alpha)]' - \mu h_m^{(1)}(\alpha)[p\alpha j_n(p\alpha)]'} \tag{2.27}$$

where μ_1 and μ being the magnetic permeabilities of the sphere and the surrounding medium, respectively. Furthermore, α is the size parameter and p is the relative refractive index between the surrounding medium and the sphere, and are defined as

$$\alpha = ka = \frac{2\pi a}{\lambda},\ p = \frac{n_1}{n} \tag{2.28}$$

In Eq. (2.28), a is the sphere's radius, λ the wavelength of incident light and n_1 and n are the refractive index of sphere and surrounding medium, respectively.

These Mie coefficients can be simplified more by considering the magnetic permeabilities of the surrounding medium and particle to be equal to one and by using Ricatti-Bessel functions as

$$\psi_m(\rho) = \rho j_m(\rho), \xi_m(\rho) = \rho h_m^1(\rho) \tag{2.29}$$

with $\rho = kr$.

Under these conditions, the Mie coefficients can be expressed as

$$a_m = \frac{p\psi_m(p\alpha)\psi'_m(\alpha) - \psi_m(\alpha)\psi'_m(p\alpha)}{p\psi_m(p\alpha)\xi'_m(\alpha) - \xi_m(\alpha)\psi'_m(p\alpha)} \tag{2.30}$$

$$b_m = \frac{\psi_m(p\alpha)\psi'_m(\alpha) - p\psi_m(\alpha)\psi'_m(p\alpha)}{\psi_m(p\alpha)\xi'_m(\alpha) - p\xi_m(\alpha)\psi'_m(p\alpha)} \tag{2.31}$$

2.2.3 Scattering, Extinction and Absorption Efficiencies

The cross section (C) can be defined as the ratio of the net rate at which electromagnetic energy (V) crosses the surface of an imaginary sphere centered on the particle to the incident irradiation (P). The absorption and scattering cross sections can be expressed as

$$C_{sca} = \frac{V_{sca}}{P};\ C_{abs} = \frac{V_{abs}}{P} \tag{2.32}$$

The scattered, extinction and absorbed electromagnetic energy are given by

$$\begin{aligned} V_{ext} &= \frac{1}{2}\mathrm{Re}\int_0^{2\pi}\int_0^{\pi}(E_{i\phi}H^*_{s\theta} - E_{i\theta}H^*_{s\phi} - E_{s\theta}H^*_{i\phi} + E_{s\phi}H^*_{i\theta})r^2\sin\theta d\theta d\phi, \\ V_{sca} &= \frac{1}{2}\mathrm{Re}\int_0^{2\pi}\int_0^{\pi}(E_{s\theta}H^*_{s\phi} - E_{s\phi}H^*_{s\theta})r^2\sin\theta d\theta d\phi, \\ V_{abs} &= V_{ext} - V_{sca} \end{aligned} \tag{2.33}$$

After solving these equations, the cross sections can be expressed in terms of Mie coefficients as

$$\begin{aligned} C_{sca} &= \frac{2\pi}{k^2}\sum_{m=1}^{\infty}(2m+1)(|a_m|^2 + |b_m|^2), \\ C_{ext} &= \frac{2\pi}{k^2}\sum_{m=1}^{\infty}(2m+1)\,\mathrm{Re}(a_m + b_m), \\ C_{abs} &= C_{ext} - C_{sca}. \end{aligned} \tag{2.34}$$

The extinction, scattering and absorption efficiencies can be obtained by dividing these cross-sections mentioned in eq. (2.34) to the geometrical cross area of the particle (G). For a sphere, $G=\pi a^2$, and the efficiencies become

$$\begin{aligned} Q_{sca} &= \frac{2}{\alpha^2}\sum_{m=1}^{\infty}(2m+1)(|a_m|^2+|b_m|^2), \\ Q_{ext} &= \frac{2}{\alpha^2}\sum_{m=1}^{\infty}(2m+1)\,\mathrm{Re}(a_m+b_m), \\ Q_{abs} &= Q_{ext}-Q_{sca}. \end{aligned} \tag{2.35}$$

For infinite series, n is truncated to n_{max} i.e.

$$n_{\max} = \alpha + 4\alpha^{1/3} + 2 \tag{2.36}$$

2.3 Finite Difference Time Domain Method

From all the full wave techniques which are used to solve electromagnetic problems, FDTD is the flexible and efficient modeling method. In 1966, K. Yee was the first to introduce the FDTD method [118] and later developed by Taflove and others [119-122]. This technique employs approximations of finite differences to both the temporal and spatial derivatives that are present in Maxwell's time dependent curl equations. The approximated derivatives of the function are very well expressed by Taylor's series expansion. The central finite difference approximation of function $f(x)$ at point x_0 with an offset of g is given by

$$\left.\frac{df(x)}{dx}\right|_{x=x_0} \approx \frac{f(x_0+g)-f(x_0-g)}{2g}+O(g^2) \tag{2.37}$$

All the terms which are not shown explicitly are represented by "O" term and the value in bracket i.e. g^2 shows the lowest order of g in these terms. If g is very small, then in equation (2.37) all the terms represented by "O" can be neglected. Also, note that this finite difference expressed in Eq. (2.37) just gives the approximation of the function's derivative at x_0, but the function is not sampled there. The function is actually sampled at the neighborhood points x_0+g and x_0-g.

2.3.1 Yee's Algorithm

Consider an isotropic medium in which Maxwell's equations (Ampere's and Faraday's laws) are expressed as

$$\begin{aligned} \nabla \times \vec{E} &= -\mu \frac{\partial \vec{H}}{\partial t} \\ \nabla \times \vec{H} &= \sigma \vec{E} + \varepsilon \frac{\partial \vec{E}}{\partial t} \end{aligned} \tag{2.38}$$

In the rectangular coordinate system, the vector equation (2.38) produces a system of six scalar equations written as

$$\begin{aligned} \frac{\partial H_x}{\partial t} &= \frac{1}{\mu}\left(\frac{\partial E_y}{\partial z} - \frac{\partial E_z}{\partial y}\right), \\ \frac{\partial H_y}{\partial t} &= \frac{1}{\mu}\left(\frac{\partial E_z}{\partial x} - \frac{\partial E_x}{\partial z}\right), \\ \frac{\partial H_z}{\partial t} &= \frac{1}{\mu}\left(\frac{\partial E_x}{\partial y} - \frac{\partial E_y}{\partial x}\right), \\ \frac{\partial E_x}{\partial t} &= \frac{1}{\varepsilon}\left(\frac{\partial H_z}{\partial y} - \frac{\partial H_y}{\partial z} - \sigma E_x\right), \\ \frac{\partial E_y}{\partial t} &= \frac{1}{\varepsilon}\left(\frac{\partial H_x}{\partial z} - \frac{\partial H_z}{\partial x} - \sigma E_y\right), \\ \frac{\partial E_z}{\partial t} &= \frac{1}{\varepsilon}\left(\frac{\partial H_y}{\partial x} - \frac{\partial H_x}{\partial y} - \sigma E_z\right) \end{aligned} \tag{2.39}$$

The steps of using Yee's algorithm are as follows:

1. All the derivatives in equation (2.39) are replaced by finite differences. Discretize space and time i.e. space is divided into small segments known as cells and time is quantized into small steps. This makes magnetic and electric fields staggered in space and time. These cells are known as Yee or FDTD cells. A three dimensional volume called FDTD mesh can be obtained by multiple Yee cells.
2. Work out the resulting finite difference equations to find the (future) unknown fields in terms of (past) known fields which are known as "update equations".
3. Evaluation of electric fields one time step into future so that they are known (past fields)
4. Evaluation of magnetic fields one time step into future so that they are known (past fields)

5. To find the fields over the desired duration, the previous two steps are repeated. This process is known as leap frog method.

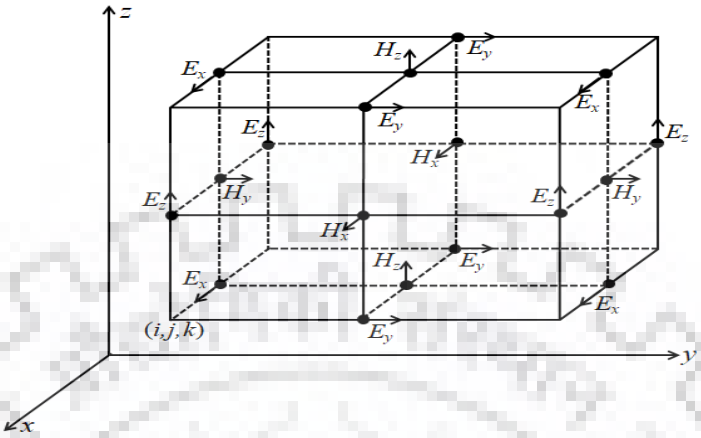

Figure 2.2 *Positions of the field components in a unit cell of the Yee's lattice (Adapted from Ref. 118).*

Let us define a grid point and any function of time and space in the solution region as

$$(a,b,c) \equiv (a\Delta x, b\Delta y, c\Delta z)$$
$$F^m(a,b,c) \equiv F(a\delta, b\delta, c\delta, m\Delta t) \tag{2.40}$$

where $\delta = \Delta x = \Delta y = \Delta z$ is the increment in space, Δt is the increment in time and *a, b,c, m* are integers. Using Eqs. (2.37) and (2.40), we get

$$\frac{\partial F^m(a,b,c)}{\partial x} = \frac{F^m(a+1/2,b,c) - F^m(a-1/2,b,c)}{\delta}$$
$$\frac{\partial F^m(a,b,c)}{\partial t} = \frac{F^{m+1/2}(a,b,c) - F^{m-1/2}(a,b,c)}{\Delta t} \tag{2.41}$$

Fig. (2.2) depicts the positions of the components of $\vec{E}$ and $\vec{H}$ about a unit cell of the lattice developed by Yee. In applying equation (2.41) to all the space and time derivatives in equation (2.39), the field components are solved at alternate half time steps. Therefore, the finite difference approximation of equation (2.39) is obtained as

$$H_x^{m+1/2}(a,b+1/2,c+1/2) = H_x^{m-1/2}(a,b+1/2,c+1/2) + \frac{\Delta t}{\mu(a,b+1/2,c+1/2)\delta} \times$$
$$[\{E_y^m(a,b+1/2,c+1) - E_y^m(a,b+1/2,c+1)\} +$$
$$\{E_z^m(a,b,c+1/2) - E_z^m(a,b+1,c+1/2)\}] \tag{2.42a}$$

$$H_y^{m+1/2}(a+1/2,b,c+1/2)=H_y^{m-1/2}(a+1/2,b,c+1/2)+\frac{\Delta t}{\mu(a+1/2,b,c+1/2)\delta}\times$$
$$[\{E_z^m(a+1,b,c+1/2)-E_z^m(a,b,c+1/2)\}+ \quad (2.42b)$$
$$\{E_x^m(a+1/2,b,c)-E_x^m(a+1/2,b,c+1)\}]$$

$$H_z^{m+1/2}(a+1/2,b+1/2,c)=H_z^{m-1/2}(a+1/2,b+1/2,c)+\frac{\Delta t}{\mu(a+1/2,b+1/2,c)\delta}\times$$
$$[\{E_x^m(a+1/2,b+1,c)-E_x^m(a+1/2,b,c)\}+ \quad (2.42c)$$
$$\{E_y^m(a,b+1/2,c)-E_y^m(a+1,b+1/2,c)\}]$$

$$E_x^{m+1}(a+1/2,b,c)=\left(1-\frac{\sigma(a+1/2,b,c)\Delta t}{\varepsilon(a+1/2,b,c)}\right)E_x^m(a+1/2,b,c)+\frac{\Delta t}{\varepsilon(a+1/2,b,c)\delta}\times$$
$$[\{H_z^{m+1/2}(a+1/2,b+1/2,c)-H_z^{m+1/2}(a+1/2,b-1/2,c)\}+ \quad (2.42d)$$
$$\{H_y^{m+1/2}(a+1/2,b,c-1/2)-H_y^{m+1/2}(a+1/2,b,c+1/2)\}]$$

$$E_y^{m+1}(a,b+1/2,c)=\left(1-\frac{\sigma(a,b+1/2,c)\Delta t}{\varepsilon(a,b+1/2,c)}\right)E_y^m(a,b+1/2,c)+\frac{\Delta t}{\varepsilon(a,b+1/2,c)\delta}\times$$
$$[\{H_x^{m+1/2}(a,b+1/2,c+1/2)-H_x^{m+1/2}(a,b+1/2,c-1/2)\}+ \quad (2.42e)$$
$$\{H_z^{m+1/2}(a-1/2,b+1/2,c)-H_z^{m+1/2}(a+1/2,b+1/2,c)\}]$$

$$E_z^{m+1}(a,b,c+1/2)=\left(1-\frac{\sigma(a,b,c+1/2)\Delta t}{\varepsilon(a,b,c+1/2)}\right)E_z^m(a,b,c+1/2)+\frac{\Delta t}{\varepsilon(a,b,c+1/2)\delta}\times$$
$$[\{H_y^{m+1/2}(a+1/2,b,c+1/2)-H_y^{m+1/2}(a-1/2,b,c+1/2)\}+ \quad (2.42f)$$
$$\{H_x^{m+1/2}(a,b-1/2,c+1/2)-H_x^{m+1/2}(a,b+1/2,c+1/2)\}]$$

Hence, Fig. (2.2) and Eqs (2.42a)-(2.42f) depict that $\vec{E}$ and $\vec{H}$ components are interlaced within unit cell in three spatial dimensions and are calculated at alternately half time steps.

2.3.2 Stability and Accuracy Criterion

To make sure the accuracy of the obtained results, the spatial grid δ should be sufficient to resolve the smallest feature of the field to be calculated. Generally, this is done by the wavelength in the material, or in some cases, by the geometry of the device. So, for the efficient and accurate results, the grid spacing should be smaller than the wavelength or $\leq \lambda/10$. This amounts for ten or more cells per wavelength. To assure the stability of

finite difference method of equations (2.42a)-(2.42f), one must satisfy the following Courant condition [119,123] which relates temporal and spatial step size as:

$$u_{\max}\Delta t \le \frac{1}{\sqrt{(1/\Delta x^2 + 1/\Delta y^2 + 1/\Delta z^2)}} \tag{2.43}$$

where u_{max} is the maximum wave phase velocity in the model. For practical applications, the ratio of time increment to the spatial increment must be selected as large as possible yet fulfilling equation (2.43) [114].

2.3.3 Boundary Conditions in FDTD

In FDTD method, there is a requirement of artificial mesh boundary conditions which truncates the solution or simulation region. These artificial truncation conditions are known as absorbing boundary conditions as they absorb incident or transmitted fields. The accuracy of FDTD formulation is dictated by the proper choice of boundary conditions. So, the boundary conditions at the edges of computational domain must be carefully considered. The need for accuracy has resulted in various type of absorbing boundary conditions which are discussed in Ref. [124-130]. These include periodic boundary, symmetric or anti-symmetric boundary, perfect electric or magnetic conductor, and perfectly matched layer. One of the most effective and widely accepted absorbing boundary condition is perfectly matched layer (PML) [127-130].

In the PML termination technique, a layer consists of several grid points placed in the region of the outer boundary of simulation domain and is designed to act as an absorbing or highly lossy material. The goal of this boundary condition is to make sure that when a incident plane wave is incident from FDTD region to the PML region then it should be completely absorbed by PML region without any reflections.

2.4 Simulation Tools

In the previous sections, we have discussed the Mie theory and FDTD method. We have developed a Matlab code in house for Mie theory which calculates the scattering efficiency of nanoparticles. In this thesis, we have carried out most of the work with the incorporation of nanoparticles layer at different layers in the organic light emitting diode and organic solar cell structures.

The proposed multilayer design of OLED has been numerically analyzed with commercially available software Lumerical FDTD Solutions [131]. This software is based on finite difference time domain method. FDTD Solutions is useful for finding the electromagnetic fields as a function of wavelength by solving Fourier transforms during the computation. It gives complex-valued fields and other derived quantities like the reflection, transmission, Poynting vector, and far field projections as a function of wavelength. So, by obtaining the fields, we can calculate the light extraction efficiency of OLED.

For the simulation and analysis of multilayer design of organic solar cell, commercially available software RSoft Cad Full Wave and Solar Cell Utility has been utilized [132]. This software uses FDTD method to find the fields in the OSC structure. Full Wave is used to calculate the light absorption in the active layer of the structure whereas Solar Cell utility calculates the current-voltage (*J*-*V*) characteristics and optical efficiency of the solar cell.

These softwares can only take optical effects into account. Other numerical and physical parameters such as temporal grid, spatial grid, finite computational domain, boundary conditions, length of time for the simulation, material properties, sources, monitors are also considered in the software.

2.5 Conclusions

In this chapter, firstly, we have provided a brief introduction of the spherical particle (nanoparticle) theory and numerical methods to study the propagation of electromagnetic in multilayer structures. We then discussed the mathematical formulation of Mie theory to calculate the scattering, absorption and extinction efficiencies of nanoparticle. We have also discussed the finite difference time domain method which efficiently solves the time dependent Maxwell's equations. Lastly, we have done a brief discussion about the simulation tools based on Mie theory and FDTD method which are used to carry out the work of this thesis.

CHAPTER - 3

Improvement in Light Extraction Efficiency of OLED by using Dielectric Nanoparticles*

3.1 Introduction

OLEDs have attracted a great deal of attention due to their advantages of high internal quantum efficiency, low power consumption and cost, high brightness and contrast than those of semiconductor based LEDs. Organic materials are easier to deposit on flexible substrate because of their intrinsic properties. In OLEDs, the emission wavelength can be tuned easily by using appropriate dopants in organic emissive layer [10, 11]. OLEDs have been of keen interest due to their potential applications in illumination, flat panel displays and solid state lighting.

---

* A part of this work has been published in the following journal papers

V. Mann and V. Rastogi, "Dielectric nanoparticles for the enhancement of OLED light extraction efficiency," *Optics Communications*, vol. 387, pp. 202-207, 2017.

V. Mann, B. Hooda and V. Rastogi, "Improvement of light extraction efficiency of organic light emitting diodes using dielectric nanoparticles," *Journal of Nanophotonics* , vol. 11, pp. 036010-1-036010-11, 2017.

Despite achieving almost 100% internal quantum efficiency, the external quantum efficiency of OLED is limited to 20% in conventional cases [23, 24]. A large fraction of light (~80%) is lost due to various mechanisms that take place inside the device. Substrate losses are due to the TIR taking place at substrate and air interface. Almost 30% of the generated light is lost in substrate modes [25]. Waveguided losses occur due to ITO/ organic waveguided modes. Approximately 20% of light is lost in waveguided modes [26]. Due to surface plasmons modes occur at cathode and organic interface 30% of generated light is lost [25, 26] . Various approaches have been reported in the literature to extract power from these modes and thereby to increase the extraction efficiency of OLED. Use of textured substrate, surface roughening and micro lens arrays has been suggested to extract the power from substrate mode of OLED [27-34]. Use of photonic crystals, gratings, microstructures and nanostructures has been reported to extract the power from waveguide and surface plasmons modes [40-51]. Use of nanoparticles based optical scattering is another approach to improve the extraction efficiency of OLED. Metal, dielectric, semiconductor and magnetic nanoparticles are used for this purpose [133-140]. Ma et al. reported that incorporation of silver (Ag) nanoparticles between emitting layer and metal cathode increases the efficiency by 50-fold [135]. An Enhancement of 38% in efficiency of OLED is achieved with incorporation of gold (Au) nanoparticles in hole transport layer whereas with the silica (SiO_2) nanoparticles in hole transport layer, the current efficiency of OLED increases by 66% [136, 137]. In another work, the efficiency of device improved by 3 times when semiconductor ZnO nanoparticles are deposited at anode [138]. Magnetic nanoparticles of CoFe material incorporated in emissive layer enhance the efficiency of OLED by 32% [139]. Core- shell nanoparticles can also enhance the efficiency of OLEDs [141-143]. Liu et al. shows that with the incorporation of silica coated silver nanoparticles ($Ag@SiO_2$) in the emissive layer, the efficiency of the device is improved by a factor of 3 [141]. In another approach, deposition of polystyrene (PS) coated gold core shell (Au@PS) nanoparticles in the hole transport layer leads to an enhancement of 42% in efficiency [143]. Incorporation of polymer layer dispersed with scattering nanoparticles between the glass substrate and anode also improves the efficiency of the device [144-146]. Al_2O_3 nanoparticles dispersed in polystyrene increases the light extraction efficiency by 40% whereas TiO_2 nanoparticles dispersed in transparent photoresist material enhances the efficiency by 1.96 times [144, 146].

In this chapter, we have proposed two designs of OLED involving dielectric nanoparticles and numerically demonstrate the enhancement in light extraction efficiency of the device. In design 1, we have incorporated the nanoparticles layer at glass substrate. In design 2, the nanoparticles layer is incorporated at the anode (ITO). These nanoparticles act as scattering medium for the light trapped modes inside the OLED device. Various parameters like diameter, interparticle spacing and refractive indices of nanoparticles have been optimized to achieve the maximum enhancement in light extraction efficiency of OLED.

3.2 Dielectric nanoparticles at glass substrate

Loss in OLED in the form of waveguide modes occur at the ITO/organic interface arises due to TIR inside the device. Due to these modes, light comes out from the sides of the device. So, to reduce these losses, we have proposed to incorporate the nanoparticles (act as scatterers) layer at the glass substrate.

3.2.1 *Proposed Structure and Analysis*

The conventional OLED device considered as reference is shown in Fig. 3.1. The structure consists of a glass substrate, indium tin oxide (ITO) as anode, N,N-Di(naphthalene-1-yl)-N,N'-diphenyl-benzidine (NPD) acting as hole transport layer (HTL), tris(8-quinolinolato) aluminium (Alq_3) as emissive layer (EL), Lithium Fluoride (LiF) as electron transport layer (ETL), aluminium (Al) acting as cathode. The proposed structure shown in Fig. 3.2 consists of a single layer of dielectric nanoparticles at glass substrate followed by ITO/NPD/Alq_3/LiF/Al. We have also placed an additional layer of ITO which works as planarization layer to avoid the roughness caused by distribution of nanoparticles. There will not be any problem of absorption by nanoparticles as dielectric material is optically lossless. Nanoparticles are assumed to be spherical in shape.

Mie theory and finite difference time domain method discussed in chapter 2 have been used to analyze the effect of nanoparticles. As there is no dissipation in the visible region by dielectric nanoparticles, $Q_{abs} = 0$, so, Eq. (2.35) gives $Q_{sca} = Q_{ext}$.

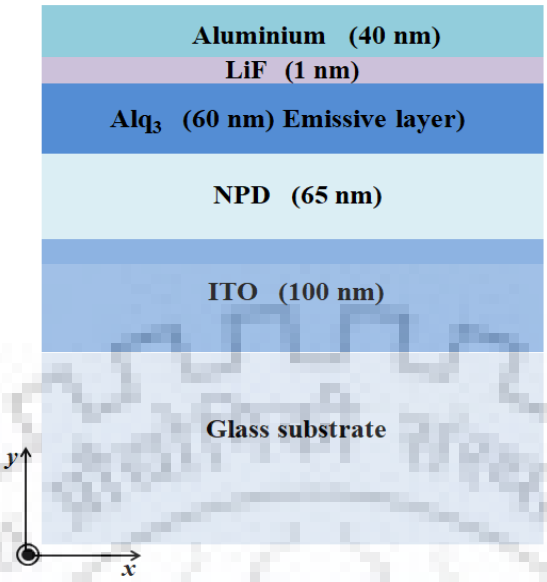

Figure 3.1 *Schematic design of conventional OLED.*

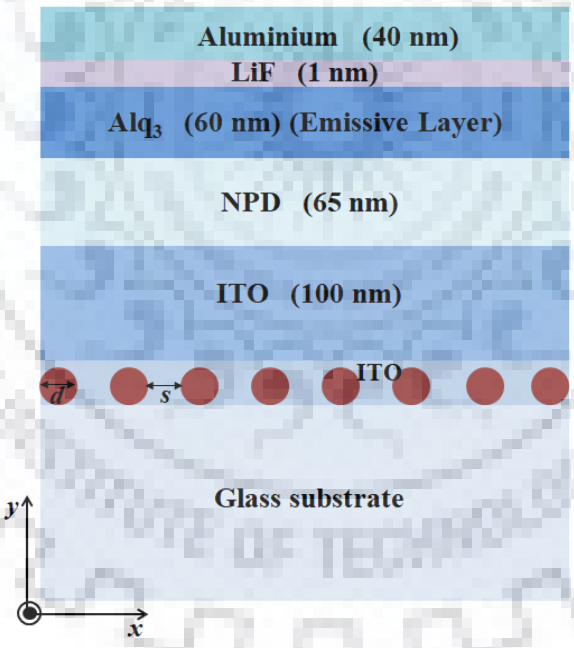

Figure 3.2 *Schematic design of proposed OLED with nanoparticles.*

To calculate the enhancement in light extraction efficiency of proposed structure we have used FDTD method. FDTD is an efficient way of solving Maxwell's equations at very small scales and is also very applicable for the study of OLED devices [147]. We have numerically studied the proposed structure using the simulation software

Lumerical FDTD solutions [131]. Though 3D simulations provide more reliable results but to save simulation time, we did 2D FDTD simulations with transverse electric polarizations as FDTD simulations are computationally very heavy. J. -H. Park et al. showed that the relative enhancement ratios for 2D and 3D simulations are same [148]. They also found that external quantum efficiency ratio observed in the experiment was close to that obtained from the FDTD simulation. The following parameters were chosen for the numerical simulation. Thicknesses of layers were set to be as: ITO (100 nm), NPD (65 nm), Alq_3 (60 nm), LiF (1 nm), Al (40 nm). It may be noted that 100 nm thickness of ITO layer is above the dielectric nanoparticle layer. Diameter (d) and interparticle separation (s) of nanoparticles were optimized for maximum extraction of light from the device. Refractive indices and extinction coefficients of ITO, NPD, Alq_3 and Al were taken from literature [149-151] whereas refractive indices of glass substrate and LiF were set to be 1.5 and 1.39 respectively. Refractive index (n_{np}) of dielectric nanoparticles has been varied from 1.1 to 2.1. The dielectric materials considered for nanoparticles can be synthesized by the sol-gel process.

Generation of light takes place in the emissive layer as the injected electrons and holes recombine to generate photons. The photons are generated through spontaneous emission process and each photon has random direction, phase and polarization. The exact treatment of this process can be described quantum mechanically in terms of photons but the generation of light has been considered classically by using electromagnetic point dipole sources. A single dipole was chosen for finite computation and placed in the centre of emissive layer. Since, FDTD simulations directly calculate the various field components i.e. it is vectorial in nature; we can not expect an incoherent addition of fields by placing two sources together in the same simulation. So, in order to have a point dipole source we need to make use of transverse electric (TE) polarized dipoles with orthogonal orientations in two separate simulations and then add the two responses incoherently. In order to estimate the total power generated in emissive layer, the dipole source was surrounded by a monitor. To avoid the unnecessary reflection of light, perfectly matched layer (PML) boundary conditions have been placed at all boundaries except at cathode side [127]. We used the metallic boundary at cathode side. The FDTD mesh size is a very crucial aspect as this decides the convergence of calculated fields and the results as well. The mesh size along x and y-directions have been chosen as 5 nm. The time increment of 5.5×10^{-18}s has been

considered. The span of the simulation region needs to be large enough such that there is enough propagation distance for the light to be fully extracted from the emission layer. The enhancement in the light extraction efficiency has been determined by calculating the far field distribution of emissive dipole source. The far field intensity distribution has been detected by monitor placed in the air above the glass substrate.

3.2.2 Results and Discussion

3.2.2.1 Scattering Efficiency of Nanoparticle

We have studied the optical scattering properties of dielectric nanoparticles in order to examine their suitability for enhanced performance of OLED. All these dielectric nanoparticles do not have dissipative properties in the spectral range of operation of OLED and hence they have an added advantage of not absorbing a part of incident energy and losing it in the form of joule heating. The dielectric nanoparticles do not exhibit the dipolar plasmonic resonances as they have positive dielectric constant over visible range.

(a) Effect of size of nanoparticle

Fig. 3.3 shows the calculated scattering efficiencies of isolated dielectric nanoparticle (n_{np} = 1.32) with diameter varying from 25 nm - 160 nm in an ambient medium of ITO. From the figure, it is visible that the scattering efficiency increases from d = 25 nm to d =160 nm. This means larger nanoparticles are generally desirable for extracting light from the device due to their greater ability to scatter more light. Large size nanoparticles tend to induce significant electrical effects [152]. However, in the proposed structure the nanoparticles being between glass and anode layer do not fall in the path of current and so are not expected to alter the electrical properties.

(b) Effect of refractive index

Fig. 3.4 shows the scattering efficiencies of dielectric nanoparticle (diameter = 100 nm) with refractive index varying from 1.1 to 2.1. Nanoparticle with n_{np} = 1.1 shows the maximum scattering efficiency and with n_{np} = 1.8 shows the minimum scattering efficiency. The ITO medium refractive index is not fixed to 1.8 but it is varying with wavelength [151]. That's why there will be scattering by nanoparticles of n_{np} = 1.8.

This shows that the scattering of light by nanoparticles strongly depends on the refractive index contrast between nanoparticles and embedding medium.

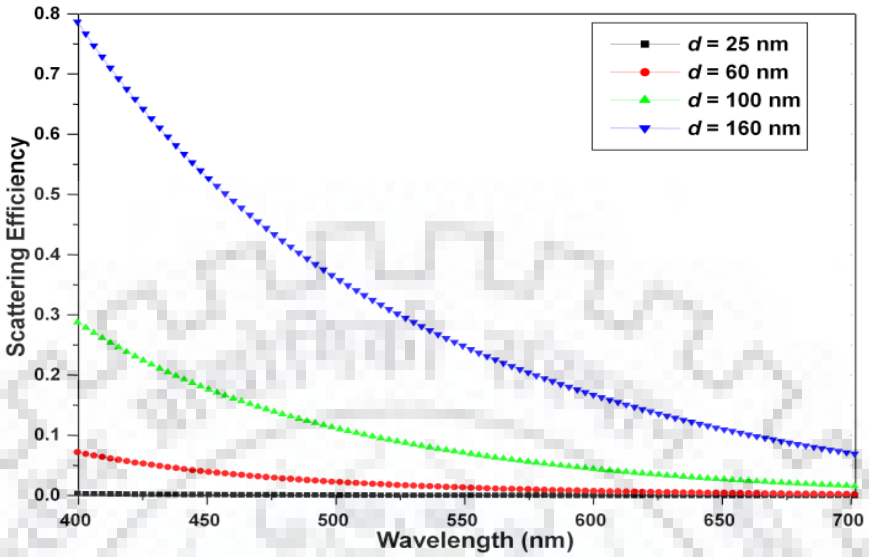

Figure 3.3 *Scattering efficiency as a function of wavelength for different diameters of nanoparticles.*

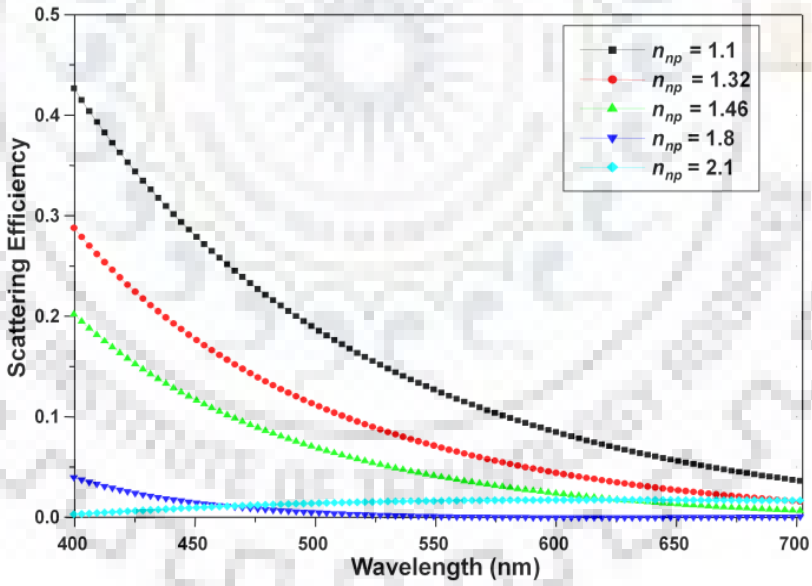

Figure 3.4 *Scattering efficiency as a function of wavelength for different refractive indices of nanoparticles.*

3.2.2.2 Far field distribution pattern

Fig. 3.5 (a) and 3.5 (b) show the far field intensity distribution for conventional OLED and OLED with nanoparticles. From the patterns, we can see that by adding the

dielectric nanoparticles more radiation is directed outside the emission layer of OLED. Addition of nanoparticles in the OLED design results in scattering and hence coupling-out of the emitted light from waveguide modes.

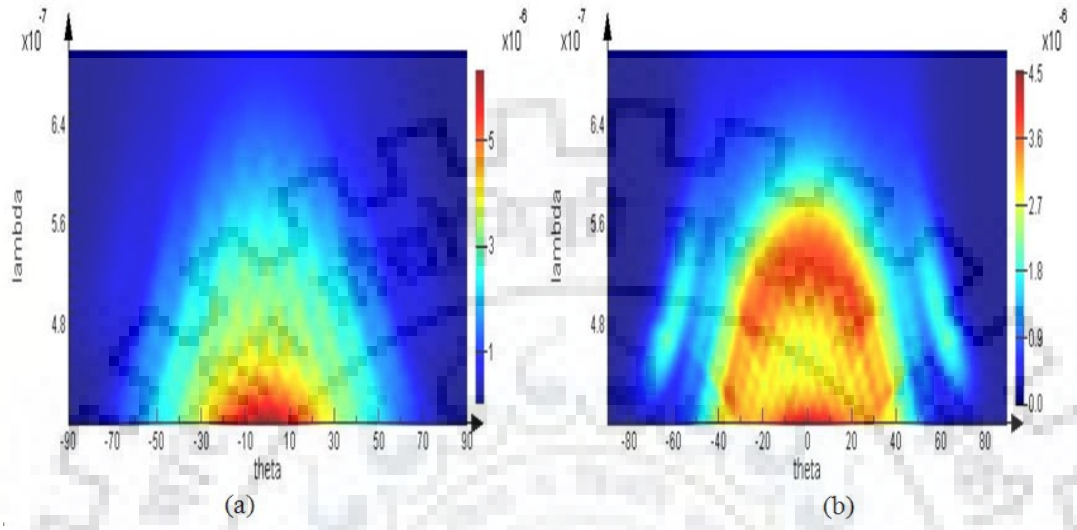

Figure 3.5 *Far field intensity distribution pattern for (a) conventional OLED (b) proposed OLED with nanoparticles.*

3.2.2.3 Enhancement in Light Extraction Efficiency

When calculating the light extraction efficiency, we calculate the fraction of power extracted from the OLED device relative to the total power emitted from the active layer. In FDTD simulation, the monitor placed in air receive the power emitted from the device with nanoparticles and conventional OLED for various parameters. The enhancement was calculated by the ratio of light extraction efficiencies of OLED with nanoparticles to the conventional OLED. Even with the use of dielectric nanoparticles, the light could not be completely extracted because the organics and metals absorb the light before it is coupled out of the device. To achieve the maximum enhancement in light extraction efficiency, several parameters like diameter (d), interparticle separation (s) and refractive index (n_{np}) of nanoparticles were optimized.

(a) Effect of size of nanoparticles

Diameter of nanoparticles plays an important role in scattering out the light from the device. To find the effect of diameters in light extraction, enhancement in light

extraction efficiency was calculated as a function of wavelength for different diameters of nanoparticles as shown in Fig. 3.6 while all other parameters such as refractive index and interparticle separation were kept fixed to 1.1 and 0 nm (i.e. no spacing). The diameter was varied from 25 nm to 160 nm. As we can see from the plot that enhancement in light extraction efficiency increases as d increases from 25 nm to 100 nm but at d = 160 nm it starts decreasing. This shows that for the larger diameter, the light extraction efficiency does not increase because the number of scattering sources becomes smaller in the simulation region of analysis. The enhancement can be seen in the wavelength range from approximately 440 nm to 600 nm. Therefore, one can achieve extraction efficiencies higher than that of planar OLED by setting the operating wavelength of OLED at any of these wavelengths So, in our structure approximately 1.7 times enhancement can be seen with d = 100 nm at around 500 nm wavelength.

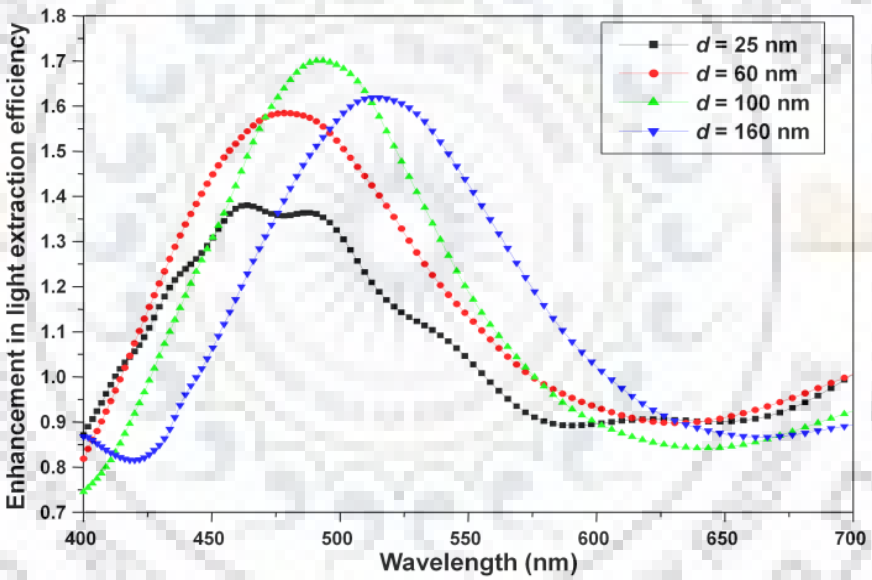

Figure 3.6 *Enhancement in light extraction efficiency as a function of wavelength for different size of nanoparticles.*

(b) Effect of interparticle separation

Any change in the interparticle separation of nanoparticles also affects the scattering, which results in a change in light extraction efficiency. To show this, we have investigated the effect of interparticle separation of dielectric nanoparticles on the enhancement in light extraction efficiency with wavelength and the results are shown in Fig. 3.7. We have fixed the diameter and refractive index of nanoparticles to 100 nm and 1.1. Interparticle separation was varied from 0 nm to 100 nm. As seen from the

figure, enhancement in extraction efficiency decreases from 1.7 times to 1.58 times as the interparticle separation increases from 0 nm to 100 nm. Also, there is peak wavelength shift of approximately 10 nm as the interparticle separation is raised from 0 nm to 100 nm. The peak experiences a blue shift and reduced strength with increasing interparticle separation indicating the diminishing of coupling effect between two spherical nanoparticles. These reductions in peak strength with interparticle spacing reflect the decay of field distribution between the particles. From the figure, we note that maximum enhancement (almost 1.7 times) is achieved with no interparticle spacing (i.e. s = 0 nm).

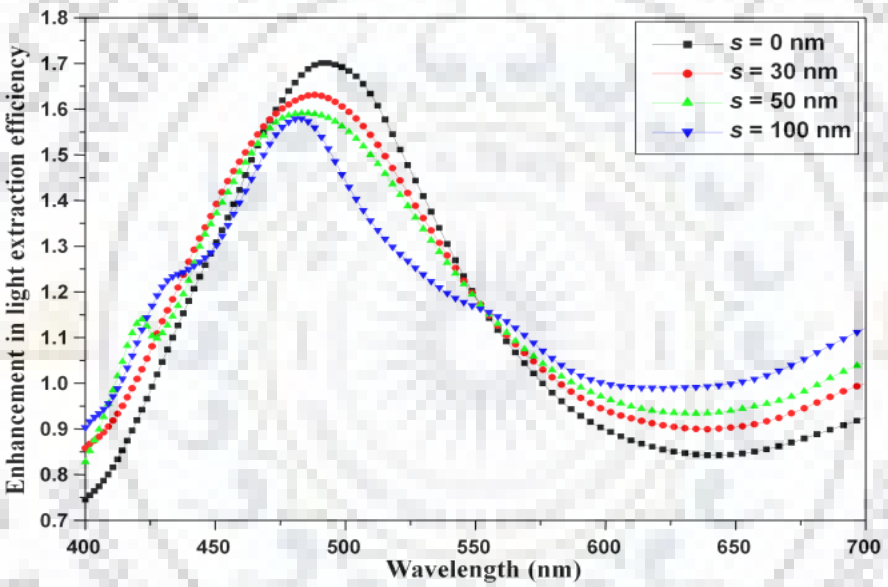

Figure 3.7 *Enhancement in light extraction efficiency as a function of wavelength for various interparticle separations of nanoparticles.*

(c) Effect of refractive indices

Next, we have studied the effect of refractive index of nanoparticles on enhancement in light extraction efficiency. To illustrate this, in Fig. 3.8 we have plotted the enhancement in light extraction efficiency with wavelength corresponding to different refractive index of nanoparticles. Diameter of nanoparticles was fixed to 100 nm with no interparticle separation (s = 0 nm). The curve shows the maximum enhancement of almost 1.7 times with refractive index 1.1. The scattering of light by the nanoparticles strongly depends on refractive index contrast. Here, the index contrast is in between

refractive index of dielectric nanoparticles and ITO (n = 1.8). We have varied the refractive index of nanoparticles from 1.1 to 2.1. From the figure, we can infer that enhancement in light extraction efficiency decreases from 1.7 times to 1.4 times as n_{np} increases from 1.1 to 1.46 whereas it increases from 1.4 times at n_{np} = 1.8 to 1.55 times at n_{np} = 2.1. Low refractive index (n_{np} = 1.1 and n_{np} = 1.32) dielectric nanoparticles show the enhancement in light extraction efficiency in the wavelength range 430 nm - 570 nm whereas high refractive index (n_{np} = 1.8 and n_{np} = 2.1) nanoparticles show the enhancement in wavelength range 400 nm - 500 nm and 630 nm - 700 nm. Enhancement can be seen in the whole visible spectrum with n_{np} = 1.46. This is due to the scattering efficiency of nanoparticles and absorption of light by various layers in the device. The scattering efficiency is more for high index contrast between embedded medium (ITO) and nanoparticles. In the visible region, the extinction coefficient of ITO first decreases and then increases with wavelength. An interplay between the scattering efficiency and the absorption of light for given refractive index of nanoparticles gives rise to the peak at particular wavelength. So, one can use refractive index of dielectric nanoparticles according to the choice of operating wavelength. Hence, mesoporous silica ($n_{np} \approx 1.1$), teflon ($n_{np} \approx 1.3$), silica ($n_{np} \approx 1.46$), aluminium oxide ($n_{np} \approx 1.8$) and zirconia ($n_{np} \approx 2.1$) dielectric materials can be used for nanoparticles.

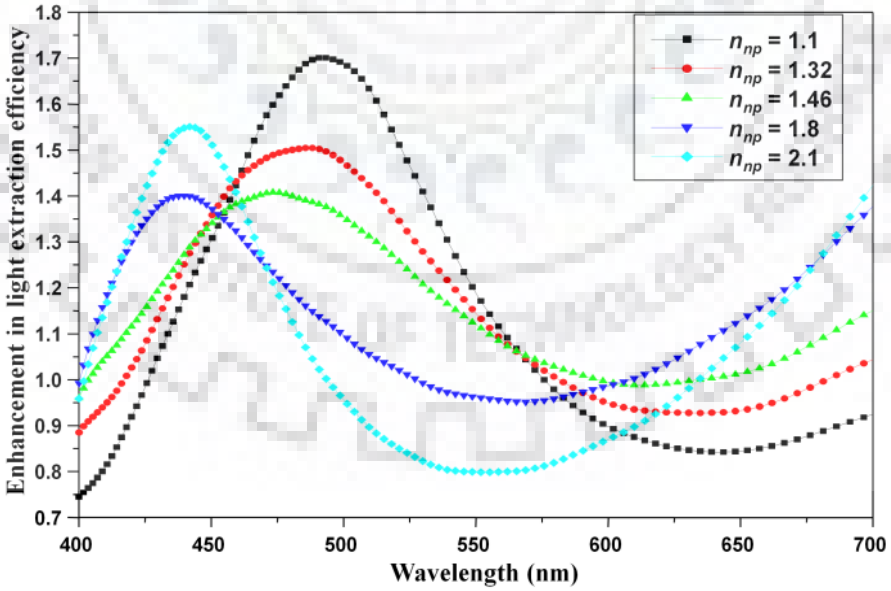

Figure 3.8 *Enhancement in light extraction efficiency as a function of wavelength for different refractive indices of nanoparticles.*

(d) Effect of assorted size nanoparticles

We have also investigated the effect of assorted size dielectric nanoparticles layer (deposited on glass substrate) on the enhancement of light extraction efficiency. Fig. 3.9(a) shows the structure containing assorted diameter dielectric nanoparticles and Fig. 3.9(b) shows the plot of corresponding enhancement in light extraction efficiency with wavelength. The diameters of nanoparticles range from 80 nm to 120 nm in a random manner while keeping the refractive index of nanoparticles as 1.1 with no interparticle spacing (i.e. s = 0 nm). The figure shows that enhancement of 1.5 times in light extraction efficiency is achieved with assorted diameter nanoparticles.

3.2.2.4 Comparison between 2D and 3D simulations

Although, 3D FDTD simulations provide the realistic results but the relative enhancement for both 2D and 3D simulations are same [142]. To verify this, we have carried out 3D FDTD simulation of the proposed structure for d = 100 nm, s = 0 nm, n_{np} = 1.1 and compared our results with 2D simulation. Fig. 3.10 shows the plot of enhancement in light extraction efficiency versus wavelength for 2D and 3D FDTD simulation. From the curve, we can see that the enhancement ratios of light extraction efficiency for both 2D and 3D simulations are quite same. This confirms that 2D simulation can be used to estimate the light extraction efficiency. Therefore, in order to save computational efforts and time, we have limited ourselves to 2D simulations.

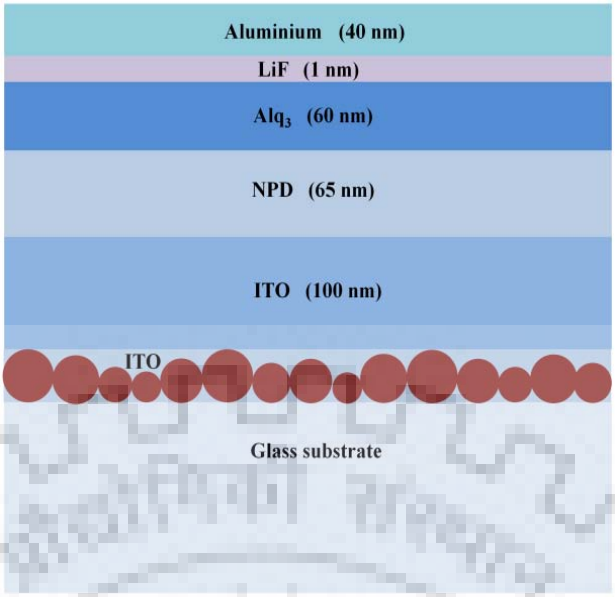

(a)

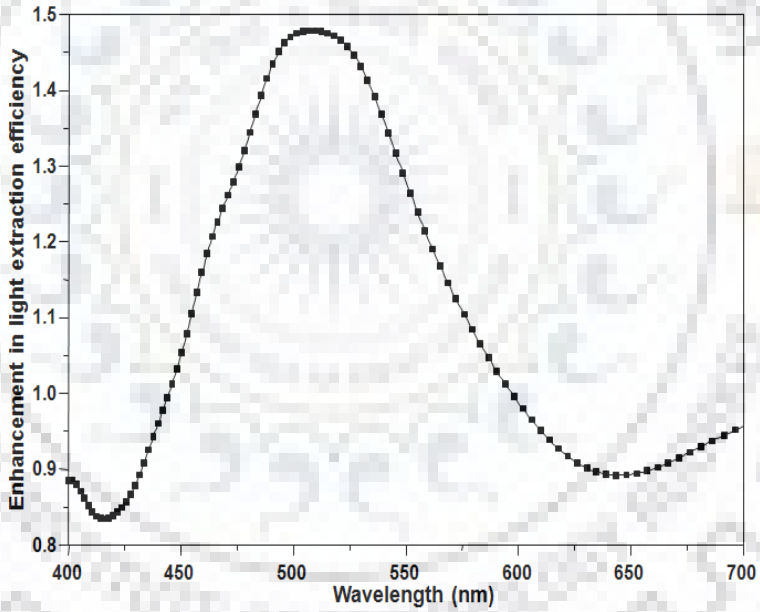

(b)

Figure 3.9 *(a) Proposed structure with assorted diameter nanoparticles. (b) Enhancement in light extraction efficiency as a function of wavelength for assorted diameter nanoparticles.*

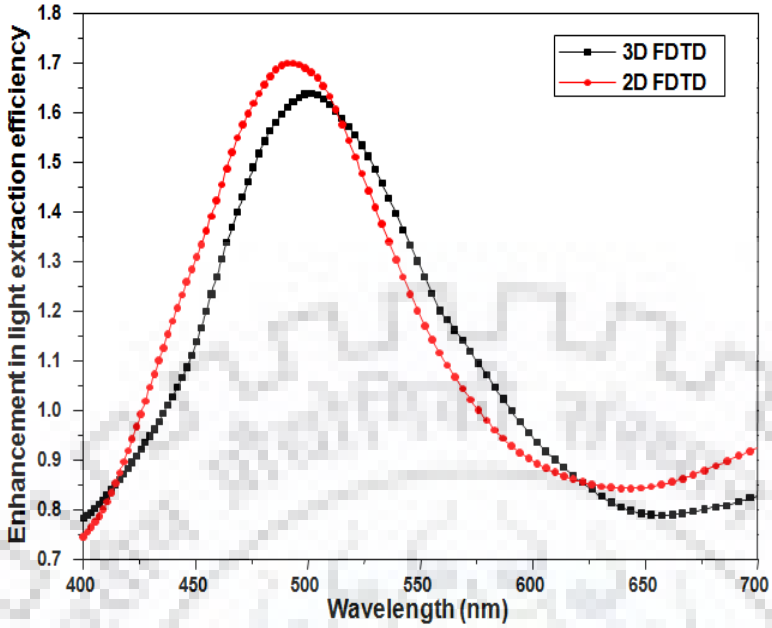

Figure 3.10 *Comparison of enhancement in light extraction efficiency for 2D and 3D FDTD simulation.*

3.3 Dielectric nanoparticles at anode (ITO)

In this study, we have placed the nanoparticles layer at anode to break the waveguided modes formed at ITO/organic interface.

The mode profile of conventional OLED structure has been calculated at 500 nm wavelength as shown in Fig. 3.11. The mode profile of the conventional OLED structure has been calculated by using Lumerical Mode solution [153]. The effective index of TE_0 mode comes out to be 1.63669. As it can be seen from the figure, most of the light remains inside the device and get dissipated in the glass layer. When nanoparticles layer is added in the structure then the interface between ITO and NPD layer becomes corrugated. Due to this corrugation, total internal reflection does not take place and guided mode is not formed. This helps in preventing loss of light in the guided mode.

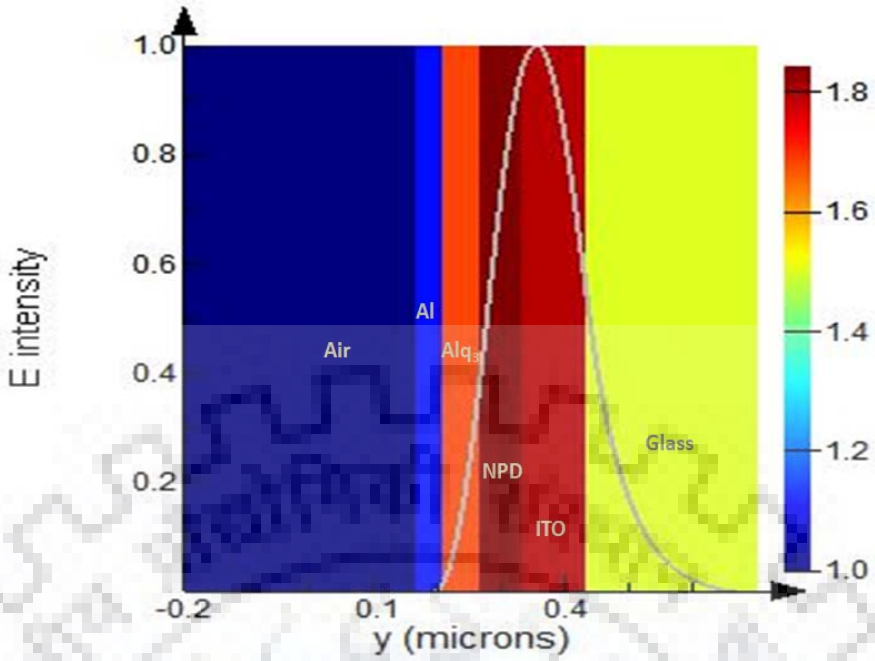

Figure 3.11 *Mode profile for the conventional OLED structure.*

3.3.1 Proposed Structure and Analysis

Fig. 3.1 shows the schematic for the conventional OLED considered in this study. A layer of dielectric nanoparticles has been placed at ITO in the proposed structure as shown in Fig. 3.12. We have considered the nanoparticles to be spherical in shape. As the dielectric material is optically lossless so there will not be any problem of absorption by nanoparticles. Mie theory and finite difference time domain (FDTD) method already discussed in chapter 2 have been used to analyze the effect of nanoparticles.

To find the enhancement in light extraction efficiency of proposed structure we have used FDTD method. The proposed OLED structure has been numerically analyzed by using the simulation software Lumerical FDTD solutions. Though 3D simulation provides more realistic results but to save simulation time, we carried out 2D FDTD simulation with transverse electric (TE) polarization. We have also carried out the 3D FDTD simulation for optimal solution obtained from 2D FDTD simulation. The parameters considered for the device like thicknesses of the layers of device, refractive index and extinction coefficients of materials are kept same as discussed in section 3.2.1. To extract the maximum light out of the device, diameter (d) and interparticle separation (s) of nanoparticles has been optimized. Refractive index (n_{np}) of dielectric

nanoparticles has been varied from 1.1 to 2.1. In 2D FDTD, the size of computational domain of 5 μm × 3 μm has been used.

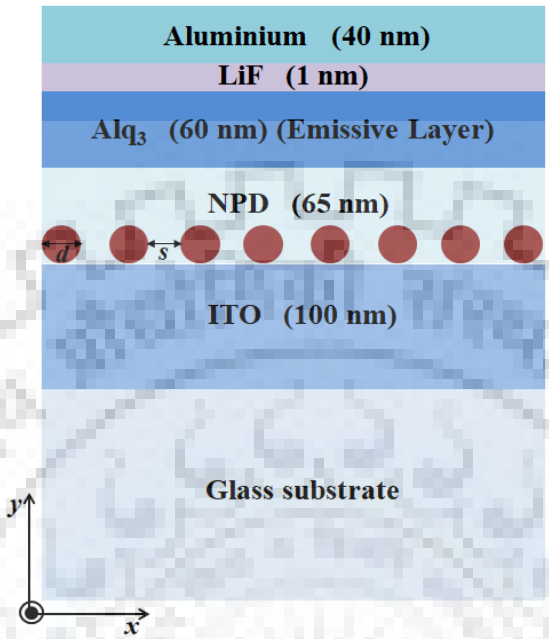

Figure 3.12 *Schematic design of proposed OLED with nanoparticles.*

A single dipole source placed at the centre of the emissive layer has been chosen for computation in this case also. The dipole source placed in the centre of emitting layer was surrounded by a monitor to estimate the total power generated in the layer. PML boundary conditions have been placed at all boundaries except at cathode side. 12 number of PML layers have been used in the simulation. The metallic boundary has been considered at the cathode side. To decide the convergence and to reduce the error in calculated fields and efficiency, the spatial grid size in FDTD is a very crucial aspect. The mesh size along x and y-direction has been chosen as 5 nm. We have verified that a grid size of 2 nm gives the same results. The time increment of 5.5×10^{-18}s has been considered. The span of the simulation region needs to be large enough such that there is enough propagation distance for the light to be fully extracted from the emission layer. The simulation time of 500 fs is used. Enhancement in the light extraction efficiency has been analyzed by calculating the far-field distribution of emissive dipole source. The far field intensity distribution has been recorded by placing the monitor in air above the glass substrate.

3.3.2 Results and Discussion

3.3.2.1 Scattering Efficiency of Nanoparticle

To check the suitability of dielectric nanoparticles for the enhanced performance of the OLED, their optical scattering properties have been studied using Mie theory. The dielectric nanoparticles have an added advantage of not absorbing the part of incident light and losing it in the form of heat as they do not have dissipative properties in the spectral range of OLED's operation. As the particles have positive dielectric constant over the visible range so they do not exhibit the dipolar plasmonic resonances.

(a) Effect of size of nanoparticles

Fig. 3.13 shows the calculated scattering efficiencies as a function of the wavelength of the isolated dielectric nanoparticle of refractive index (n_{np}) 1.32 with diameter varying from 20 nm to 60 nm embedded in the medium of NPD. The curve shows that the scattering efficiency increases as the nanoparticle size increases. This can be explained as the particle size increases, the higher modes get excited due to which the scattering efficiencies increase. The scattering efficiency is maximum for diameter of 60 nm. This depicts that larger size nanoparticles can be considered for extracting out the light from the device due to their greater tendency to scatter more light. The curve also shows that the scattering efficiency is highly dependent on wavelength. The scattering efficiency of the nanoparticles decreases as the incident wavelength increases.

(b) Effect of refractive index

The calculated scattering efficiency as a function of the wavelength of the dielectric nanoparticle of diameter (d) = 50 nm with refractive index (n_{np}) varying from 1.1 to 2.1 is shown in Fig. 3.14. The curve shows the maximum scattering efficiency for nanoparticle with n_{np} = 1.1. The scattering efficiency is small for nanoparticle with refractive indices 1.8 and 2.1. The refractive index of the medium (NPD) in which nanoparticle is embedded is not fixed but it is varying from 2.1 to 1.75 with wavelength. The scattering efficiency for nanoparticles with n_{np} = 1.8 and 2.1 is low owing to small index contrast with NPD in the entire wavelength range. This shows that the light scattered by nanoparticles strongly depends on the index contrast of the nanoparticles and embedded medium.

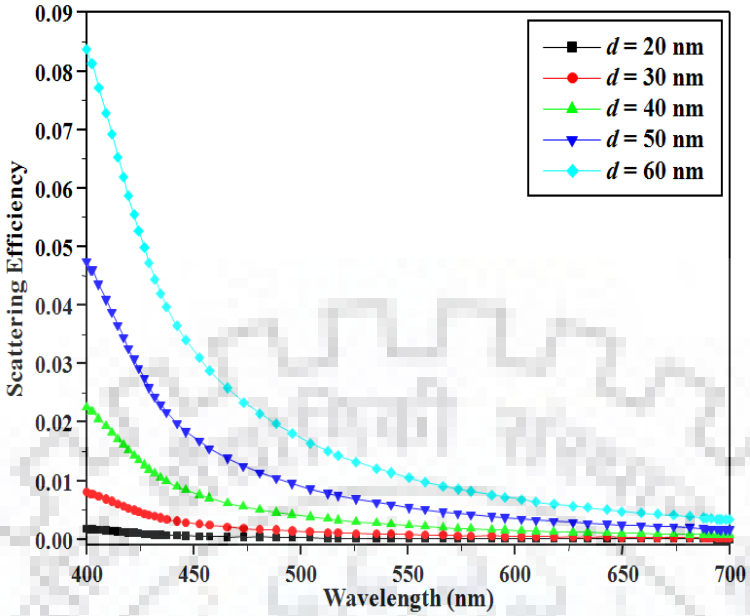

Figure 3.13 *Scattering Efficiency as a function of wavelength for different size of nanoparticles.*

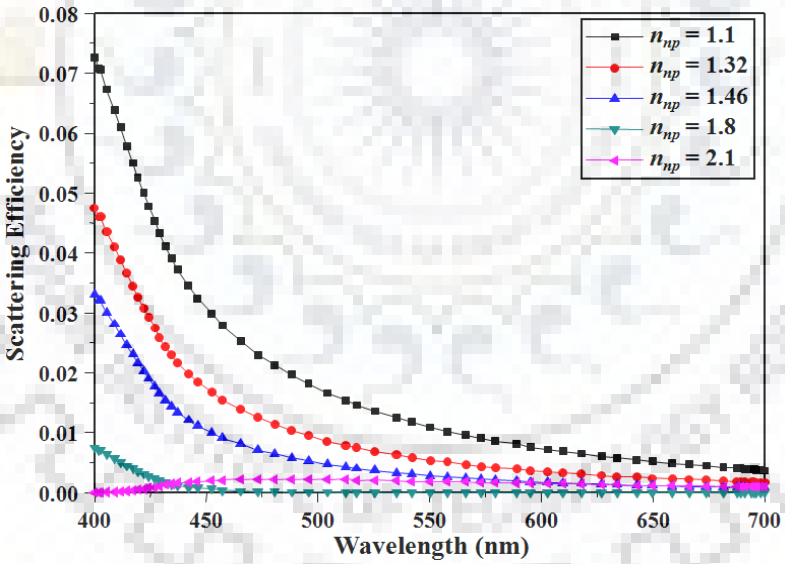

Figure 3.14 *Scattering Efficiency as a function of wavelength for different refractive indices of nanoparticles.*

3.3.2.2 Far Field Distribution Pattern

We have analyzed the entire OLED device with and without nanoparticles using Lumerical FDTD Solutions. The far field intensity distribution patterns proportional to $|E|^2$, where E is the electric field, for conventional OLED and OLED with nanoparticles

are shown in Fig. 3.15(a) and 3.15(b) respectively. The parameters of nanoparticles used for the intensity distribution pattern of Fig. 3.15(b) are as follows: d = 50 nm, s = 0 and n_{np} = 1.32. It can be clearly seen from the patterns that by inserting the layer of nanoparticles, more radiation is directed outside of the emissive layer of the device. This means that the addition of nanoparticles results in scattering, and hence, coupling-out of the emitted light from waveguide modes.

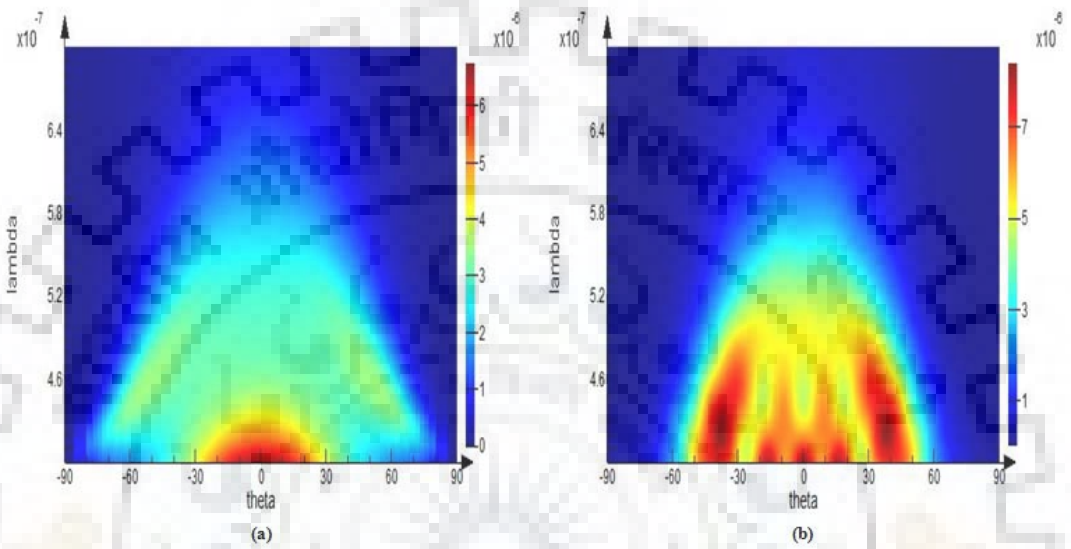

Figure 3.15 *Far field intensity distribution pattern for (a) conventional OLED (b) proposed OLED with nanoparticles.*

3.3.2.3 Enhancement in Light Extraction Efficiency

We have calculated the fraction of useful power emitted from the OLED device relative to the total power emitted from the emitting layer while determining the light extraction efficiency. In FDTD simulation, the monitor placed in air receive the light emitted from the conventional OLED and from the OLED having nanoparticles. The enhancement factor in light extraction has been obtained by the ratio of light extraction efficiencies of the OLED with nanoparticles and the conventional OLED. The light could not be fully extracted even with the use of dielectric nanoparticles because metals and organics absorb the light before it is coupled out of the device. Enhancement in the light extraction efficiency by dielectric nanoparticles is related to three factors: diameter (d), interparticle separation (s) and refractive index (n_{np}) of the nanoparticles. These parameters have been optimized to achieve the better light extraction from the OLED device.

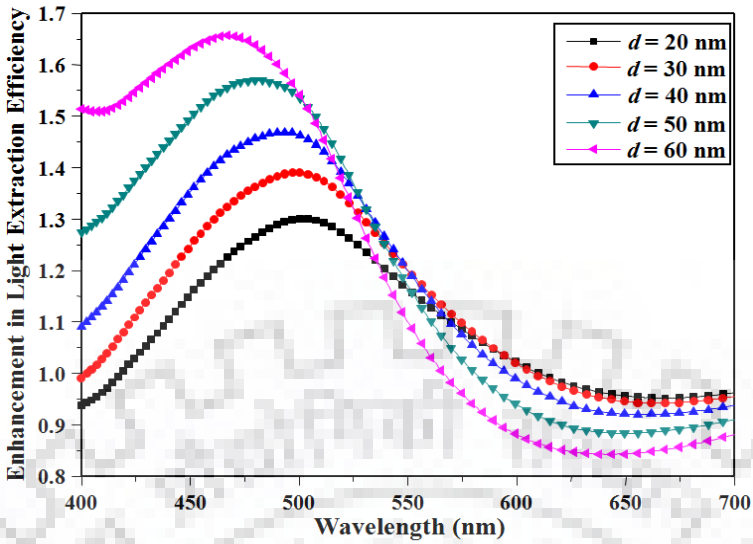

Figure 3.16 *Enhancement in light extraction efficiency as a function of wavelength for different size of nanoparticles.*

(a) Effect of size of nanoparticles

The diameter of nanoparticles plays an important role in scattering out the light from the device. The enhancement in light extraction efficiency as a function of wavelength has been calculated for different diameters of nanoparticles as shown in Fig. 3.16. The other parameters of nanoparticles like interparticle separation and refractive index were kept fixed at 0 nm (i.e. no spacing) and 1.32 respectively. The diameter (*d*) of particles has been varied from 20 nm to 60 nm. The plot shows that the enhancement in light extraction efficiency increases from 1.3 times to 1.65 times as the diameter of nanoparticles increases from 20 nm to 60 nm. This is because the larger size nanoparticles have the tendency to scatter more light as seen in Fig. 3.13. Light has to be extracted out of waveguided modes of ITO/organic interface. There is a wavelength shift of around 35 nm towards blue region as the diameter is increased from 20 nm to 60 nm. The enhancement can be seen in the wavelength range from approximately 400 nm to 550 nm. This means that the nanoparticles are able to enhance the light extraction efficiency in blue-green region only. As Alq_3 (emissive layer) emits the light in the green region. By doping the Alq_3 with small amount of DCM (4-(Dicyanomethylene)-2-methyl-6-(4-dimethylaminostyryl)-4H-pyran) dye we can shift the emission from green region to red region [11]. By setting the operating wavelength of OLED at any of these wavelengths, one can achieve the extraction efficiencies higher than that of the

conventional device. So, approximately 1.65 times enhancement can be seen with d = 60 nm around 470 nm wavelength.

(b) Effect of interparticle separation

Any alteration in the interparticle separation of nanoparticles also affects the scattering, which results in a change in extraction efficiency. To show this, we have studied the effect of interparticle separation of dielectric nanoparticles on the enhancement in light extraction efficiency as a function of wavelength and the results are shown in Fig. 3.17. The diameter and refractive index of the nanoparticles were fixed to 50 nm and 1.32 respectively. Interparticle separation (s) has been varied from 0 nm to 50 nm. The curve shows that as the interparticle separation increases from 0 nm to 50 nm, the enhancement in light extraction efficiency decreases from 1.57 times to 1.36 times. As the interparticle separation is increased from 0 nm to 10 nm, the shift of approximately 10 nm in wavelength is noticed. This curve also shows the enhancement in the wavelength range from 400 nm to 550 nm. The peak experiences a red shift and reduced strength with increase in interparticle separation. This signifies the diminishing of coupling effect between two spherical nanoparticles. These reductions in peak strength with interparticle spacing reflect the decay of field distribution between the particles. From the figure, we note that approximately 1.57 times enhancement is seen with no interparticle separation (i.e. s = 0 nm) around 480 nm wavelength.

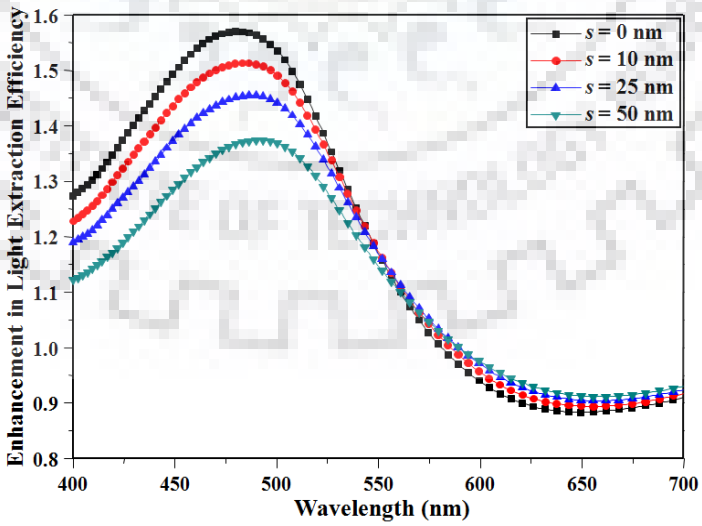

Figure 3.17 *Enhancement in light extraction efficiency as a function of wavelength for various interparticle separations of nanoparticles.*

(c) Effect of refractive index of nanoparticles

Next, we have studied the effect of refractive index of nanoparticles on enhancement in light extraction efficiency. To illustrate this, in Fig. 3.18 we have plotted the enhancement in light extraction efficiency as a function of the wavelength corresponding to different refractive index of nanoparticles. We have fixed the diameter of nanoparticles to 50 nm with no interparticle separation (s = 0 nm). It can be depicted from the curve that the enhancement in light extraction efficiency of almost 1.7 times is obtained with refractive index (n_{np}) of 1.1. The scattering of light by the nanoparticles strongly depends on index contrast. Here, the index contrast is between refractive index of dielectric nanoparticles and NPD (the embedded medium). The refractive index of NPD is not fixed but it is varying from 2.1 to 1.75 with wavelength. We have varied the refractive index of nanoparticles from 1.1 to 2.1. From the figure, we can infer that enhancement in light extraction efficiency decreases from 1.7 times to 1.2 times as n_{np} increases from 1.1 to 1.8. But no significant enhancement is seen with refractive index 2.1. This is because the index contrast is quite low for refractive index 2.1. There is a wavelength shift of approximately 20 nm towards red region as the refractive index of nanoparticles increased from 1.1 to 1.8. The dielectric nanoparticles show the enhancement in light extraction efficiency in the wavelength range 400 nm to 550 nm. So, one can use the refractive index of dielectric nanoparticles according to the choice of operating wavelength. The maximum enhancement of 1.7 times is obtained with nanoparticles of refractive index 1.1 around 475 nm wavelength. However, the incorporation of dielectric nanoparticles of refractive index 1.1 although help in increasing the optical efficiency of the device but at the cost of poor electrical efficiency particularly in the case of no interparticle separation. One should therefore, have to optimize the interparticle separation, refractive index and diameter of the particles, in order to improve overall efficiency. The dielectric materials that can be used for nanoparticles are as follows: mesoporous silica ($n_{np} \approx 1.1$), teflon ($n_{np} \approx 1.3$), silica ($n_{np} \approx 1.46$), aluminium oxide ($n_{np} \approx 1.8$) and zirconia ($n_{np} \approx 2.1$).

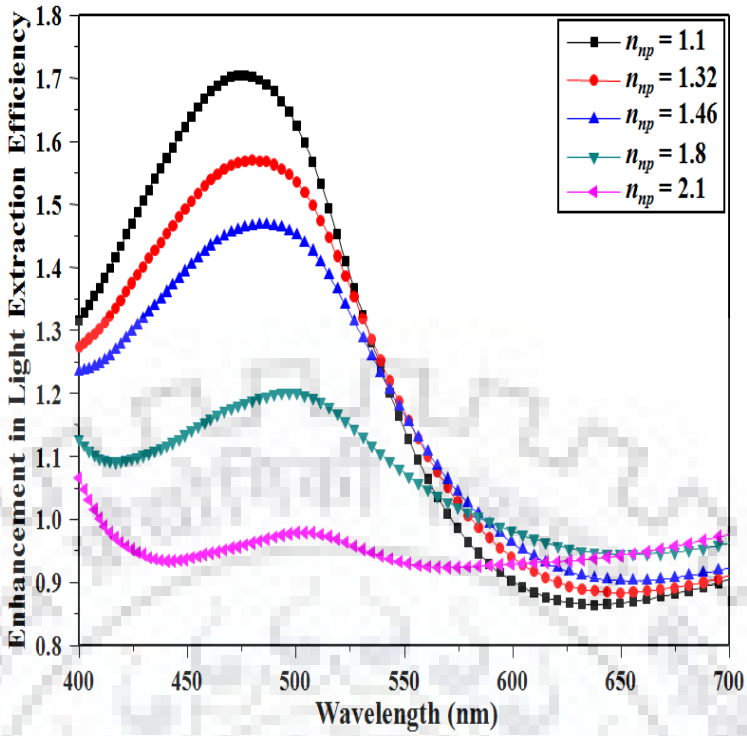

Figure 3.18 *Enhancement in light extraction efficiency as a function of wavelength for different refractive indices of nanoparticles.*

(d) Effect of assorted size nanoparticles

We have also investigated the effect of assorted diameters and interparticle spacings of spherical dielectric nanoparticles layer (deposited on ITO layer) on the enhancement of light extraction efficiency. We have varied the diameter from 30 nm to 50 nm and spacing from 10 nm to 30 nm in a random manner while keeping the refractive index of nanoparticles as 1.32. The plot of enhancement in light extraction efficiency as a function of wavelength is shown in Fig. 3.19. Fig. 3.16 shows that the enhancement in peak extraction efficiency increases from 1.3 times to 1.65 times as the diameter of nanoparticles increases from 20 nm to 60 nm and Fig. 3.17 shows that as the interparticle separation increases from 0 nm to 50 nm, the enhancement in peak extraction efficiency decreases from 1.57 times to 1.36 times. So, the accumulative effect of both diameter and interparticle spacing decreases the enhancement in peak efficiency of device to 1.41 times when assorted diameters and interparticle spacings of nanoparticles are added.

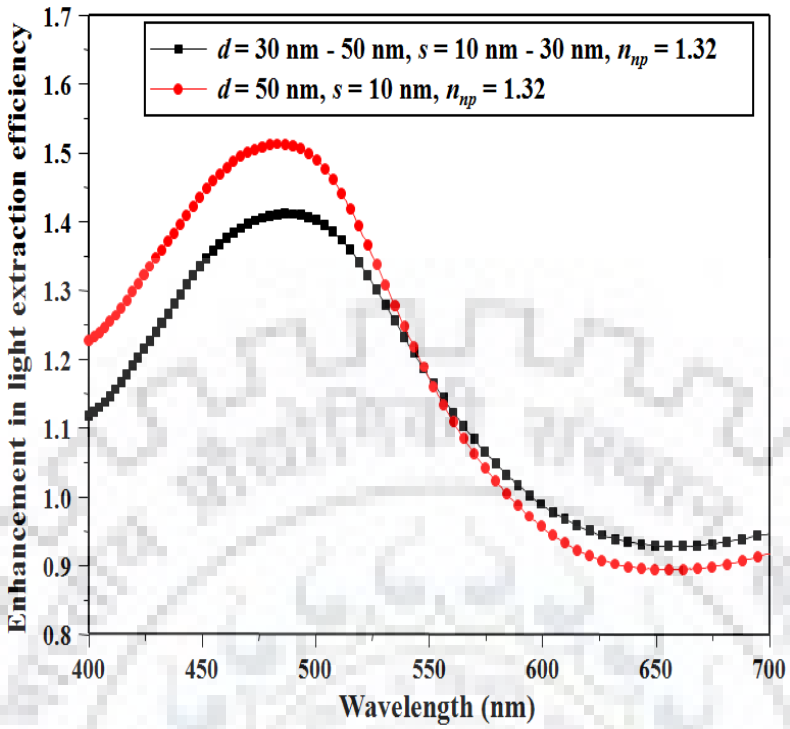

Figure 3.19 *Enhancement in light extraction efficiency as a function of wavelength for assorted diameters and interparticle separations of nanoparticles.*

3.3.2.4 Comparison between 2D and 3D simulations

One should in principle perform 3D simulation for more reliable results. However, 3D simulations are highly computationally extensive and time consuming. To verify this, we have also carried out 3D FDTD simulation of the proposed OLED structure for diameter (d) 50 nm, inter-particle spacing (s) 50 nm, refractive index (n_{np}) 1.32 and compared our results with 2D simulation. In 3D FDTD, the computational domain of 5 µm × 5 µm × 3 µm has been considered. All other parameters like simulation time and number of PML layers were kept same as those in 2D simulations. The enhancement in light extraction efficiency as a function of wavelength for 2D and 3D FDTD simulations are shown in Fig. 3.20. From the curve, we can see that the enhancement ratios of light extraction efficiency for both 2D and 3D simulations are not significantly different. The peak wavelength has shifted from 490 nm (2D) to 470 nm (3D). This confirms that 2D simulation can be used to examine the trend of the light extraction efficiency. So, to save computational efforts and time, we have limited ourselves to 2D simulations.

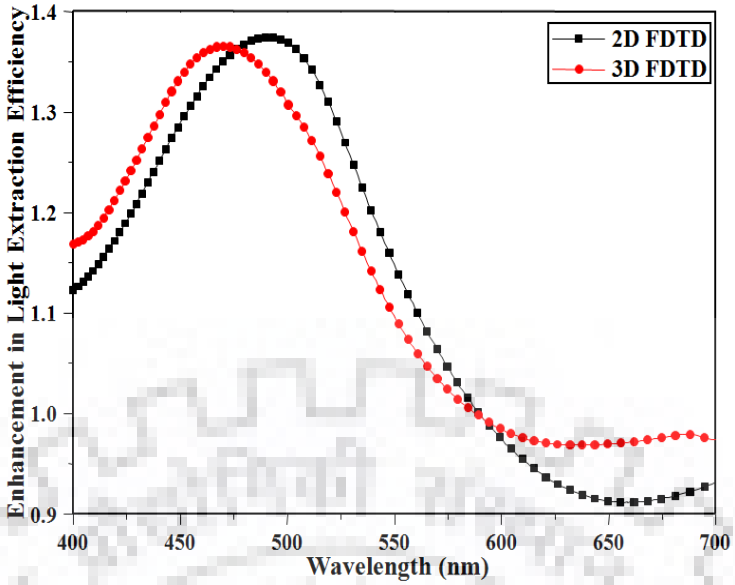

Figure 3.20 *Comparison of enhancement in light extraction efficiency for 2D and 3D FDTD simulation.*

The results clearly show that the trapped light in waveguide modes can be coupled out from the device using dielectric nanoparticles that act as a scattering medium.

3.4 Conclusions

In this chapter, we have presented two multilayer structures based on dielectric nanoparticles for the enhancement in light extraction efficiency of OLED. These nanoparticles help in extracting out the trapped light inside the device. In design 1, the dielectric nanoparticles layer is deposited at glass substrate. Effects of refractive index, diameter and interparticle separation of dielectric nanoparticles were investigated to obtain the maximum enhancement in light extraction efficiency. As a result, it was estimated that the light extraction efficiency of the dielectric nanoparticles OLED could be enhanced upto 1.7 times than that of conventional device for the nanoparticles refractive index 1.1, the diameter of 100 nm and no interparticle separation.

In design 2, the layer of dielectric nanoparticles was incorporated at anode. For this design, the light extraction efficiency of the device could be enhanced up to 1.7 times with nanoparticles of refractive index 1.1, diameter 50 nm, and no interparticle spacing. In this chapter, the results of enhancement in light extraction efficiency (LEE) are same for both cases. But the pattern of enhancement is quite different in both the cases. 1.7 times enhancement in LEE is obtained at around 490 nm wavelength in first case

whereas it is obtained at around 470 nm for second case. The difference between two patterns is due embedding medium. The ITO and NPD have different refractive index and extinction coefficient over the visible spectrum. So, the scattering by nanoparticles and absorption of light by embedding medium give rise to different patterns of both the structures.

From the results, we also found that 2D simulation could be used for saving computation time.

CHAPTER-4

Enhanced Absorption in Organic Solar Cells by use of Dielectric Nanoparticles *

4.1 Introduction

Organic solar cells (OSCs) have attracted great attention in the past few years because of their low-cost roll-to-roll manufacturing, suitability with flexible substrates and high absorption coefficient [154]. However, when compared with silicon based conventional solar cells, the power conversion efficiency of OSCs is still low. One of the factors which limit the efficiency of OSCs is the mismatch between the optical absorption length and exciton diffusion length. The absorption and exciton diffusion length are around 100 nm and less than 10 nm respectively in the commonly used active layer material poly(3-exylthiophene):(6,6)-phenyl-C61-butyric-acid-methyl ester (P3HT:PCBM) [155]. Many photons are left unharvested due to the thin active layer.

A part of this work has been presented in the following conference

V. Mann and V. Rastogi, "Role of Dielectric Nanoparticles in the enhancement of Organic Solar Cell Efficiency", *Fiber Optics and Photonics–PHOTONICS*, IIT Kanpur, Uttar Pradesh, India, December 5-8, 2016, OSA proceeding (Th4B.2).

By using new materials for the active layer, the efficiency is achieved up to 14% [156]. For the tandem structures, the efficiency is around 17% [157]. Another approach to increase the efficiency of OSCs is to use the light trapping techniques. These techniques help in improving the efficiency of the cell by enhancing the photon absorption in the active layer.

Various light trapping techniques have been numerically and experimentally reported to increase the light absorption in the active layer of the cell. These techniques include the use of photonic crystals [108-110], diffraction gratings [95-98], nanoparticles [99-104] in the different layers of the device. Numerous works have been reported on increasing the efficiency by the incorporation of metal nanoparticles such as Au [99], Ag [158] or semiconducting nanoparticles like CdSe, CdTe, PbSe and ZnO [159-162]. By incorporating Au nanoparticles in both hole transport layer and active layer, the PCE has been improved by 22% [99]. With the insertion of Ag nanoparticles in the active layer, the light absorption in the active layer could be enhanced by a factor of 1.56 [158]. S. H. Oh et al. reported that the efficiency of the OSC is increased by 23% by incorporating semiconducting ZnO nanoparticles in the active layer [162]. To avoid the absorption by metal nanoparticles, recent studies show that the efficiency can be enhanced by the incorporation of dielectric, metal core/shell and magnetic nanoparticles [163-166]. The reason for the enhanced efficiency after the insertion of nanoparticles is due to the enhancement in light absorption in the active layer by scattering property of nanoparticle. Approximately 13% enhancement in PCE can be seen by incorporating the SiO_2 dielectric nanoparticles in the active layer of OSCs [163]. P. Shao et al. reported that SiO_2 nanoparticles embedded in transport layer exhibits 17.5% increase in short circuit current density [164]. 25% enhancement in the light absorption is reported when the $Ag@SiO_2$ nanoparticles are incorporated on top of anode (ITO) [165]. Recent studies show 10% improvement in short circuit current density (J_{sc}) of the device by incorporating Fe doped tin oxide magnetic nanoparticles in the active layer [166]

In this chapter, we have proposed the design of organic solar cell based on dielectric nanoparticles and numerically demonstrate the enhancement in light absorption in the active layer and short circuit current density of the device. In the proposed design, we have incorporated the nanoparticles layer at glass substrate. The nanoparticles layer will

act as scattering medium and help to increase the optical path length of the device. Several parameters like diameter, interparticle spacing and materials of nanoparticles have been optimized in order to achieve the maximum enhancement in light absorption and optical efficiency of the organic solar cell.

4.2 Proposed Structure and Analysis

The conventional organic solar cell structure set as reference is presented in Fig. 4.1. The structure consists of a glass substrate, indium tin oxide (ITO) as an transparent anode, polymer poly(3,4-ethylenedioxythiophene) polystyrene sulfonate (PEDOT:PSS) with good thermal and chemical stability acting as a buffer layer, commonly used polymer poly(3-hexylthiophene):phenyl-C61-butyric acid methyl ester (P3HT:PCBM) with 1:1 weight ratio as an active layer, aluminium (Al) acting as a cathode. The proposed structure shown in Fig. 4.2 consists of a single layer of dielectric nanoparticles at glass substrate followed by ITO/PEDOT:PSS/P3HT:PCBM/Al layers. The nanoparticles have been considered to reduce the optical loss due to reflection at the glass/ITO interface. The dielectric material used for nanoparticles has been assumed to be loss-less at optical frequencies and therefore, there would not be any absorption of light by the nanoparticles themselves. We have considered spherical nanoparticles in our simulations.

The effect of nanoparticles on the optical performance of organic solar cell has been analyzed by using the Mie theory and FDTD method discussed in chapter 2. As there is no dissipation in the visible regime by dielectric nanoparticles, $Q_{abs} = 0$, so, Eq. (2.35) becomes

$$Q_{sca} = Q_{ext}$$

To calculate the enhancement in light absorption in active layer and improvement in optical efficiency of proposed structure of organic solar cell we have used FDTD method. FDTD is a powerful way of solving Maxwell's equations at every point in space [147] and is also very useful for the study of organic solar cell devices. The proposed OSC structure has been designed and simulated by using the Synopsys software RSoft's Full Wave and Solar Cell Utility [132]. Though three dimensional (3D) simulations provide more realistic results, the FDTD simulations being computationally extensive, we have carried out two dimensional (2D) FDTD simulations with transverse

electric (TE) polarizations to save time. For comparison purpose, 3D simulations have also been carried out only for the optimal parameters obtained from 2D simulations. The following parameters were chosen for the numerical simulations. Thicknesses of layers were set to be as: ITO (150 nm), PEDOT:PSS (60 nm), P3HT:PCBM (100 nm), Al (80 nm). Diameter (*d*) and interparticle separation (*s*) of nanoparticles were optimized for maximum enhancement in the light absorption in the active layer of the OSC. Refractive index and extinction coefficient of ITO, PEDOT:PSS and P3HT:PCBM were taken from literature [167] whereas refractive index of glass substrate was set to be 1.5. RSoft's material library has been used for data of Al material. Material properties of dielectric TiO_2 and SiC used for nanoparticles were taken from literature [168, 169].

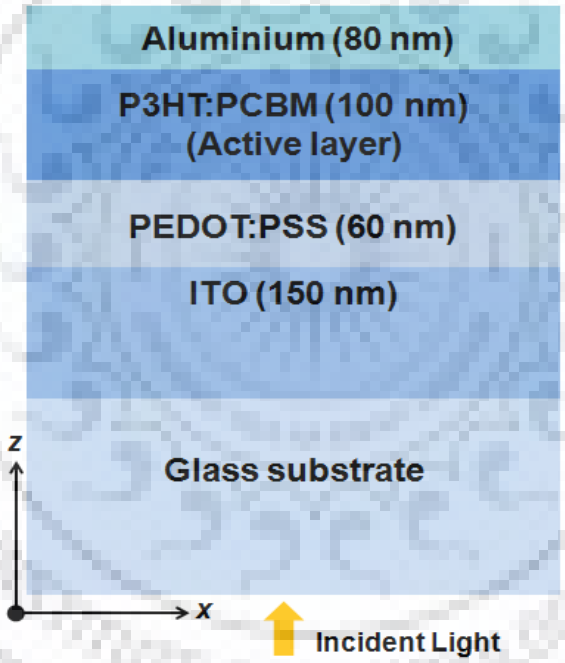

Figure 4.1 *Schematic design of conventional organic solar cell*

The solar cell was exposed to light where the incident light source has power density of $1kW/m^2$ in order to mimic direct sunlight. Light with electric field normal to the nanoparticles is normally incident from air into the solar cell (see Fig. 4.1), and it passes through all the layers of the device. The default parameters in the Solar Cell Utility match the AM 1.5 criteria. Some of the light gets absorbed in anode, active layer and cathode and rest of it is reflected away from the solar cell. In order to estimate the total light absorbed in active layer of the solar cell, the active layer was surrounded by a

monitor. Perfectly matched layer (PML) boundary conditions have been used at all boundaries [127]. The FDTD mesh size is an important simulation parameter as this decides the convergence of calculated fields. The grid sizes making up the mesh are set to 3 nm, which is smaller enough than the smallest diameter of nanoparticles in order to have the accurate results. We have considered time increment of 7.01×10^{-18}s. The span of the simulation region needs to be large enough so that the light can be propagated fully through the device. Full Wave as well as Solar cell utility, can only take the optical effects into account. The light absorption in the active layer has been studied by using FDTD based Full Wave. The J-V characteristics and optical efficiency of the device have been calculated by Solar Cell Utility. Computations have been performed using monochromatic excitations over the wavelength range 400 nm - 800 nm.

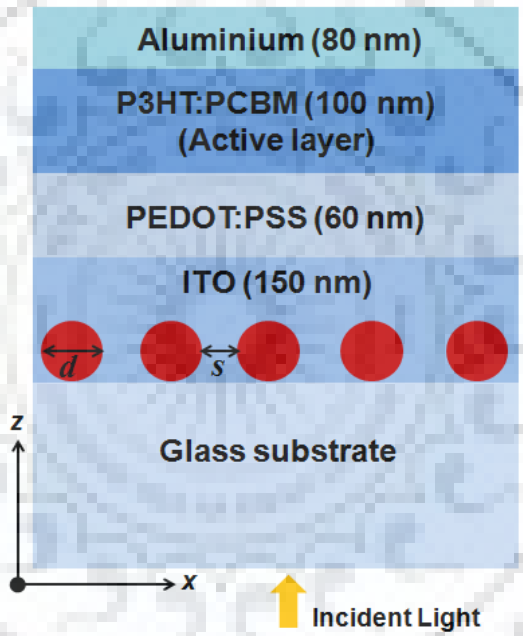

Figure 4.2 *Schematic design of proposed organic solar cell with nanoparticles*

4.3 Results and Discussion

4.3.1 Scattering Efficiency of Nanoparticle

In order to examine the suitability of dielectric nanoparticles for the enhanced performance of OSC, we have studied their optical scattering properties. The dielectric nanoparticles have positive dielectric constant over visible range so they do not exhibit the dipolar plasmonic resonances. Also, the dielectric nanoparticles have an added advantage of not absorbing a part of incident energy and losing it in the form of joule

heating as they do not have dissipative properties in the spectral range of operation of OSC. Improvement in the light absorption of the OSC in such a structure is primarily based on the scattering of solar light by the nanoparticles; we have first studied the effect of size and material of the nanoparticle on scattering efficiency by using the Mie theory. To carry this out, we have considered a single nanoparticle in ITO surrounding. Such a study helps in efficient optimization of size and material of nanoparticles while considering them in the complete structure as shown in Fig. 4.2. So, the results presented in Figs. 4.3 and 4.4 are based on Mie theory while all the other results have been produced by the FDTD method.

(a) Effect of size of nanoparticle

Fig. 4.3 shows the calculated scattering efficiencies of isolated TiO_2 dielectric nanoparticle with diameter in range from 50 nm – 100 nm embedded in ITO. We have considered material dispersion of ITO in the simulation. It can be seen from the curve that scattering efficiency increases from d = 50 nm to d =100 nm. This means larger nanoparticles are generally more desirable for absorbing light in the active layer of the device due to their greater ability to scatter more light.

(b) Effect of refractive index

Fig. 4.4 shows the scattering efficiencies of dielectric nanoparticle (diameter = 75 nm) with TiO_2 and SiC materials. SiC nanoparticle shows higher scattering than that obtained by using the TiO_2 nanoparticle because the refractive index of SiC is higher than that of TiO_2. This shows that the scattering of light by nanoparticles strongly depends on the refractive index contrast between the embedding medium and the nanoparticle material.

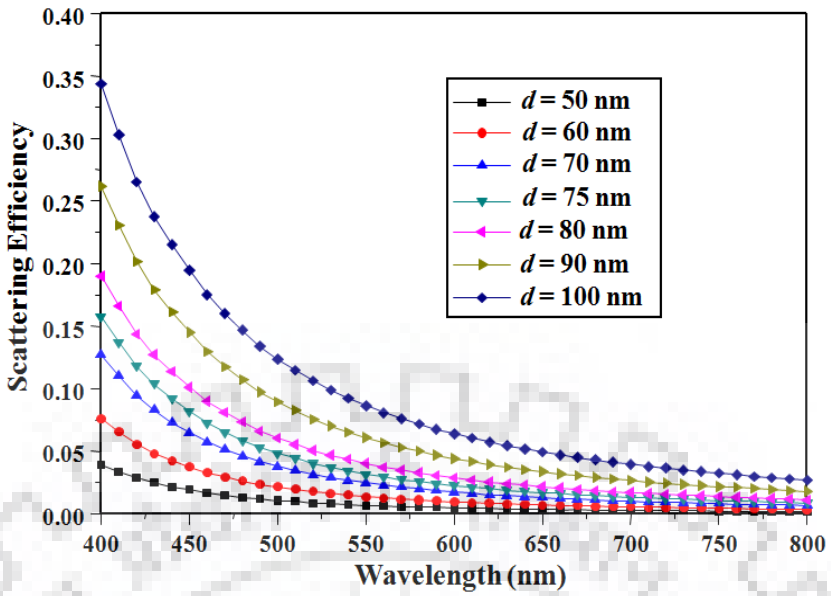

Figure 4.3 *Scattering efficiency as a function of wavelength for different diameters of nanoparticles*

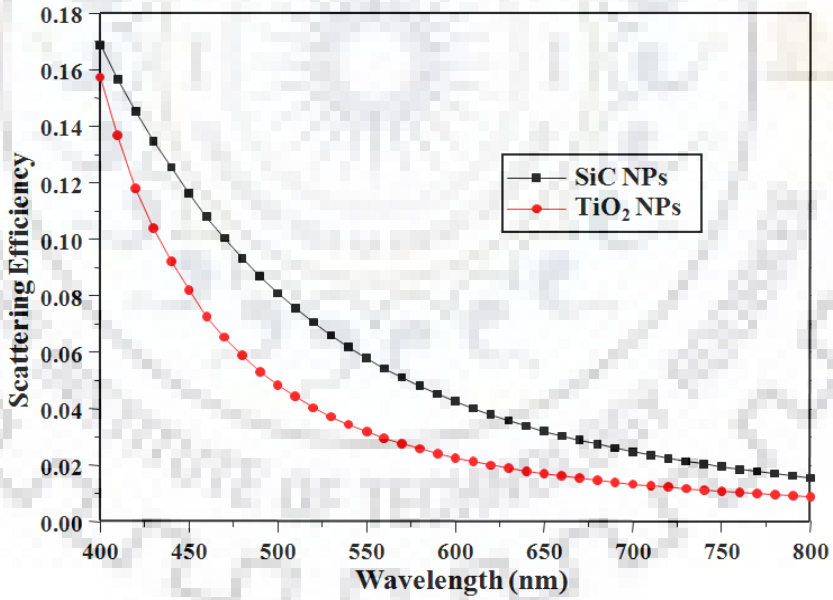

Figure 4.4 *Scattering efficiency as a function of wavelength for different materials of nanoparticles*

4.3.2 Electric field distribution pattern

Fig. 4.5 shows the electric field component of the incident light for the conventional OSC and OSC with nanoparticles for SiC and TiO_2 at wavelength 500 nm. We have considered the diameter 75 nm and interparticle spacing 30 nm for SiC and TiO_2 nanoparticles. From the figure, we can see that the surrounding field dissipates as the light strikes the nanoparticles. This means that the addition of nanoparticles in the solar cell design shows scattering effect and hence incident light gets absorbed in the active layer.

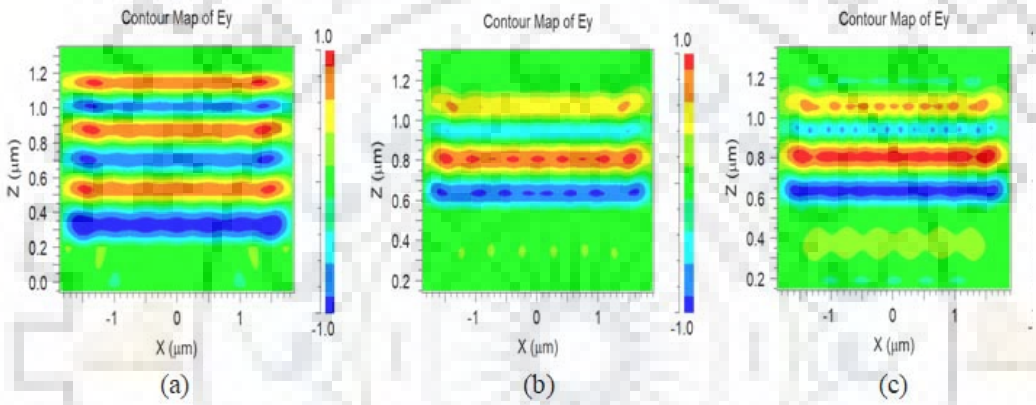

Figure 4.5 *Contour plot of spatial variation of electric field (a) without nanoparticles (b) TiO_2 nanoparticles (c) SiC nanoparticles.*

4.3.3 Enhancement in Light Absorption and Short circuit current density

We have studied organic solar cell with nanoparticles and without nanoparticles. The absorption spectrum in the active layer of the device can be obtained directly with Full Wave utility. Even with the use of dielectric nanoparticles, the light could not be completely absorbed because of the reflection that takes place at different interfaces. The effect of several parameters like diameter (*d*), interparticle separation (*s*) and refractive index of nanoparticles were investigated to achieve the maximum enhancement in light absorption in the active layer of the solar cell.

(a) Effect of size of nanoparticles

Diameter of nanoparticles plays an important role in scattering the light. To find the effect of diameters on incident light absorption, we have plotted the light absorption in the active layer with wavelength and AM 1.5G solar spectrum for TE and TM polarizations as shown in Fig. 4.6 (a) and 4.6 (c). Fig. 4.6 (b) and 4.6 (d) show the J-V characteristics of the organic solar cell for TE and TM polarizations, respectively. All the figures have been plotted for TiO_2 nanoparticles with interparticle separation 0 nm (i.e. no spacing). The diameter has been varied from 50 nm to 100 nm. As we can see from the Figs. 4.6 (a) and 4.6 (c) the light absorption in the active layer increases from d = 50 nm to 75 nm but it starts decreasing after d = 75 nm. This shows that for the larger size of nanoparticles, light absorption decreases as the number of scatterers become smaller in a given region. There is an increase of light absorption in the active layer of the device by 15% for d = 50 nm, 18.9% for d = 75 nm and 17.1% for d = 100 nm for TE polarization. For TM polarization, the absorption in the active layer increases by 14.5% for d = 50 nm, 18.5% for d = 75 nm and 16.7% for d = 100 nm. Also, Fig. 4.6 (b) shows that the short circuit current density (J_{sc}) increases from d = 50 nm to d = 75 nm and decreases after d = 75 nm. The J_{sc} increases by 14.7% for d = 50 nm and 16.8% for d = 100 nm. Fig. 4.6 (d) shows that for TM polarization the J_{sc} increases by 14.4% for d = 50 nm and 16.7% for d = 100 nm. So, in case of TE polarization, the incorporation of TiO_2 nanoparticles in the organic solar cell increases light absorption by 19% and the current density by 18.9% whereas for TM polarization the light absorption increases by 18.7% and the current density by 18.5% for d = 75 nm and no interparticle spacing.

The enhancement in light absorption shown in Fig. 4.6 (c) is primarily dominated by the absorption spectrum of P3HT:PCBM. The slight variation in the spectrum due to insertion of nanoparticles is due to the periodic structure formed by an array of nanoparticles which gives maximum scattering at a particular wavelength. Hence, any variation in size and interparticle spacing of nanoparticles will change the resonance wavelength.

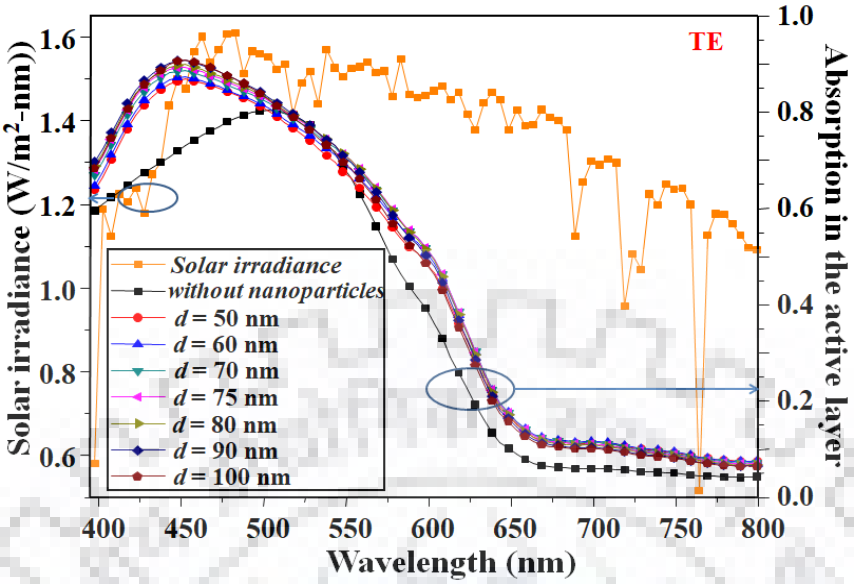
TE
Solar irradiance
without nanoparticles
d = 50 nm
d = 60 nm
d = 70 nm
d = 75 nm
d = 80 nm
d = 90 nm
d = 100 nm
Solar irradiance (W/m²-nm))
Absorption in the active layer
Wavelength (nm)
1.6
1.4
1.2
1.0
0.8
0.6
1.0
0.8
0.6
0.4
0.2
0.0
400
450
500
550
600
650
700
750
800

(a)

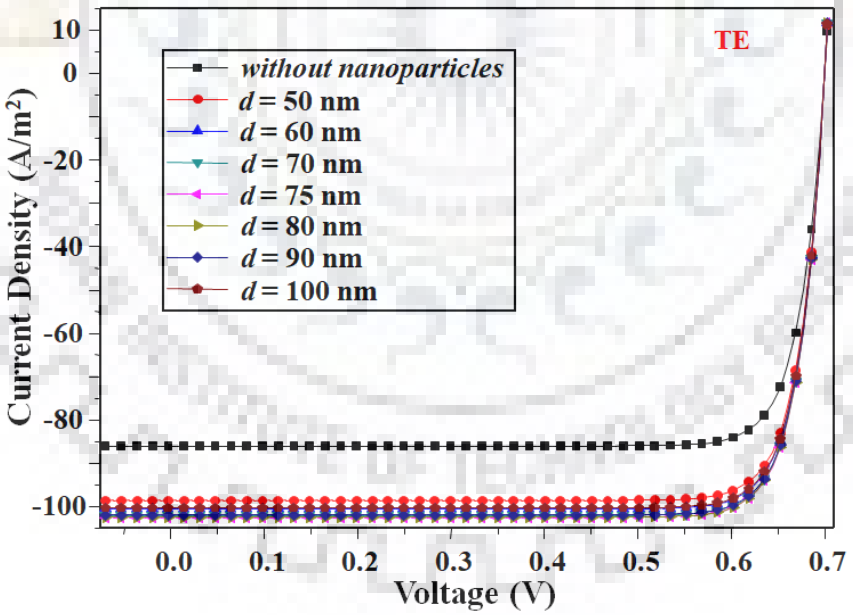
TE
without nanoparticles
d = 50 nm
d = 60 nm
d = 70 nm
d = 75 nm
d = 80 nm
d = 90 nm
d = 100 nm
Current Density (A/m²)
Voltage (V)
10
0
-20
-40
-60
-80
-100
0.0
0.1
0.2
0.3
0.4
0.5
0.6
0.7

(b)

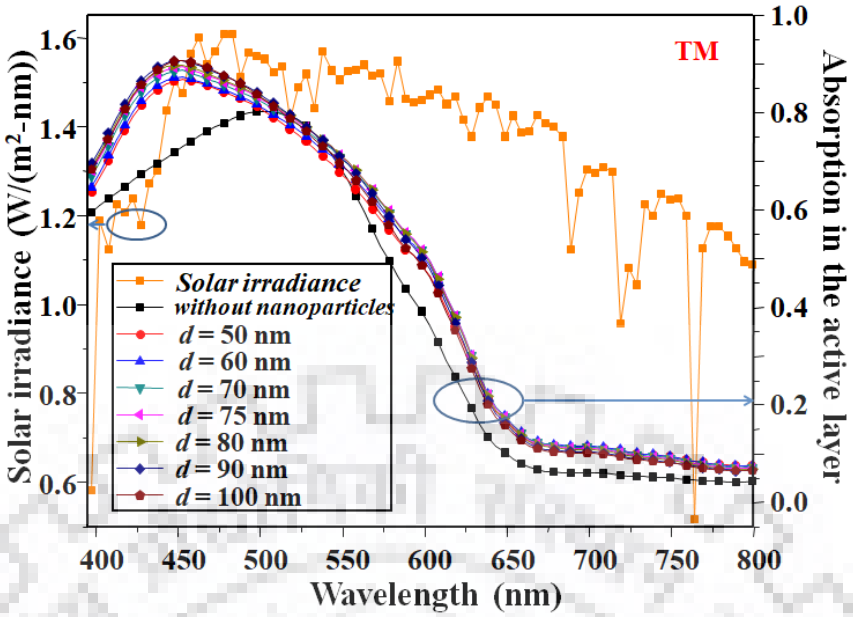

(c)

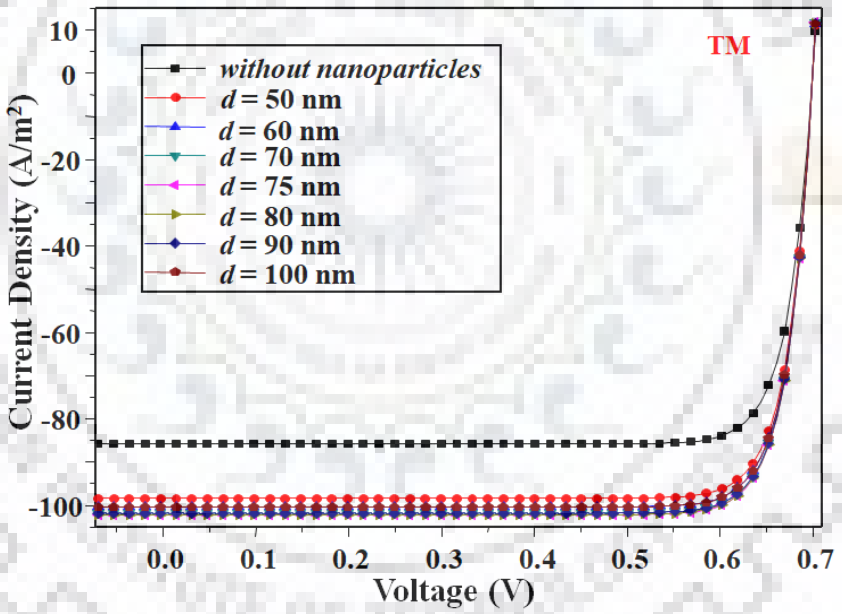

(d)

Figure 4.6 *(a) Absorption in the active layer as a function of wavelength for TE polarization (b) J-V characteristics of the cell for different diameters of nanoparticles for TE polarization (c) Absorption in the active layer as a function of wavelength for TM polarization (d) J-V characteristics of the cell for different diameters of nanoparticles for TM polarization*

(b) Effect of interparticle separation

Any change in the interparticle separation of nanoparticles also affects the absorption of incident light in the active layer of the device. To show this, the effect of interparticle separation of dielectric nanoparticles on the light absorption in the active layer with wavelength for TE and TM polarizations has been investigated and the results are shown in Fig. 4.7 (a) and 4.7 (c). We have considered the TiO_2 nanoparticles with diameter 75 nm. Interparticle separation has been varied from 0 nm to 100 nm. The curve shows that the enhancement in light absorption decreases as the interparticle separation increases. For TE polarization, the enhancement decreases from 19% to 13% whereas for TM polarization, the enhancement decreases from 18.7% to 10% as spacing *(s)* increases from 0 nm to 100 nm. Fig. 4.7 (b) and 4.7 (d) show the J-V characteristics of the cell for various interparticle separations for TE and TM polarizations. As seen from the Figs. 4.7 (b) and 4.7 (d), the current density decreases from 18.9% to 14.8% as the interparticle separation increases from 0 nm to 100 nm for TE polarization and it decreases from 18.5% to 10.5% as the interparticle separation increases from 0 nm to 100 nm. This shows that as the interparticle separation increases, the electric field enhancement becomes smaller. This is due to the decoupling between neighboring dielectric nanoparticles. From the figure, we note that maximum enhancement of 19% in light absorption and 18.9% in the short circuit current density of the cell could be achieved with no interparticle separation (i.e. s = 0 nm) for TE polarization. For TM polarization the enhancement in light absorption increases by 18.7% and the current density by 18.5% for particles with no interparticle spacing.

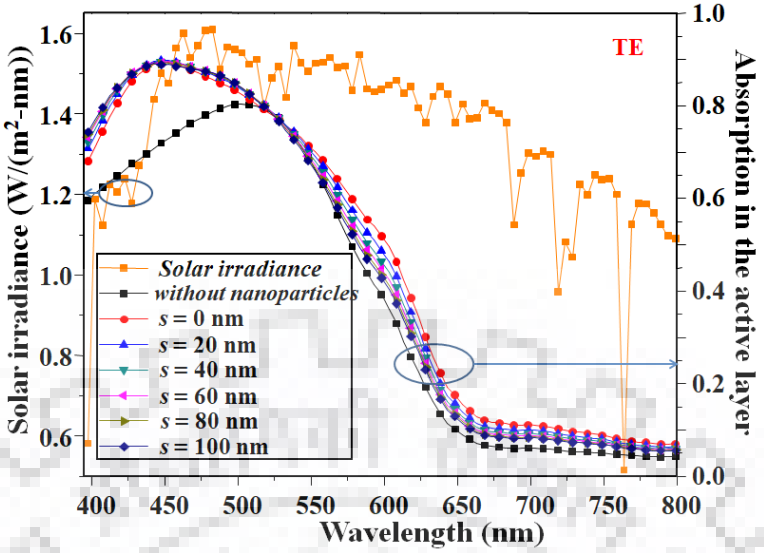
TE
Solar irradiance
without nanoparticles
s = 0 nm
s = 20 nm
s = 40 nm
s = 60 nm
s = 80 nm
s = 100 nm
Solar irradiance (W/(m²-nm))
Absorption in the active layer
Wavelength (nm)

(a)

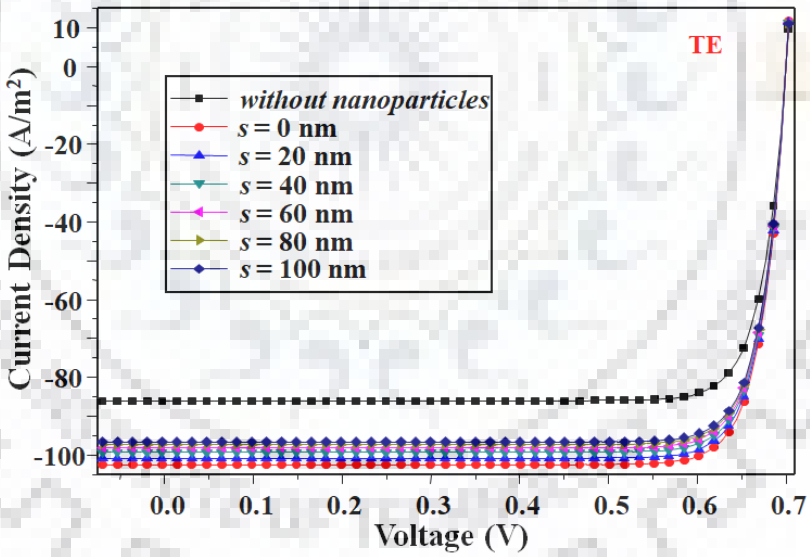
TE
without nanoparticles
s = 0 nm
s = 20 nm
s = 40 nm
s = 60 nm
s = 80 nm
s = 100 nm
Current Density (A/m²)
Voltage (V)

(b)

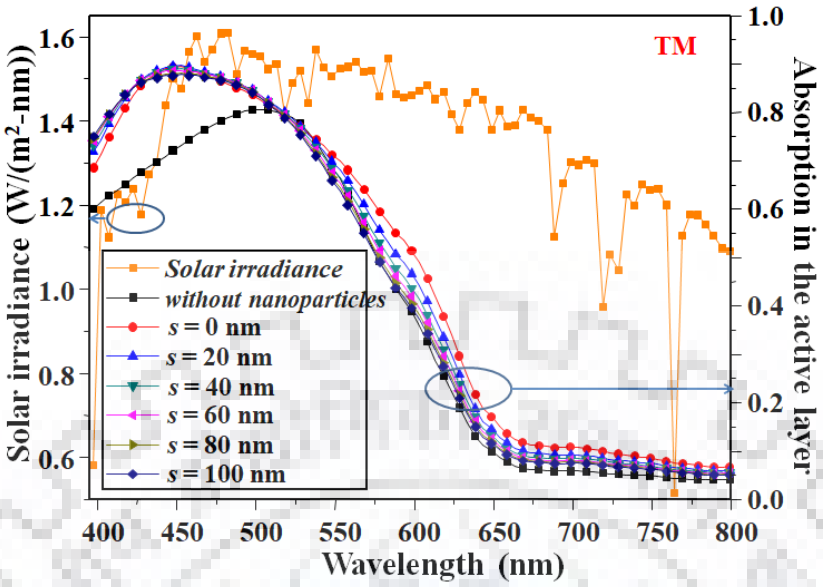

(c)

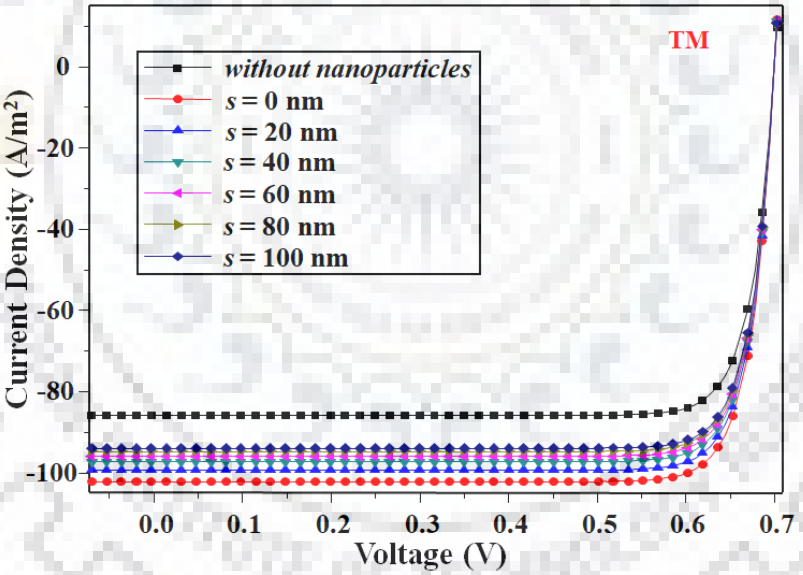

(d)

Figure 4.7 *(a) Absorption in the active layer as a function of wavelength for TE polarization (b) J-V characteristics of the cell for different interparticle separations for TE polarization (c) Absorption in the active layer as a function of wavelength for TM polarization (c) J-V characteristics of the cell for different interparticle separations for TM polarization.*

(c) Effect of material of nanoparticles

Next, we have studied the effect of material of nanoparticles on absorption of incident light and J-V characteristics of the cell. To illustrate this, we have plotted the light absorption in the active layer with wavelength for TE and TM polarizations as shown in Figs. 4.8 (a) and 4.8 (c). Figs. 4.8 (b) and 4.8 (d) show the J-V characteristics of the cell corresponding to different materials of nanoparticles for TE and TM polarization. TiO_2 and SiC nanoparticles have been considered in our study. Diameter of nanoparticles was fixed to 75 nm with no interparticle separation (s = 0 nm). Figs. 4.8 (a) and 4.8 (c) shows that the increment in light absorption in the active layer is more for SiC than TiO_2. The refractive index of SiC is higher than that of TiO_2 so SiC nanoparticles scatter more light. This shows that the scattering of light by the nanoparticles strongly depends on the refractive index contrast between the material of nanoparticles and ITO. The light absorption in the active layer increases by 19% with TiO_2 nanoparticles and by 20.4% with SiC nanoparticles for TE polarization. For TM polarization, with TiO_2 nanoparticles the light absorption in the active layer increases by 18.7% and with SiC nanoparticles by 20.1%. Fig. 4.8 (b) shows that the presence of TiO_2 nanoparticles increases the J_{sc} by 18.9% and SiC nanoparticles increase it by 19.8%. Fig. 4.8 (d) shows that the presence of TiO_2 nanoparticles increases the J_{sc} by 18.5% and SiC nanoparticles increase it by 19.6%.

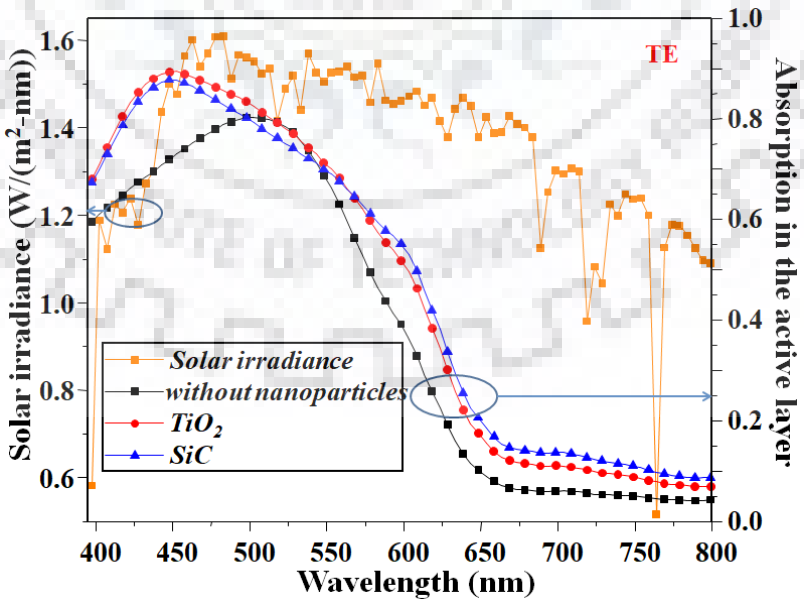

(a)

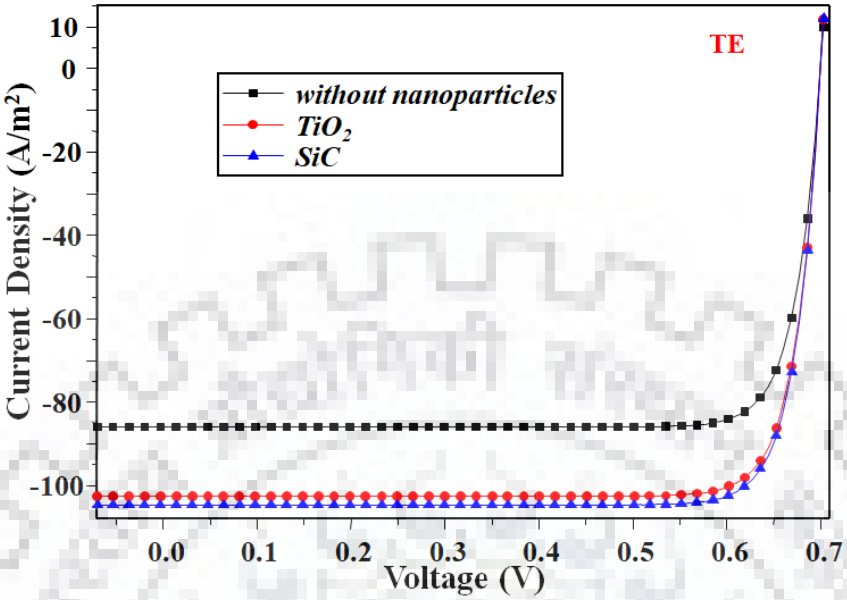
TE
without nanoparticles
TiO2
SiC
Current Density (A/m2)
Voltage (V)
10
0
-20
-40
-60
-80
-100
0.0
0.1
0.2
0.3
0.4
0.5
0.6
0.7

(b)

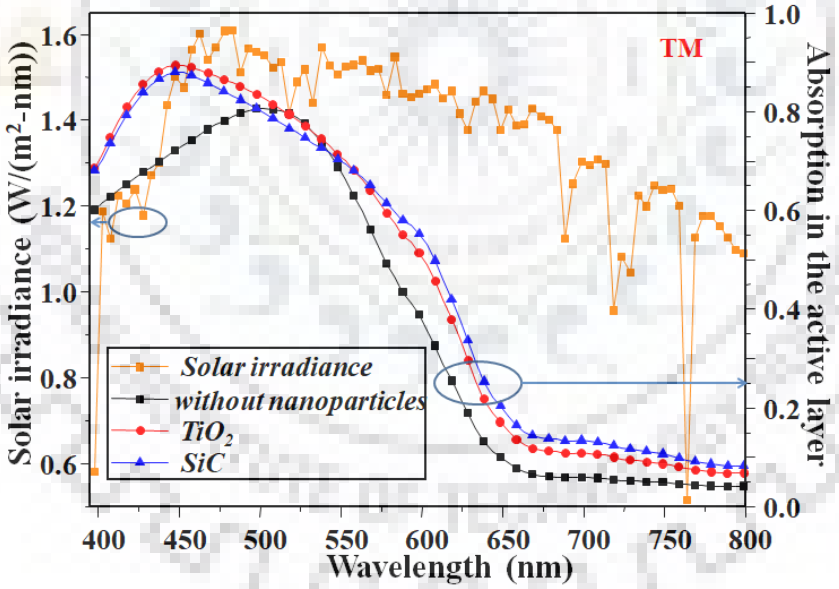
TM
Solar irradiance
without nanoparticles
TiO2
SiC
Solar irradiance (W/(m2-nm))
Absorption in the active layer
Wavelength (nm)
1.6
1.4
1.2
1.0
0.8
0.6
1.0
0.8
0.6
0.4
0.2
0.0
400
450
500
550
600
650
700
750
800

(c)

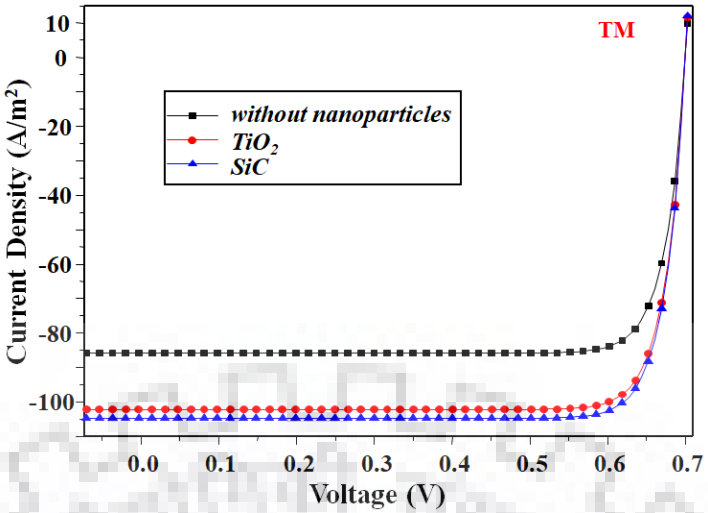

(d)

Figure 4.8 *(a) Absorption in the active layer as a function of wavelength for TE polarization (b) J-V characteristics of the cell for different materials of nanoparticles for TE polarization (c) Absorption in the active layer as a function of wavelength for TM polarization (d) J-V characteristics of the cell for different material of nanoparticles for TM polarization*

(d) Effect of assorted size and interparticle spacing

In a fabricated device, the size and the separation between the nanoparticles may vary randomly. To take this into account, we have also investigated the effect of assorted diameter dielectric nanoparticles layer (deposited on glass substrate) on the light absorption in the active layer and current density of the device for TE polarization. We have varied the diameter from 70 nm to 90 nm and interparticle separation from 10 nm to 30 nm in a random manner for TiO_2 and SiC nanoparticles. The plots of light absorption in the active layer as a function of wavelength and J-V characteristics of the cell are shown in Figs. 4.9 (a) and 4.9 (b). The accumulative effect of both diameter and interparticle separation decreases the short circuit current density of the device to 18.7% for SiC nanoparticles and 17% for TiO_2 nanoparticles when assorted diameters and interparticle separations of nanoparticles are added.

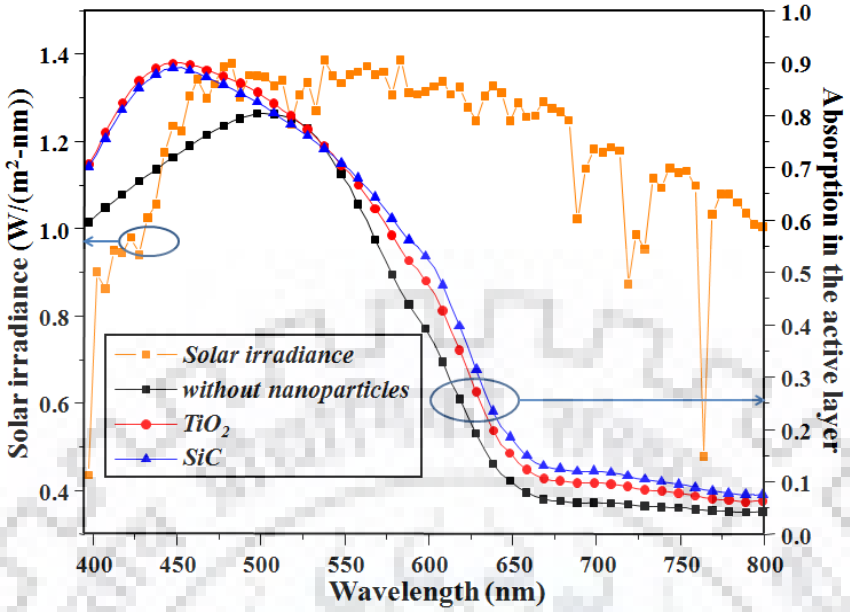

Figure 4.9 *(a) Absorption in the active layer as a function of wavelength for TE polarization (b) J-V characteristics of the cell for assorted size and interparticle separations of nanoparticles for TE polarization*

4.3.4 Comparison between 2D and 3D simulations

One should in principle perform 3D simulations for more reliable results. However, 3D simulations are computationally heavy and are time consuming. Also, for simulations related to nanoparticles, researchers have shown that 2D model gives similar results as those obtained from 3D model [170]. To verify this, we have also carried out 3D FDTD simulation of the proposed structure for TiO_2 nanoparticles with d = 80 nm, s = 20 nm for TE polarization and compared our results with 2D simulation. Figs. 4.10 (a) and 4.10 (b) show the plot of light absorption in the active layer with wavelength and J-V characteristics of the organic solar cell for 2D and 3D FDTD simulation. From the curve, we can see that the light absorptions in the active layer for both 2D and 3D simulations are not significantly different. In 2D simulation, the obtained improvement in short circuit current density is 17.5% while it is 16.7% using 3D simulations. This confirms that 2D simulation can be used to examine the trend of the light absorption in the active layer and short circuit current density of the device. So, we have limited ourselves to 2D simulations to save computational time and memory.

4.3.5 Comparison between TE and TM polarizations

We have also carried out the studies for both TE and TM polarizations for 2D and 3D geometries. The comparison of results is shown in Figs. 4.11 (a), 4.11 (b) and 4.11 (c). We have considered the SiC material with diameter 80 nm and spacing 20 nm for the simulations. The results of Fig. 4.11 (a) and Fig. 4.11 (b) show that when we consider TE and TM polarizations individually then the short circuit current density for 2D and 3D simulations are not significantly different. We have also compared the results of TE and TM polarization for 3D simulation as shown in Fig. 4.11 (c). The figure shows that the there is polarization dependence. The improvement in current density is larger for TE polarization in comparison to TM polarization.

The results clearly show that incorporation of nanoparticles will lead to scattering owing to the Mie Scattering theory and thereby increases the optical absorption in the active layer and hence the optical efficiency of organic solar cell.

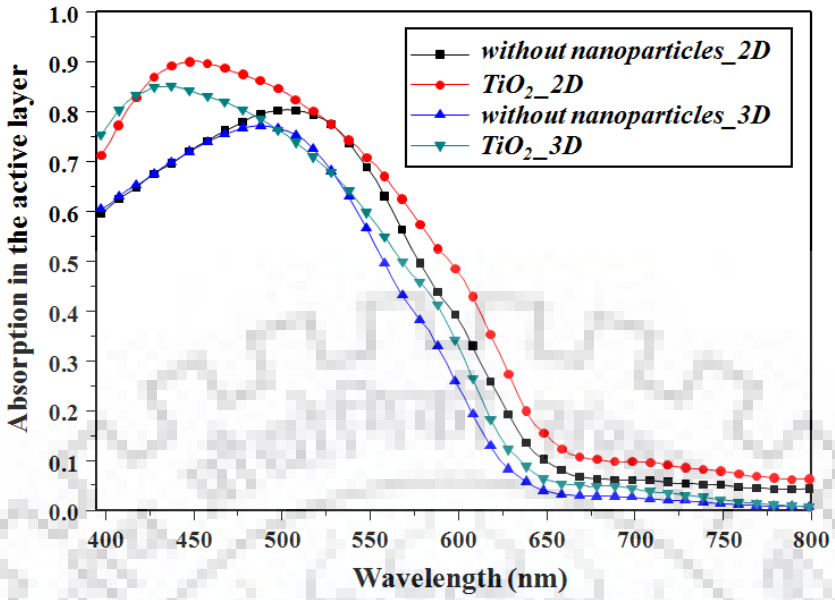

(a)

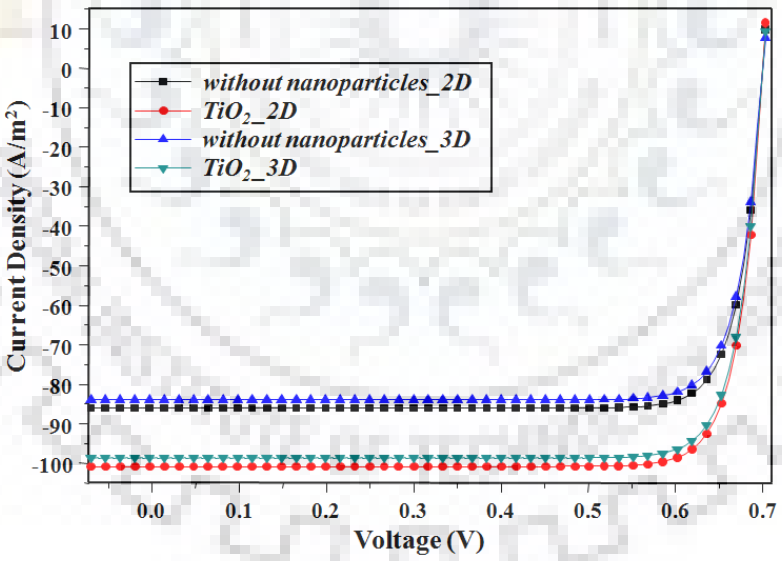

(b)

Figure 4.10 *Comparison of (a) absorption in the active layer as a function of wavelength for TE polarization (b) J-V characteristics of the cell for 2D and 3D FDTD simulation for TE polarization*

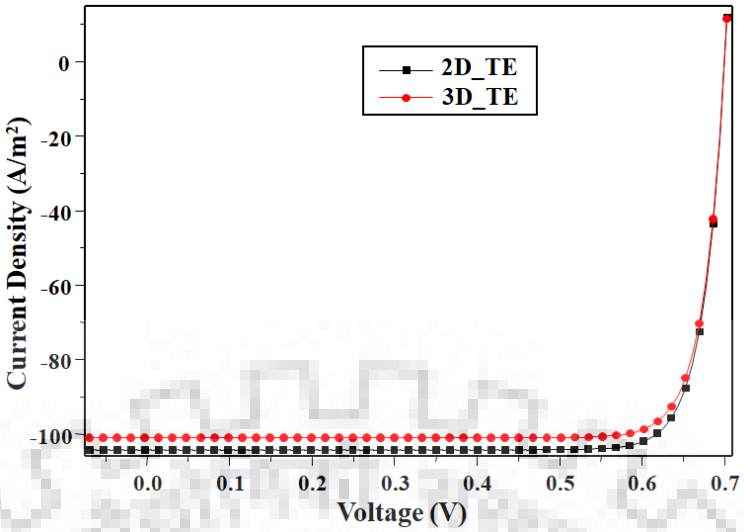

(a)

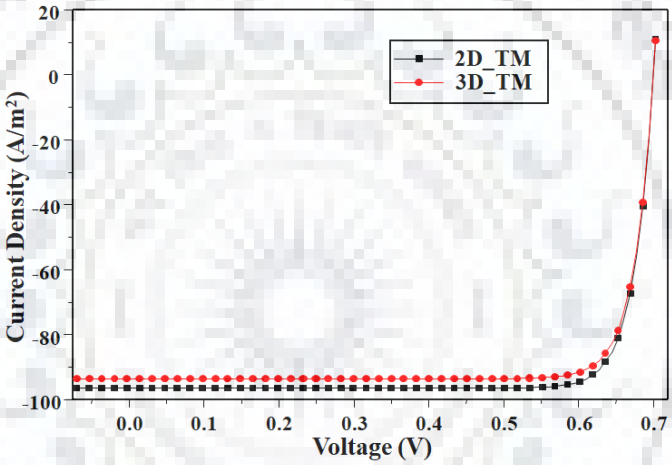

(b)

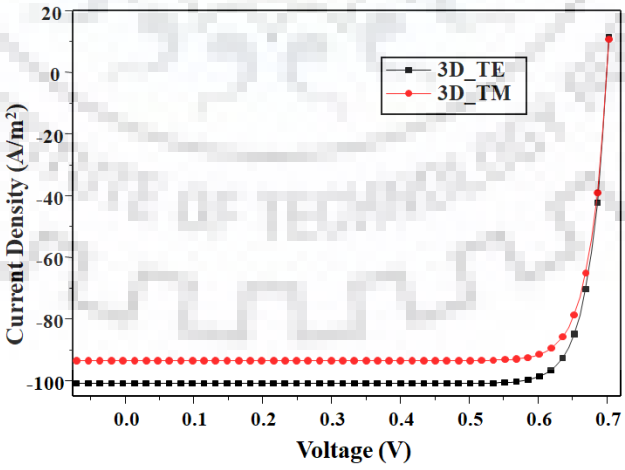

Figure 4.11 *J-V characteristics of the cell for 2D and 3D simulation for (a) TE polarization (b) TM polarization (c) Comparison of J-V characteristics of the cell for 3D simulation for TE and TM polarizations*

4.4 Conclusions

In this chapter, we have proposed the multilayer structure based on dielectric nanoparticles for the enhancement of light absorption in the active layer and short circuit current density of the organic solar cell. These nanoparticles will help in scattering the incident light. In proposed design, the dielectric nanoparticles layer has been incorporated at glass substrate. Effects of material, diameter and interparticle separation of dielectric nanoparticles were examined in order to obtain the maximum enhancement in light absorption. Improvement in the light absorption by 19% by considering TiO_2 nanoparticles and by 20.4% with SiC nanoparticles can be obtained. It has also been shown that the current density and hence the optical efficiency of proposed OSC can be improved by 18.5% by using TiO_2 nanoparticles and by 19.8% by using SiC nanoparticles.

CHAPTER-5

Use of Dielectric Grating for Improving Absorption in Organic Solar Cells *

5.1 Introduction

In the last chapter, we have proposed to incorporate the layer of nanoparticles at the glass substrate to trap the incident light and to study the enhancement in light absorption in the active layer of the OSC device. Use of diffraction gratings is another technique to trap the light by coupling the incident light to diffraction orders of grating propagating outside the escape cone in the active layer of the device. The diffraction grating splits up or diffract the incoming solar light into discrete and multiple beams.

Initially the work on gratings was numerically carried out by Sheng et al. for amorphous silicon solar cells [176]. Most of the work has also been performed for organic solar cells using metallic gratings [177-180]. C. Min et al. showed that optical absorption can

---

* A part of this work has been presented in the following conference

V. Mann and V. Rastogi "Increasing the efficiency of organic solar cell using dielectric grating" Progress in Electromagnetic Research Symposium (PIERS), Nanyang Technological University, Singapore, November 19-22, 2017.

be enhanced up to 50% by inserting periodic metallic grating in top transparent electrode [177]. P. T. Dang found that the short circuit current density increases up to 47 % through the placement of metallic grating in hole transport layer [178]. Increment in optical absorption by 21 % is seen when the active layer is partially filled with metallic grating (back contact grating) [179]. Dielectric grating can also be used for the enhancement of the light absorption in the solar cell. Improvement in the absorption by 23.4% is observed by inserting dielectric grating between electrolyte and dye sensitized titania layer [181]. Shen has theoretically studied the use of multiple gratings in a solar cell [182].

In this chapter, we have proposed to incorporate the periodic dielectric diffraction grating at glass-ITO interface. Diffraction techniques describe the mechanism of changing the direction of the incident light into different directions and hence can increase the optical absorption in the cell. Several parameters like duty cycle, aspect ratio, period and height of the grating have been optimized in order to achieve the maximum enhancement in light absorption in the active layer and optical efficiency of the organic solar cell.

5.2 Proposed Structure and Analysis

A schematic of the organic solar cell structure set as reference is presented in Fig. 5.1. The device structure consists of glass/ITO/PEDOT:PSS/P3HT:PCBM/Al. The transparent anode which provides electrical contact to cell is made by indium tin oxide (ITO) of 150 nm thickness and is deposited on 60 nm thick polymer poly(3,4-ethylenedioxythiophene) polystyrene sulfonate (PEDOT:PSS) with good chemical and thermal stability used for hole transportation. The electron donor poly(3-hexylthiophene) (P3HT) and the electron acceptor phenyl-C61-butyric acid methyl ester (PCBM) with 1:1 weight ratio and thickness 100 nm is commonly used active layer. The active layer is in contact with the cathode made up of aluminium (Al). Al is used as a cathode because of its matching work functions. A transparent glass substrate has been used to provide the mechanical support to these thin layers. Refractive index and extinction coefficient of ITO, PEDOT:PSS and P3HT:PCBM were taken from literature [167] whereas refractive index of glass substrate was set to be 1.5. RSoft's material

library has been used for data of Al material. Material properties of dielectric TiO_2 for grating were taken from literature [168].

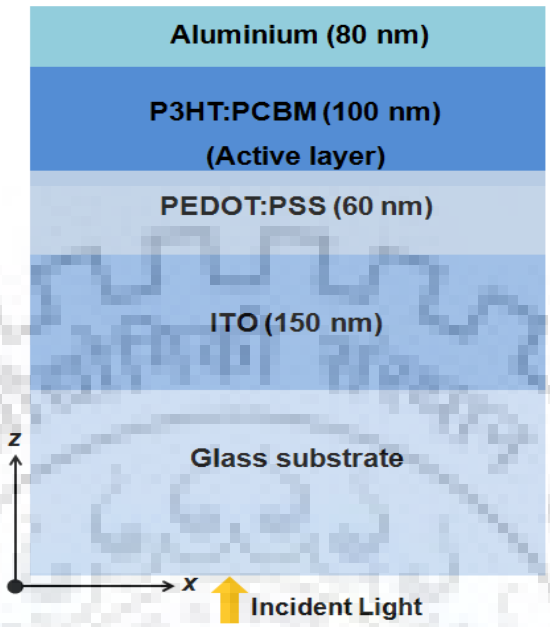

Figure 5.1 *Schematic of conventional organic solar cell*

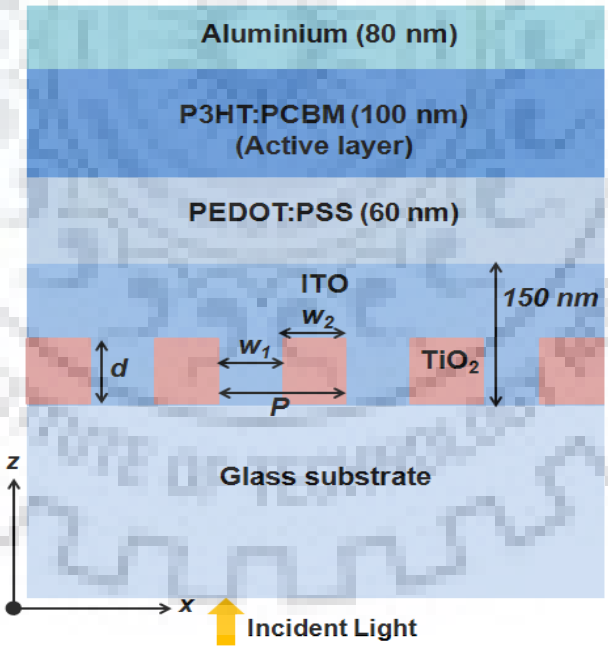

(b)

Figure 5.2 *Pictorial representation of OSC with periodic grating*

In the proposed structure, a periodic diffraction grating is inserted at the glass-ITO interface as shown in Fig. 5.2. Titanium dioxide (TiO_2) material has been used for the grating structure. We have considered the rectangular grating in our simulations.

We have employed the FDTD method to calculate the enhancement in light absorption in active layer and improvement in optical efficiency of proposed structure of organic solar cell [132]. Though three dimensional (3D) simulations provide more realistic results, the FDTD simulations being computationally extensive, we have carried out two dimensional (2D) FDTD simulations with transverse electric (TE) polarizations to save time. For comparison purpose, 3D simulations have also been carried out only for the optimal parameters obtained from 2D simulations. The grating period *P*, the grating height *d* and the width of the TiO_2 portion of grating w_2 were optimized for maximum enhancement in the light absorption in the active layer of the OSC.

The solar cell was exposed to light where the incident light source has power density of $1kW/m^2$ in order to mimic direct sunlight. Light with electric field normal to the grating is normally incident from air into the solar cell (see Fig. 5.1), and it passes through all the layers of the device. The default parameters in the Solar Cell Utility match the standard AM 1.5 solar spectrum criteria. Some of the light gets absorbed in anode, active layer and cathode and rest of it is reflected away from the solar cell. In order to estimate the total light absorbed in active layer of the solar cell, the active layer was surrounded by a monitor. Perfectly matched layer (PML) boundary conditions have been used along the z-axis (z_{min} and z_{max}). Periodic boundary conditions have been used along the x-axis (x_{min} and x_{max}). . The FDTD mesh size is an important simulation parameter as this decides the convergence of calculated fields. The grid sizes making up the mesh are set to 5 nm in order to have the accurate results. The time increment of 7.01×10^{-18}s has been considered. The span of the simulation needs to be large enough so that the light can be propagated fully through the device. Computations have been performed using monochromatic excitations over the wavelength range 300 nm - 800 nm. This wavelength range is the region of interest for the active layer material (i.e. P3HT:PCBM) and it covers most of the solar radiation spectrum.

5.3 Results and Discussion

5.3.1 Enhancement in Light Absorption and Short circuit current density

We have studied organic solar cell with diffraction grating and without grating for comparison purpose. Even with the use of dielectric grating, the light could not be completely absorbed because of the reflections that take place at different interfaces.

The effect of several parameters like grating period *P*, the grating height *d* and the width of the TiO_2 portion of grating w_2 were investigated to achieve the maximum enhancement in light absorption in the active layer of the solar cell. For the grating height *d* and periodicity *P*, the enhancement factor can be defined as

$$\frac{\sum_{\lambda} A_{grating}(\lambda, d, P) - \sum_{\lambda} A_0(\lambda)}{\sum_{\lambda} A_0(\lambda)}$$

where $A_{grating}$ and A_0 are the absorption in the active layer with grating and without grating as a function of wavelength.

(a) Effect of grating height (d)

Here, we have fixed the period of the grating as 800 nm. The duty cycle defined as the ratio of width of the grating to the period of the grating (i.e. w_2/P) is also varied by varying the width of the grating. We have varied the grating height from 40 nm to 120 nm for the duty cycle of 0.875 by considering w_2 to be 700 nm.

Fig. 5.3(a) shows the curve of optical absorption in the active layer with wavelength and 5.3(b) shows the J-V characteristics of the cell for different grating height *d*. It can be seen from the figure that the absorption increases as the *d* increases from 40 nm to 80 nm but it decreases for 100 nm. For 120 nm height no increment is seen. The enhancement in light absorption is primarily dominated by the absorption spectrum of P3HT:PCBM. The slight variation in the spectrum due to insertion of grating is due to the periodic structure of the grating which gives maximum scattering at a particular wavelength. Hence, any variation in the grating height will slightly change the resonance wavelength. The absorption increases by 15.5%, 24.2% and 14.5% respectively corresponding to grating height d = 40 nm, 80 nm and 100 nm. Also, Fig. 5 (b) shows that the short circuit current density (J_{sc}) increases from d = 40 nm to d = 80 nm and decreases for values of *d* higher than 80 nm. The J_{sc} increases by 14.9%, 20.5% and 13.3% for d = 40 nm, 80 nm and 100 nm, respectively.

So, from the above plot it can be noted that the absorption does not always increase as the depth increases. Larger depth does not mean the larger enhancement in absorption; it implies that there is an optimal groove height in the specified geometry of the grating. For very small grating heights the diffraction efficiency will be less whereas large

grating height comparable to the thickness of ITO film would lead to segmentation of the region. Here, the enhancement in light absorption and short circuit current density is largest for height 80 nm and period 800 nm. No enhancement can be seen with grating height 120 nm.

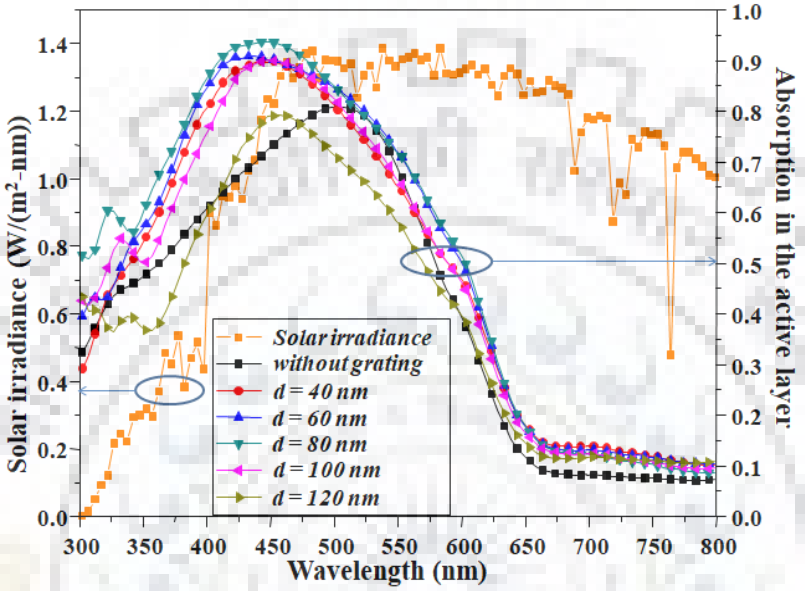

(a)

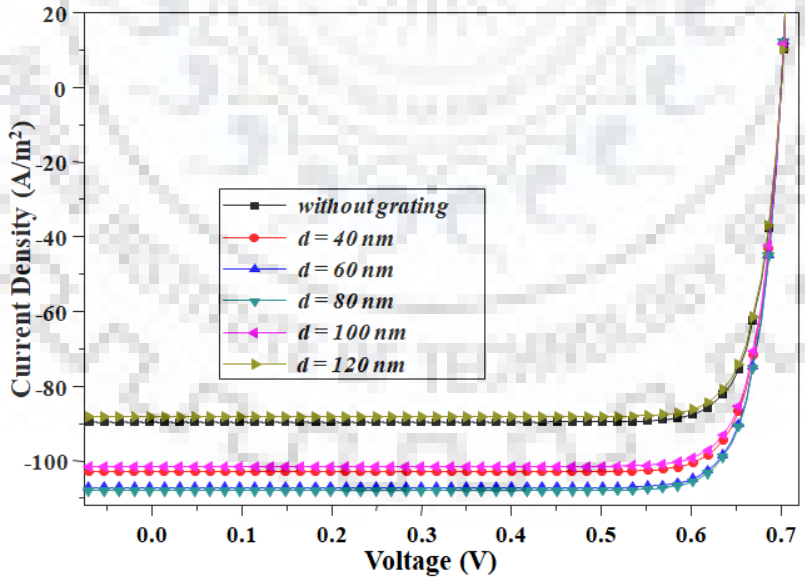

(b)

Figure 5.3 *(a) Absorption in the active layer as a function of wavelength (b) J-V characteristics of the cell for different heights of the grating*

(b) Effect of width or duty cycle of the grating (w_2)

To study the effect of the width of the grating we have fixed the period of the grating to 800 nm and d = 80 nm. As the w_2 is varied then duty cycle is also varied. The duty cycle has been varied from 0.875 to 0.375 i.e. w_2 is varied from 700 nm to 300 nm. The spectral absorption of light in the active layer is shown in Fig. 5.4 (a) and Fig. 5.4 (b) shows the J-V characteristics of the device. The plots show that the absorption and short circuit current density decreases as the duty cycle decreases. The absorption in the active layer are enhanced by 24.2%, 24.1%, 22.4%, 20.2% and 18.1% respectively corresponding to duty cycle of 0.875, 0.75, 0.625, 0.5 and 0.375. This shows that wider the width of the grating, larger the enhancement in light absorption in the active layer. Also the large amount of absorption increment is seen in the wavelength range of 300 nm to 500 nm. The short circuit current density increases from 11% to 20.5% for duty cycle from 0.375 to 0.875.

(c) Effect of grating period (P)

To study the effect of the period of the grating we have fixed the fill factor to 0.75 and d = 80 nm. If the duty cycle is kept constant it means both the width and period of the grating has been varied. For considerable diffraction of the incident light, grating period should be comparable to the wavelength of light. So, there is variation in the period of the grating from 600 nm to 1400 nm with a gap of 200 nm. Accordingly the width has been varied. The plots of absorption in the active layer and J-V characteristics for different period of the grating are shown in Fig. 5.5(a) and 5.5(b). It can be observed that for different periods, there is not much difference in the enhancement in the light absorption. All the curves have a peak at 450 nm. The absorption increases by 23%, 24.2%, 23.6%, 23.1% and 22.4% respectively for periods of 600 nm, 800 nm, 1000 nm, 1200 nm and 1400 nm. Also, the J_{sc} enhanced by 18.3%, 18.6%, 18.4%, 18.1% and 17.7% for the different periods of the grating.

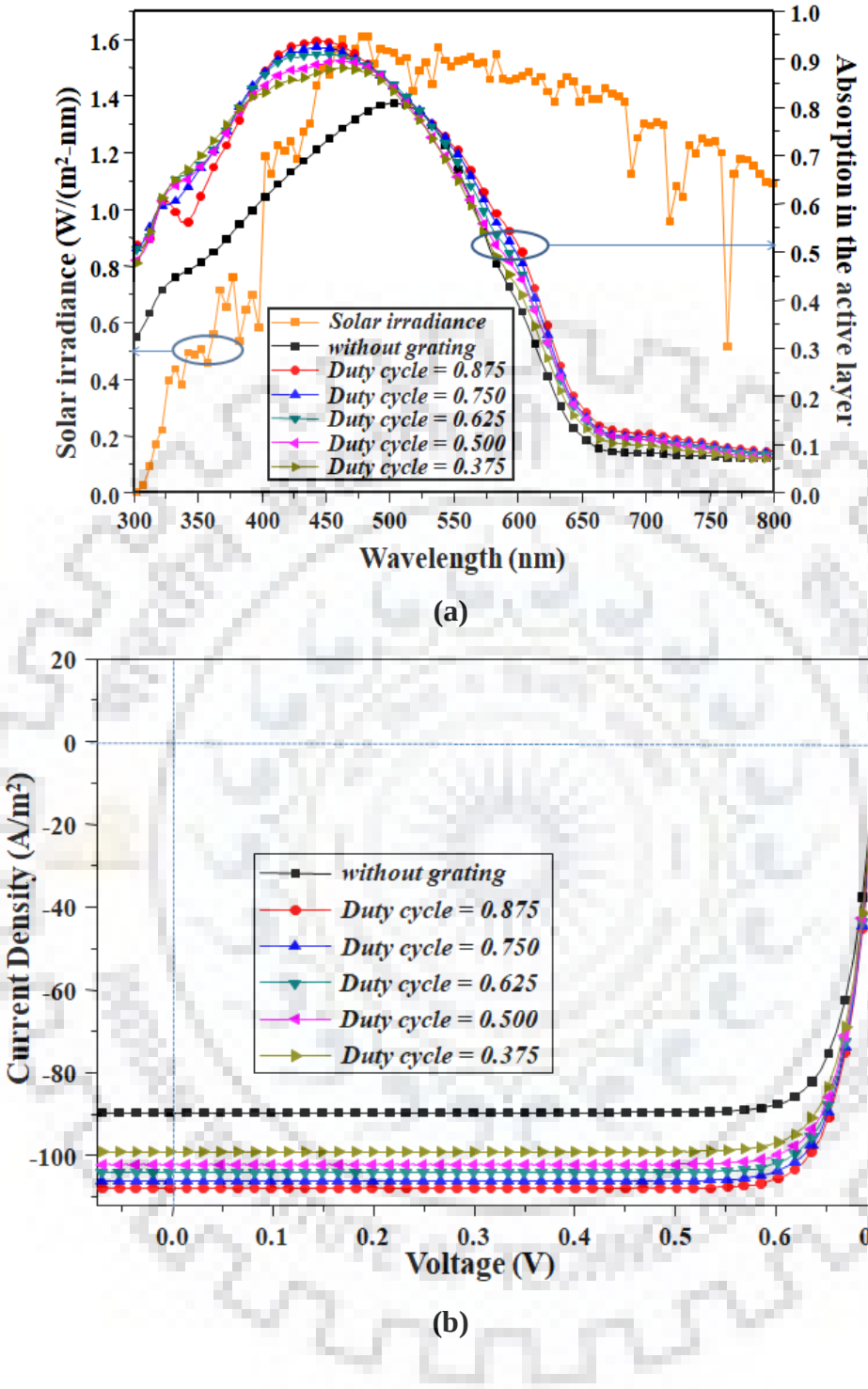

Figure 5.4 *(a) Absorption in the active layer as a function of wavelength (b) J-V characteristics of the cell for different duty cycle of the grating*

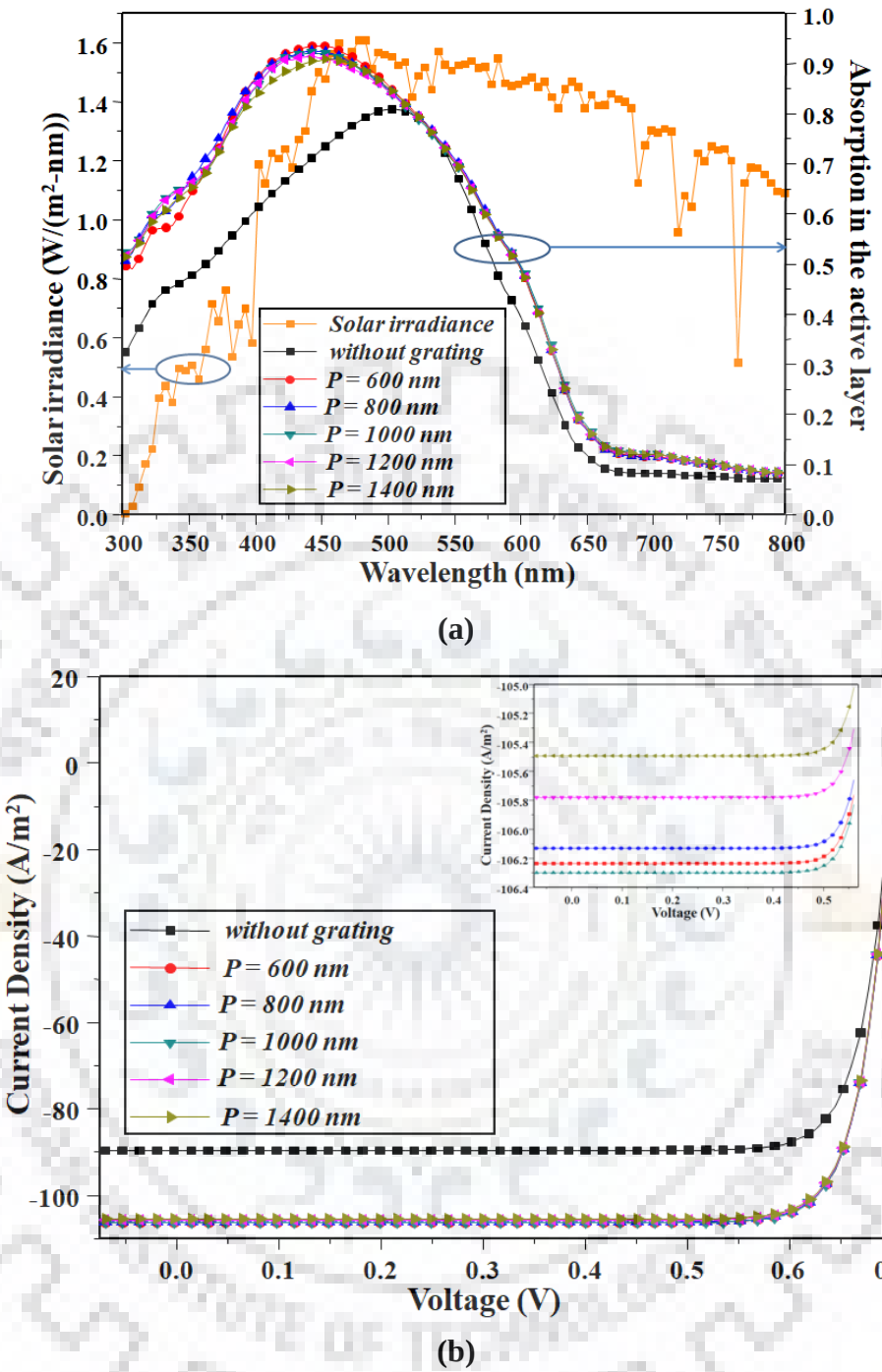

Figure 5.5 *(a) Absorption in the active layer as a function of wavelength (b) J-V characteristics of the cell for various periods of the grating*

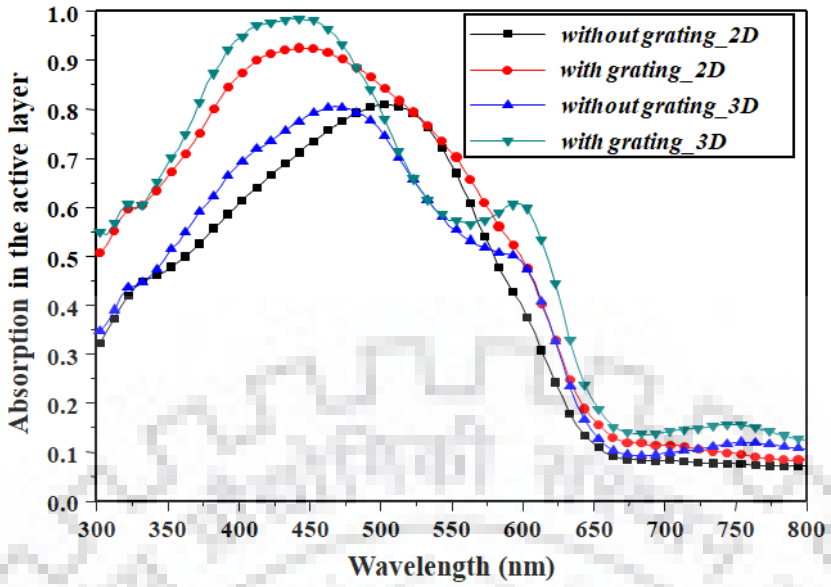

(a)

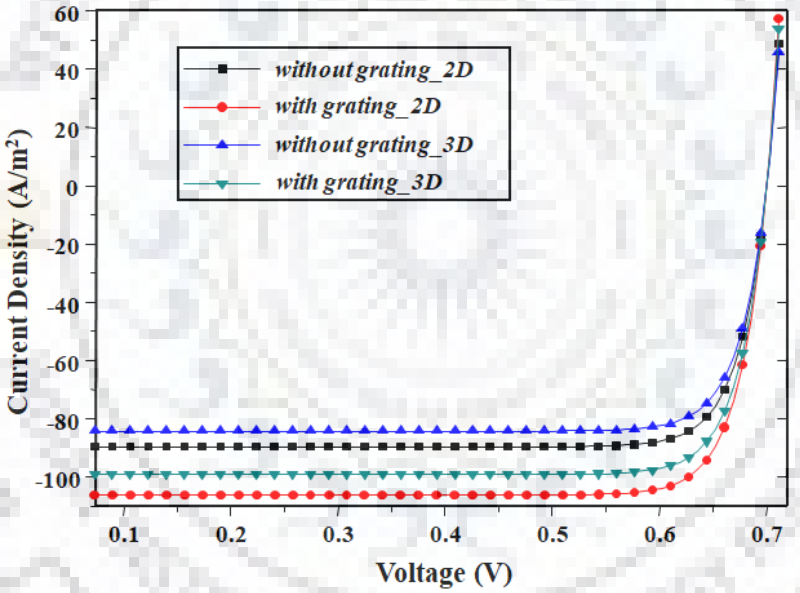

(b)

Figure 5.6 *Comparison of (a) absorption in the active layer as a function of wavelength (b) J-V characteristics of the cell for 2D and 3D FDTD simulation*

5.3.2 Comparison between 2D and 3D simulations

For the reliable results, we should perform 3D simulations. But the 3D simulations are time consuming and computationally heavy. To verify that there is not much difference in the 2D and 3D simulations, we have carried out the 3D FDTD simulation of the proposed structure for periodic diffraction TiO_2 grating with d = 80 nm, P = 800 nm and

w_2 = 400 nm. Figs. 5.6 (a) and 5.6 (b) show the plot of light absorption in the active layer with wavelength and J-V characteristics of the organic solar cell for 2D and 3D FDTD simulation. From the plots, we can see that the light absorption in the active layer for both 2D and 3D simulations are not significantly different. In 2D simulation, the obtained improvement in short circuit current density is by 18.4% while it is 17.6% using 3D simulations. This confirms that 2D simulation can be used to examine the trend of the light absorption in the active layer and short circuit current density of the device. So, we have limited ourselves to 2D simulations to save computational time and memory.

5.4 Conclusions

In this chapter, we have proposed the multilayer structure based on periodic dielectric diffraction grating for the enhancement of light absorption in the active layer and short circuit current density of the organic solar cell. The grating causes the optical path length enhancement in active layer of the cell by diffracting the incident light in different directions. The dielectric diffraction grating has been incorporated at glass substrate. To obtain the maximum enhancement in light absorption, the effects of width, height and period of the grating are examined. Improvement in the light absorption by 24.2% is obtained with d = 80 nm, w_2 = 700 nm and P = 800nm. Also, the short circuit current density and hence the optical efficiency of the proposed device is improved by 18.6%.

CHAPTER - 6

Enhancement in Absorption of Organic Solar Cell by use of Nanoparticles *

6.1 Introduction

The previously studied light trapping techniques (nanoparticles and diffraction grating) can further be implemented at other interfaces in the device to improve the performance of the organic solar cells.

Numerous works have been done by the incorporation of metal nanoparticles such as Au [183], Ag [184] or semiconducting nanoparticles like PbSe, CdTe, CdSe and ZnO [159-162] in organic solar cells to improve the efficiency. The PCE of the device is improved by 24% and 60% by incorporating Au and Ag nanoparticles in the hole transport layer [183,184]. Incorporation of CdTe nanoparticles in the active layer increases the PCE of the device by approximately 10% [160]. To avoid the absorption by metal nanoparticles, recent studies show that the efficiency can be enhanced by the incorporation of dielectric and metal core/shell nanoparticles [163-166]. P. Shao et al. reported that SiO_2 nanoparticles embedded in transport layer exhibits 17.5% increase in

*

A part of this work has been communicated to the following journal paper

V. Mann and V. Rastogi, "FDTD simulation studies on improvement of Light Absorption in Organic Solar Cells by dielectric Nanoparticles", *Opt. Quant. Electron*. (Revision submitted).

short circuit current density [164]. Approximately 13% enhancement in PCE can be seen by incorporating the SiO_2 dielectric nanoparticles in the active layer of OSCs [163]. 25% enhancement in the light absorption is reported when the $Ag@SiO_2$ nanoparticles are incorporated on top of anode (ITO) [165]. Nanoparticles (NPs) can enhance the optical absorption by the light scattering process without affecting the thickness of the active layer.

In this chapter, we have proposed to incorporate the dielectric nanoparticles at the anode (ITO). These nanoparticles will act as scattering medium and help in increase in optical path length of the device. Several parameters like diameter, interparticle spacing and materials of nanoparticles have been optimized in order to achieve the maximum enhancement in light absorption and short circuit current density of the organic solar cell.

6.2 Proposed Structure and Analysis

As a reference model, we have considered the conventional organic solar cell structure presented in Fig. 6.1. The proposed OSC structure shown in Fig. 6.2 consists of dielectric nanoparticles array deposited at ITO layer followed by PEDOT:PSS/P3HT:PCBM/Al layers. We have assumed the spherical shape of nanoparticles in our simulations. The dielectric material considered for nanoparticles has been assumed to be loss-less at the optical frequencies and hence there would not be any problem of light absorption by nanoparticles themselves. Mie theory has been used the study the optical behavior of isolated nanoparticle. Finite difference time domain (FDTD) method has been applied to for the numerical simulation of the device.

We have used the FDTD method to numerically analyze the enhancement in optical absorption in the active layer and hence the improvement in optical efficiency of the proposed organic solar cell structure.

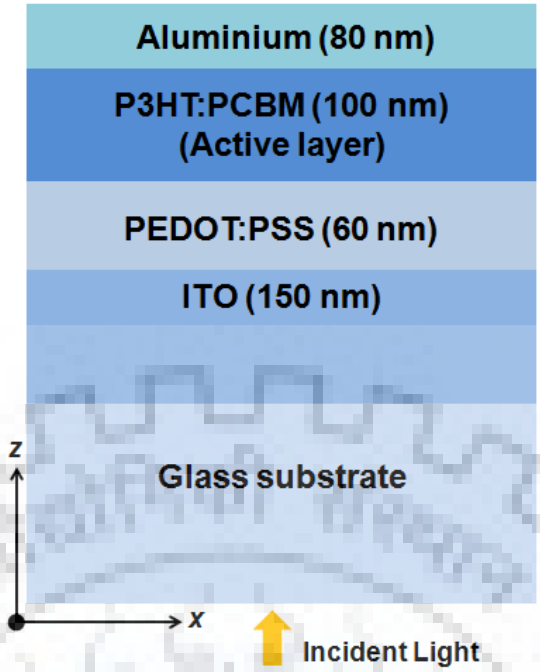

Figure 6.1 *Conventional organic solar cell set as reference*

For numerical analysis, the parameters considered for the device like thicknesses of the layers of device, refractive index and extinction coefficients of materials are kept same as discussed in section 4.2.1. In our simulations, we have included both refractive index and extinction coefficients, accounting for absorption in all layers. The nanoparticles diameter (*d*) and interparticle separation (*s*) has been optimized for the better absorption of light in the active layer of the cell. Refractive indices of dielectric materials ZrO_2, TiO_2 and SiC used for nanoparticles were taken from literature [168-169, 185]. The refractive indices of all the materials are wavelength dependent. Although three dimensional (3D) simulation provides more reliable results and FDTD simulations are computationally expensive, to save simulation time, we performed two dimensional (2D) FDTD simulations with transverse electric (TE) polarizations. We have also performed 3D simulation for the optimal parameters obtained from 2D simulation for the comparison purpose.

The solar cell structure was excited by broadband plane wave light source with a wavelength varying from 300 nm to 800 nm. The light is incident normally from air into the solar cell and it passes through all layers in the device as shown in Fig. 6.1. The default parameters in the Solar Cell Utility match the standard AM 1.5 solar spectrum criteria. There will be some absorption of light in all the layers and remaining of it is

reflected away from the cell. The active layer of the cell was surrounded by a monitor in order to collect the light absorbed by the active layer. In performing the simulation, perfectly matched layers (PML) were placed at all the boundaries. In order to have the accurate and good results, the grid size making up the spatial mesh are set to 1 nm in all the directions, which is smaller enough than the smallest diameter of nanoparticles. The execution time of the FDTD simulation needs to be sufficiently long so that the light can be propagated completely through the device. Solar cell utility, can only takes the optical effects into account.

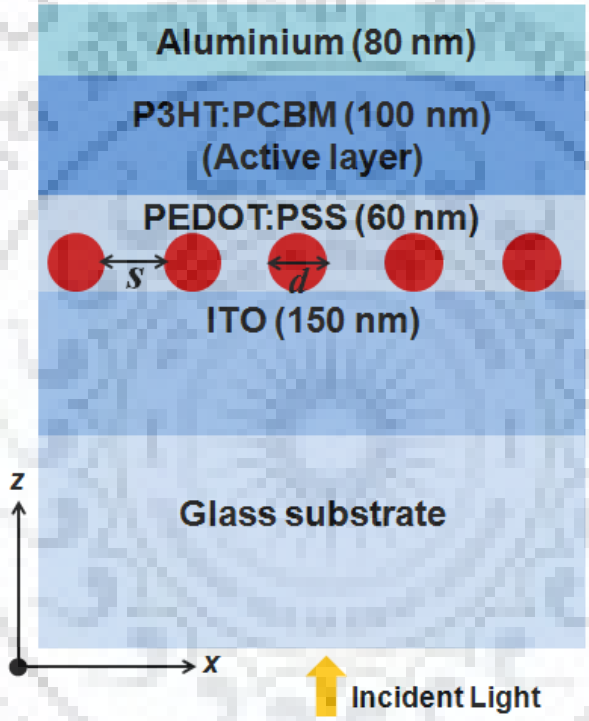

Figure 6.2 *Schematic of proposed organic solar cell with nanoparticles*

6.3 Results and Discussion

6.3.1 Scattering Efficiency of Nanoparticle

The scattering efficiency of dielectric nanoparticles has been studied to evaluate their suitability for the optimal performance of OSC. As the dielectric materials do not have dissipative properties in the incident spectrum, hence have an advantage of not absorbing the incident light and losing it in the form of heat. Also, they do not show plasmonic resonances because of their positive dielectric constant over the spectral

range. Improvement in the light absorption of the OSC in such a structure is primarily based on the scattering of solar light by the nanoparticles; we have first studied the effect of size and material of the nanoparticle on scattering efficiency by using the Mie theory. To carry this out, we have considered a single nanoparticle in PEDOT:PSS surrounding. Such a study helps in efficient optimization of size and material of nanoparticles while considering them in the complete structure as shown in Fig. 6.2. So, the results presented in Figs. 6.3 and 6.4 are based on Mie theory while all the other results have been produced by the FDTD method.

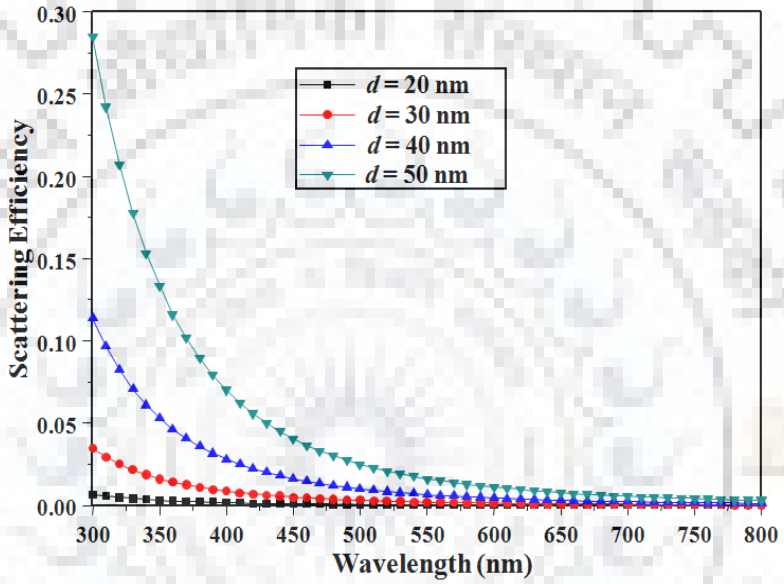

Figure 6.3 *Scattering efficiency as a function of wavelength for different diameters of nanoparticles*

(a) Effect of size of nanoparticle

Calculated spectra of scattering efficiency for various diameters of the isolated SiC nanoparticle is shown in Fig. 6.3. The diameter of nanoparticle ranges from 20 nm to 50 nm and particle is embedded in PEDOT:PSS medium. From Fig. 6.3, it can be seen that scattering efficiency of the nanoparticle increases from diameter d = 20 nm to d = 50 nm. This shows that larger sized nanoparticles have better ability to scatter the light and hence are more suitable for light absorption in the active layer of the device. Also, the scattering efficiency decreases with the increase in the wavelength of incident light.

(b) Effect of refractive index of nanoparticle

Fig. 6.4 shows the scattering efficiency as a function of wavelength for ZrO_2 and SiC nanoparticles with diameter d = 40 nm. In our simulation, we have considered the variation of refractive index of embedding medium (PEDOT:PSS) with wavelength. The scattering efficiency depends on the index contrast between the nanoparticle material and embedding medium material. The embedding medium has refractive index of 1.48 whereas ZrO_2 has 2.17; TiO_2 has 2.53 and SiC has 2.69 refractive index at wavelength 500 nm. It can be concluded from the plot that a SiC nanoparticle has higher scattering efficiency than ZrO_2 and TiO_2 nanoparticle in the wavelength range 400 nm – 800 nm. This happens because the refractive index of SiC material is higher than that of ZrO_2 and TiO_2 material and provides higher index contrast with embedding medium. This shows that the light scattering by nanoparticles strongly depends on the refractive index contrast between the embedding medium and the nanoparticles material.

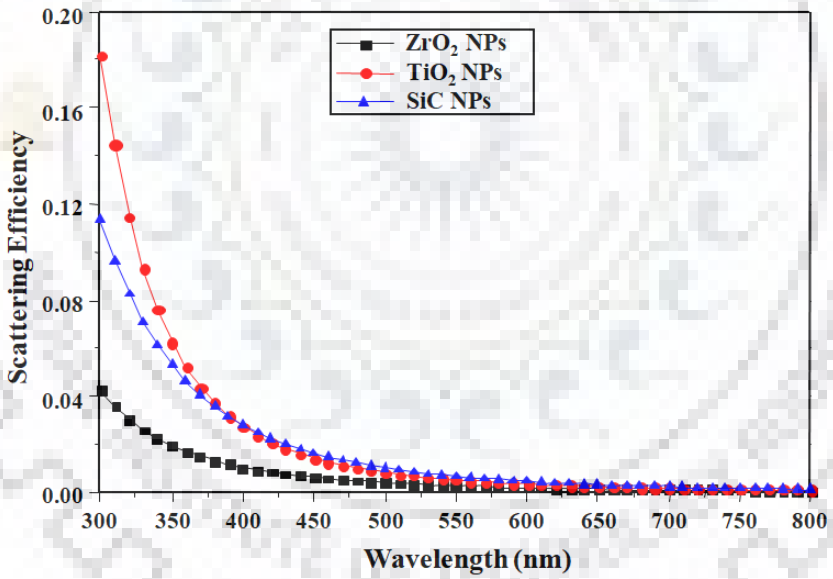

Figure 6.4 *Scattering efficiency as a function of wavelength for different materials of nanoparticles*

6.3.2 Electric field distribution

In Fig. 6.5, we have plotted the electric field component of the incident light as a function of spatial distance for conventional OSC and OSC with nanoparticles of SiC and ZrO_2 at wavelength 500 nm. We have considered the diameter 40 nm and interparticle spacing 10 nm for SiC and ZrO_2 nanoparticles. The plot of electric field

shows that as the light strikes the nanoparticles, the surrounding field dissipates. This could mean that the addition of nanoparticles in the solar cell design shows scattering effect and hence the light gets absorbed in the active layer.

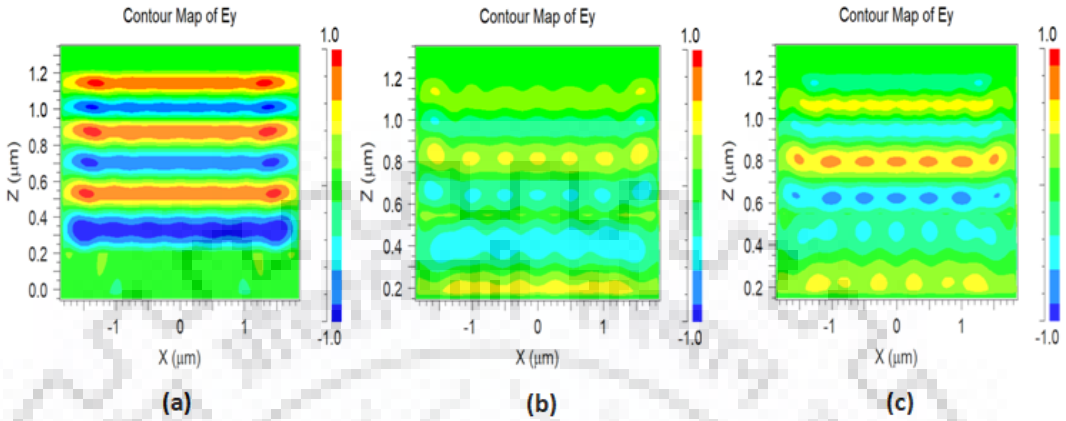

Figure 6.5 *Contour plot of spatial electric field (a) no nanoparticles (b) ZrO_2 nanoparticles (c) SiC nanoparticles.*

6.3.3 Enhancement in Light Absorption and Short circuit current density

We have numerically analyzed the OSC without and with nanoparticles. The light absorption spectrum in the active layer of the device can be obtained directly by placing the monitor over the layer. As the reflection occurs at different interfaces, the incident light could not be completely absorbed in the active layer even with the use of dielectric nanoparticles. We investigated the effect of various parameters such as diameter (*d*), interparticle separation (*s*) and refractive index of nanoparticles to achieve better light absorption in the active layer of the solar cell. All the simulations have been carried out for TE polarization.

(a) Effect of size of nanoparticles

The role of diameter of nanoparticles in scattering the incident light is significant. The dependence of incident light absorption in the active layer on the diameter of nanoparticles has been investigated and is shown in Fig. 6.6 (a) along with the AM 1.5G solar spectrum. The J-V characteristics of the organic solar cell are shown in Fig. 6.6 (b). We have considered the SiC nanoparticles with diameter varying from 20 nm to 50 nm keeping no interparticle separation in both the plots. Fig. 6.6 (a) shows that the light absorption in the active layer increases for the values of the diameter from *d* = 20 nm to

d = 50 nm. This is due to more scattering of light by large sized nanoparticles. So, there is an increase of light absorption in the active layer of the device by 27% for d = 20 nm and 43.5% for d = 50 nm. Also, the increase in the light absorption can be seen in the wavelength range from 300 nm to 490 nm and 530 nm to 800 nm but it remains almost same in the wavelength range from 490 nm to 530 nm. The scattering by nanoparticles and absorption of light by embedding medium give rise to the pattern of the figure. It can also be seen from Fig. 6.6 (b) that the short circuit current density (J_{sc}) increases for the values of the diameter from d = 20 nm to d = 50 nm. The current density increases by 20.9% for d = 20 nm and by 36.4% for d = 50 nm. The incorporation of SiC nanoparticles in the organic solar cell increases the light absorption by 40% and the short circuit current density by 33.9% for optimal diameter of 40 nm and no interparticle spacing.

(b) Effect of interparticle separation

The absorption of incident light in the active layer of the device is also affected by any change in the interparticle separation of nanoparticles. The effect of variation in interparticle separation of dielectric nanoparticles on the light absorption in the active layer with wavelength has been studied and the results are shown in Fig. 6.7 (a). We have chosen the SiC nanoparticles of 40 nm diameter. Interparticle separation has been varied from 0 nm to 50 nm. As it can be seen from the plot that the as the interparticle separation increases the enhancement in light absorption decreases. As the separation increases from 0 nm to 50 nm, the enhancement in light absorption in the active layer decreases from 40% to 26.5%. Fig. 6.7 (b) shows the J-V characteristics of the cell for different interparticle separations. As seen from the plot, the short circuit current density decreases from 33.9% to 16.9% as the interparticle separation increases from 0 nm to 50 nm. This shows that the enhancement in electric field gets smaller and smaller as the separation between the nanoparticles increases. This is due to the decoupling between neighboring dielectric nanoparticles. So, the enhancement of 40% in light absorption and 34% in short circuit current density of the cell could be achieved with no interparticle separation (i.e. s = 0 nm)

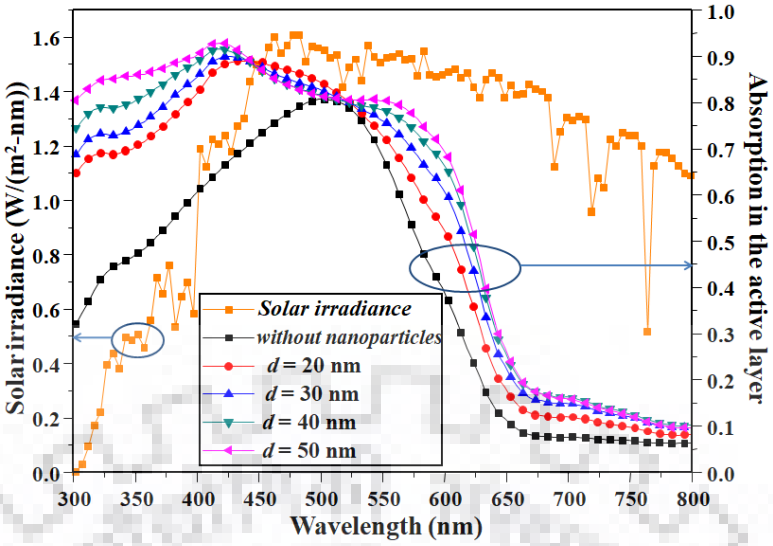

(a)

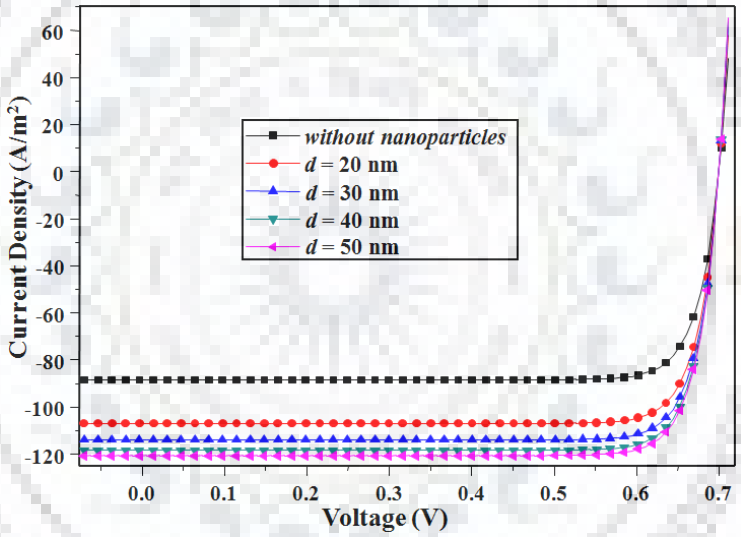

(b)

Figure 6.6 *(a) Absorption in the active layer as a function of wavelength for different diameters of nanoparticles (b) J-V characteristics of the cell for different diameters of nanoparticles*

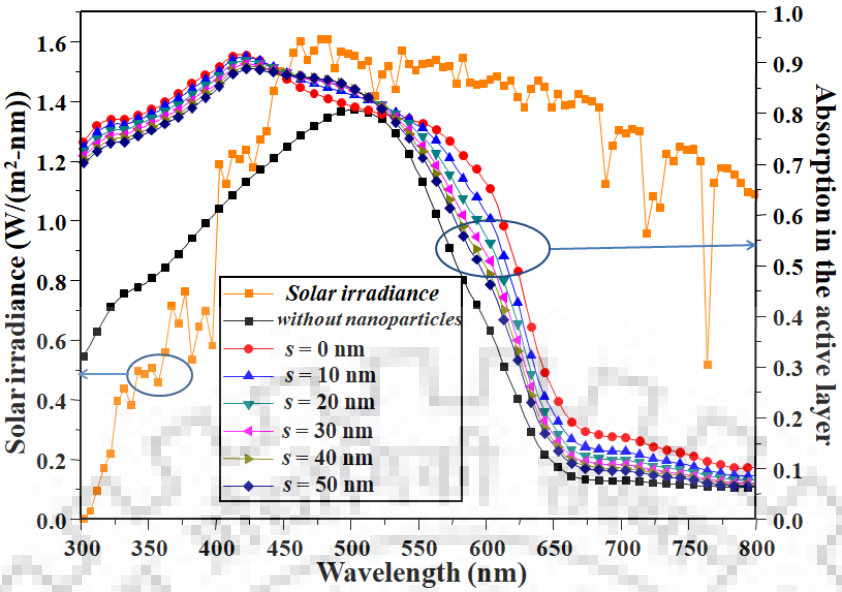

(a)

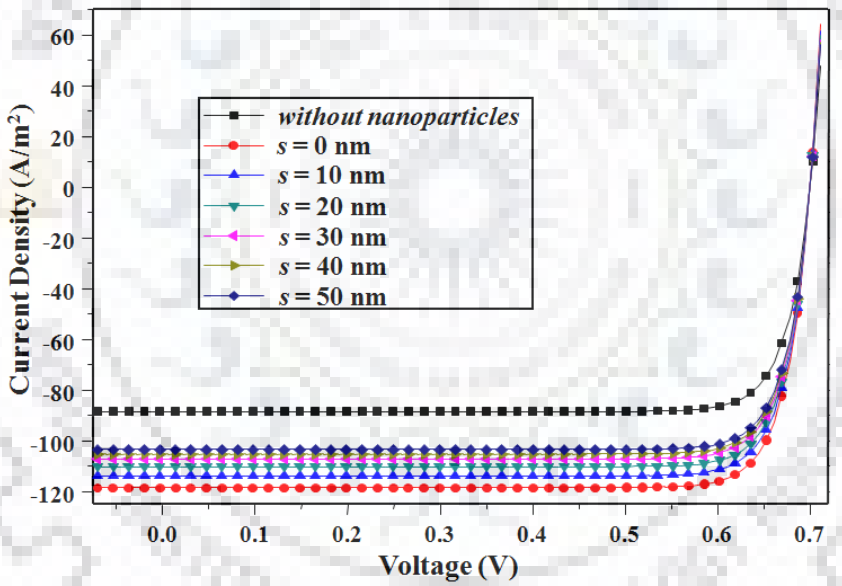

(b)

Figure 6.7 *(a) Absorption in the active layer as a function of wavelength (b) J-V characteristics of the cell for different interparticle separations of nanoparticles for TE polarization*

(c) Effect of material of nanoparticles

We have also investigated the effect of the material of nanoparticles on incident light absorption in the active layer and J-V characteristics of the cell. To show this, we have plotted the light absorption in the active layer with wavelength as shown in Fig. 6.8 (a) and Fig. 6.8 (b) shows the J-V characteristics of the cell corresponding to different material of nanoparticles. In our study, we have considered ZrO_2, TiO_2 and SiC material nanoparticles. Diameter of nanoparticles was fixed to 40 nm with no interparticle separation (s = 0 nm). It can be seen from the figure 6.8 (a) that the increase in light absorption in the active layer is more for SiC material than that of ZrO_2 and TiO_2. The light absorption in the active layer is enhanced by 29% for ZrO_2, 37% for TiO_2 and by 40% for SiC. This is due to the fact that scattering of light by the nanoparticles strongly depends on refractive index contrast. As the refractive index of SiC is more than that of ZrO_2 and TiO_2, the SiC nanoparticles scatter more light. Figure 6.8 (a) shows that the increase in light absorption is in the wavelength ranges 300 nm – 490 nm and 530 nm – 800 nm for SiC material. For ZrO_2 material, the increase in light absorption can be seen in the entire wavelength range. Figure 6.8 (b) shows that the presence of ZrO_2 nanoparticles increases the short circuit current density by 20.2%, TiO_2 nanoparticles increases J_{sc} by 32.7% and SiC nanoparticles increase it by 33.9%.

(d) Effect of assorted size and interparticle spacing of nanoparticles

In the device fabrication, the size and separation between nanoparticles may vary randomly. To take this into account, we have also studied the effect of assorted diameter and interparticle separation of dielectric nanoparticles layer (deposited on anode) on the light absorption in the active layer and current density of the device. We have varied the diameter from 30 nm to 50 nm and interparticle separation from 10 nm to 30 nm in a random manner for ZrO_2 and SiC nanoparticles. The plots for light absorption in the active layer as a function of wavelength and J-V characteristics of the cell are shown in Fig. 6.9. The accumulative effect of both diameter and interparticle separation decreases the short circuit current density of the device to 24.6% for SiC nanoparticles and to 12.7% for ZrO_2 nanoparticles when assorted diameters and interparticle separations of nanoparticles are used.

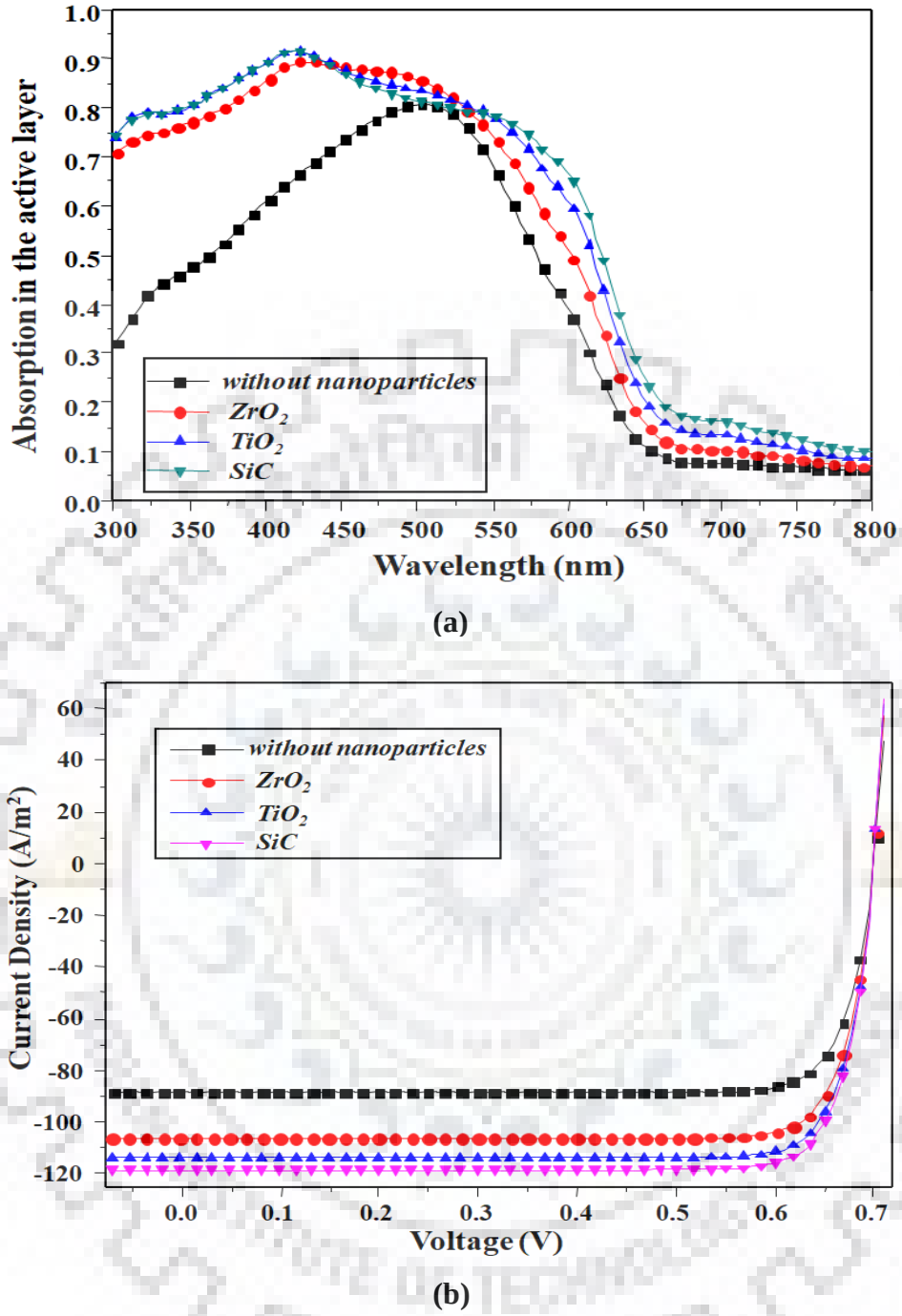

Figure 6.8 *(a) Absorption in the active layer as a function of wavelength (b) J-V characteristics of the cell for different material of nanoparticles for TE polarization*

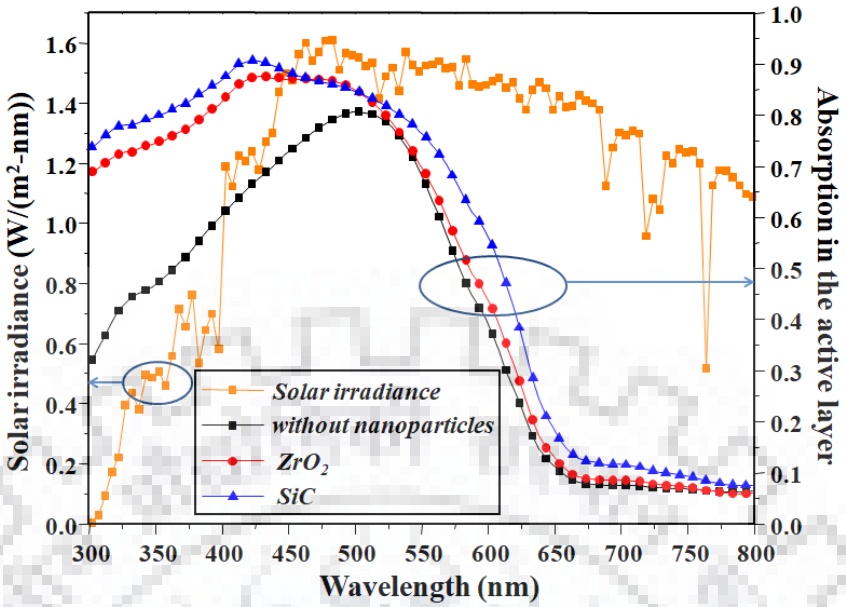

(a)

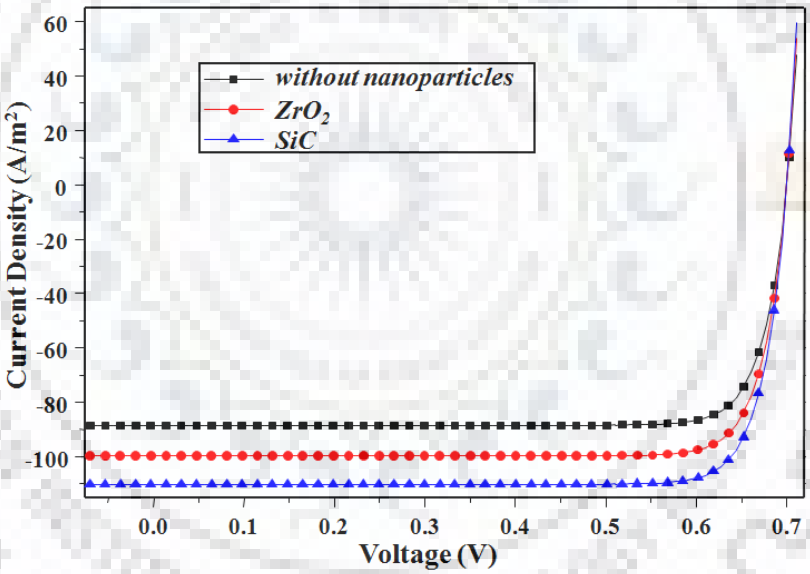

(b)

Figure 6.9 *(a) Absorption in the active layer as a function of wavelength (b) J-V characteristics of the cell for assorted diameter and interparticle separations of nanoparticles*

6.3.4 Comparison of 2D and 3D simulation

One should in principle study 3D simulations for more realistic results. However, 3D simulations are time consuming and are computationally heavy. Also, for nanoparticles related simulations, researchers have shown that a 2D model gives similar results as those obtained from a 3D model [165]. To verify this, we have numerically analyzed the 3D FDTD simulation of the proposed structure for SiC nanoparticles with d = 40 nm, s = 20 nm and compared our results with those obtained by using 2D simulations. Figs. 6.10 (a) and 6.10 (b) show the curves for light absorption in the active layer with wavelength and J-V characteristics of the device for 2D and 3D FDTD simulations. From the curve, we can find that there is no significant difference in the light absorption in the active layer for both 2D and 3D simulations. In 2D simulations, the improvement obtained in short circuit current density is 28% while it is 25% using 3D simulations. This shows that 2D simulations can be used to study the effect of nanoparticles on the light absorption in the active layer and the current density of the device. We have, therefore, restricted ourselves to 2D simulations to save computational memory and time.

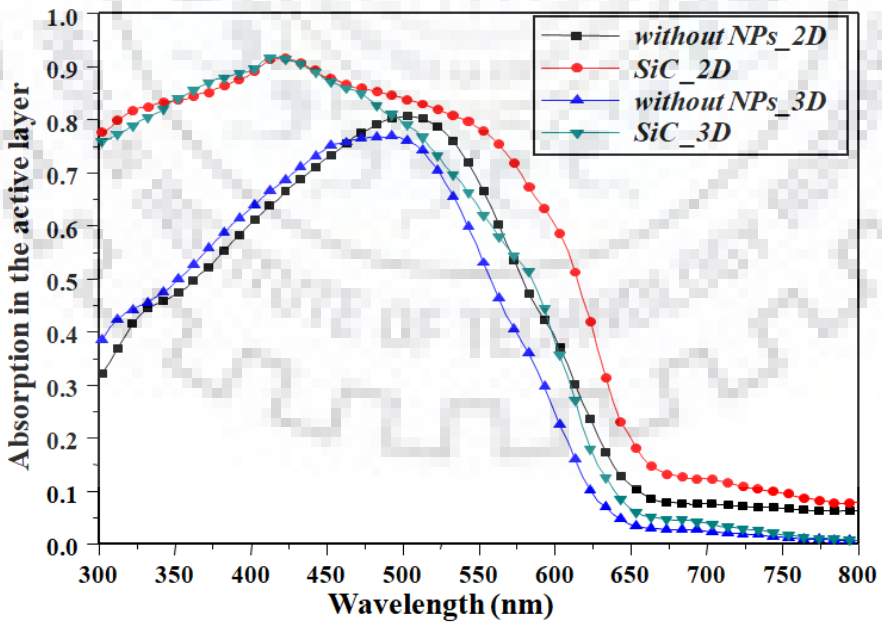

(a)

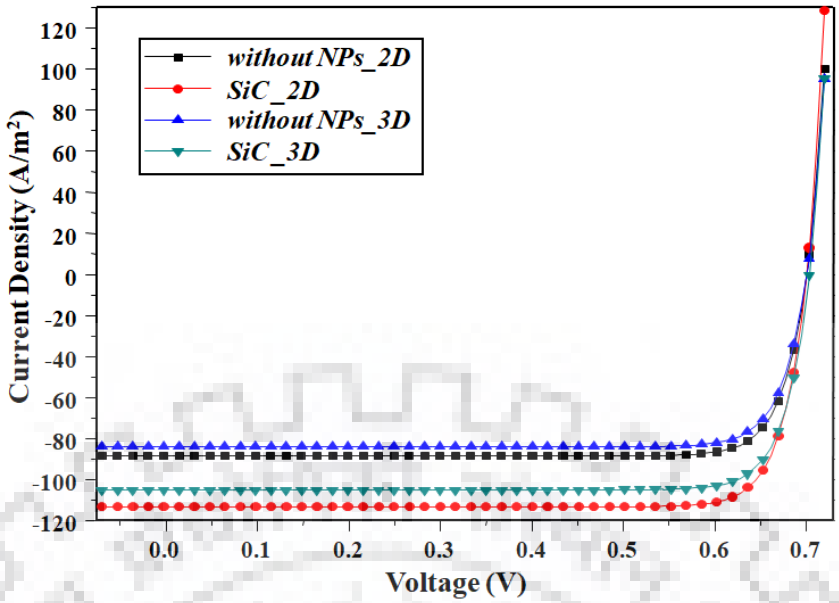

(b)

Figure 6.10 *Comparison of (a) absorption in the active layer as a function of wavelength (b) J-V characteristics of the cell for 2D and 3D FDTD simulation*

The study clearly shows that incorporation of nanoparticles helps in increasing the optical absorption in the active layer and hence the optical efficiency of the organic solar cell.

6.4 Conclusions

In this chapter, we have proposed and studied the multilayer structure for increasing the light absorption in organic solar cell by placing the dielectric nanoparticles layer at the anode. These nanoparticles will help in scattering the incident light. Effects of diameter, material and interparticle separation of dielectric nanoparticles were examined in order to obtain the maximum enhancement in light absorption. For this design, the light absorption in the active layer has been improved by 40% for SiC material, 37% for TiO_2 material and by 29% for ZrO_2 material. It has also been shown that the short circuit current density of proposed OSC can be improved by 20.2% by using ZrO_2 nanoparticles, 32.7% by TiO_2 nanoparticles and 33.9% by using SiC nanoparticles with diameter 40 nm and no interparticle separation. From the results, we also found that 2D simulation could be used for saving computation time. The proposed studies would be useful for developing high efficiency organic solar cells.

CHAPTER-7

Summary and Future Scopes

In this thesis, we have presented novel multilayer structures for optoelectronics applications. In particular, we have presented dielectric nanoparticles based designs for organic light emitting diodes and organic solar cells. We have also presented dielectric grating based multilayer designs for organic solar cells.

Our work has been mainly focused on to develop the multilayer designs to minimize the losses and hence increase the efficiency of OLEDs and OSCs. In this thesis, we have investigated the use of dielectric nanoparticles (NPs) and dielectric diffraction gratings for enhancing the efficiency of the devices.

Firstly, we have designed and analyzed two structures based on dielectric nanoparticles for OLED. In design 1, the dielectric NPs are placed at the glass substrate of the OLED structure. Effect of various parameters like diameter, interparticle separation and refractive index were studied. With this proposed design we were able to achieve the maximum enhancement in light extraction efficiency by the factor of 1.7 with diameter 100 nm, refractive index 1.1 and no interparticle separation. In second design, the dielectric nanoparticles are incorporated at anode (ITO) layer. A detailed study of this structure shows that the light extraction efficiency of OLED could be enhanced by 1.7 times with diameter 50 nm, refractive index 1.1 and no interparticle separation. Results

from both the designs show that the light trapped in waveguided modes can be coupled out from the device via use of dielectric nanoparticles which act as scattering medium.

We have further investigated the role of dielectric nanoparticles and diffraction grating in the enhancement of light absorption in the active layer and short circuit current density of OSC. In the first design, the dielectric NPs are placed at the glass substrate of the OSC structure. Optimization of diameter and interparticle separation has been carried out to achieve the maximum enhancement. Using this design, enhancement of 20.4% in light absorption and 19.8 % in short circuit current density with SiC nanoparticles has been achieved. Using TiO_2 nanoparticles, absorption could be enhanced by 19% and J_{sc} by 18.5%.

In the next design, the periodic dielectric diffraction grating has been placed at the glass substrate. We have examined the effects and optimized the width, period and height of the grating. Improvement in the light absorption by 24.2% and short circuit current density by 18.6% is obtained with optimized parameters.

Further, the dielectric nanoparticles are introduced at anode (ITO) layer. By considering this design we were able to achieve enhancement of 40% in absorption and 33.9% in J_{sc} using SiC nanoparticles. Also, the light absorption improved by 29% and J_{sc} by 20.2% with ZrO_2 material whereas for TiO_2 material, the absorption improved by 37% and J_{sc} by 32.7%.

We were able to achieve the better enhancement in the light absorption with the use of diffraction grating than that of nanoparticles when placed at the glass substrate. The enhancement in the device can be further improved by placing the nanoparticles at the anode layer.

The proposed studies would be useful for developing high efficiency OSCs.

For the fabrication purpose, the structures we have considered in our thesis can be realized by standard fabrication techniques such as spin coating, spray coating, thermal evaporation, chemical vapor deposition and pulse laser deposition. Most of dielectric materials considered for nanoparticles and grating can be synthesized by the sol-gel process which is very cost effective method.

For the future prospectus, the use of dielectric nanoparticles and dielectric grating is not limited to organic light emitting diodes and organic photovoltaics. Nanoparticles can be implemented in other optoelectronics devices such as dye sensitized solar cells, pervoskite cells, and photo detectors to enhance the device performance. Gratings can also be incorporated between the active layer and the hole transport layer. Metal shell dielectric nanoparticles can also be implemented in OLEDs and OSCs for improving the device performance.

BIBLIOGRAPHY

[1]. H. Jeon, J. Ding, A. V. Nurmikko, W. Xie, M. Kobayashi, and R. L. Gunshor, "ZnSe based multilayer p-n junctions as efficient light emitting diodes for display applications," Appl. Phys. Lett., vol. 60, 892-894, 1992.

[2]. M .R. Krames, O. B. Shchekin, R. M. -Mach, G. O. Mueller, L. Zhou, G. Harbers, and M. G. Craford, "Status and Future of High-Power Light-Emitting Diodes for Solid-State Lighting," J. Display Technol., vol. 3, 160-175, 2007.

[3]. W. -S. Sun, C. –L. Tien, J. –W. Pan, T. –H. Yang, C. –H. Tsuei, and Y. –H. Huang, "Simulation and Comparison of the Lighting Efficiency for Household Illumination with LEDs and Fluorescent Lamps," J. Opt. Soc. Korea, vol. 17, 376-383, 2013.

[4]. A. Zukauskas, M. S. Shur, and R. Caska, "Introduction to Solid-state Lighting", John Wiley and Sons, New York, 2002.

[5]. D. A. Steigerwald, J. C. Bhat, D. Collins, R. M. Fletcher, M. O. Holcomb, M. J. Ludowise, P. S. Martin, and S. L. Rudaz, "Illumination with solid state lighting technology," IEEE J. Sel. Top. Quantum Electron., vol. 8, 310-320, 2002.

[6]. E. F. Schubert and J. K. Kim, "Solid-state light sources becoming smart," Science, vol. 308, 1274-1278, 2005.

[7]. N. Holonayak and S. F. Bevacqua, "Coherent (Visible) Light Emission from $Ga(As_{1-x}p_x)$ Junctions," Appl. Phys. Lett., vol. 1, 82-83, 1962.

[8]. S. Nakamura, T. Mukai, and M. Senoh, "Candela-class high-brightness InGaN/AlGaN double-heterostructure blue-light-emitting diodes," Appl. Phys. Lett., vol. 64, 1687-1689, 1994.

[9]. https://www.nobelprize.org/nobel_prizes/physics/laureates/2014/

[10]. V. Bulovic, R. Deshpande, M. E. Thompson, and S. R. Forrest, "Tuning the color emission of thin film molecular organic light emitting devices by the solid salvation effect," Chem, Phys. Lett., vol. 308, 317-322, 1999.

[11]. H. Ulla, M. R. Kiran, B. Garudachari, M. N. Satyanarayan, G. Umesh, and A. M. Isloor, "Blue emitting halogen-phenoxy substituted 1,8-napthalimides for potential organic light emitting diode applications, Opt. Mater., vol. 37, 311-321, 2014.

[12]. K. Hong and J. –L. Lee, “Recent developments in light extraction technologies of organic light emitting diodes,” Electron. Mater. Lett., vol. 7, 77-91, 2011.

[13]. H. Ulla, M. R. Kiran, B. Garudachari, M. N. Satyanarayan, G. Umesh, and A. M. Isloor, “Blue emitting halogen-phenoxy substituted 1,8-napthalimides for potential organic light emitting diode applications, Opt. Mater., vol. 37, 311-321, 2014.

[14]. H. Sasabe and J. Kido, “Development of high performance OLEDs for general lighting,” J. Mater. Chem. C, vol. 1, 1699-1707, 2013.

[15]. K. –D. Chang, C. –Y. Li, J. –W. Pan, and K. –Y. Cheng, “A hybrid simulated method for analyzing the optical efficiency of a head-mounted display with a quasi-crystal OLED panel,” Opt. Express, vol. 22, A567-A576, 2014.

[16]. W. Helfrich and W. G. Schneider, “Recombination Radiation in Anthracene Crystals,” Phys. Rev. Lett., vol. 14, 229-232, 1965.

[17]. C. W. Tang and S. A. VanSlyke, “Organic electroluminescent diodes,” Appl. Phys. Lett., vol. 51, 913-915, 1987.

[18]. S. A. Carter, M. Angelopoulos, S. Karg, P. J. Brock, and J. C. Scott, “Polymeric anodes for improved polymer light-emitting diode performance,” Appl. Phys. Lett., vol. 70, 2067-2069, 1997.

[19]. J. Wu, M. Agrawal, H. A. Becerril, Z. Bao, Z. Liu, Y. Chen, and P. Peumans, “Organic Light-Emitting Diodes on Solution-Processesd Graphene Transparent Electrodes,” ACS Nano, vol. 4, 43-48, 2010.

[20]. R. H. Friend, R. W. Gymer, A. B. Holmes, J. Burroughes, R. N. Marks, C. Taliani, D. D. C. Bradley, D. A. Dos Santos, J. L. Bredas, M. Logdlund, and W. R. Salaneck, “Electroluminescence in conjugated polymers,” Nature, vol. 397, 121-128, 1999.

[21]. L. S. Hung, C. W. Tang, and M. G, Mason, “Enhanced electron injection in organic electroluminescence devices using an Al/LiF electrode,” Appl. Phys. Lett., vol. 70, 152-154, 1997.

[22]. M. A. Baldo and S. R. Forrest, “Highly efficient phosphorescent emission from organic electroluminescent devices,” Nature, vol. 395, 151-154, 1998.

[23]. S. R. Forrest, “The road to high efficiency organic light emitting devices,” Org. Electron., vol. 4, 45-48, 2003.

[24]. G. Gu, D. Z. Garbuzov, P. E. Burrows, S. Venkatesh, S. R. Forrest, and M. E. Thompson, “High-external-quantum-efficiency organic light-emitting devices,” Opt. Lett., vol. 22, 396-398, 1997.

[25]. J. R. Sheats, H. Antoniadis, M. Hueschen, W. Leonard, J. Miller, R. Moon, D. Roitman, and A. Stocking, “Organic Electroluminescent Devices,” Science, vol. 273, 884-888, 1996.

[26]. M. A. Baldo, D. F. O’Brien, Y. You, A. Shoustikov, S. Sibley, M. E. Thompson, and S. R. Forrest, “Highly efficient phosphorescent emission from organic electroluminescent devices,” Nature, vol. 395, 151-154, 1998.

[27]. C. F. Madigan, M. –H. Lu, and J. C. Sturm, “Improvement of output coupling efficiency of organic light-emitting diodes by backside substrate modification,” Appl. Phys. Lett., vol. 76, 1650-1652, 2000.

[28]. S. S. Jeong and J. –H. Ko, “Optical Simulation Study on the Effect of Diffusing Substrate and Pillow Lenses on the Outcoupling Efficiency of Organic Light Emitting diodes,” J. Opt. Soc. Korea, vol. 17, 269-274, 2013.

[29]. Y. H. Cheng, J. L. Wu, C. H. Cheng, K. C. Syao, and M. C. M. Lee, “Enhanced outcoupling in a thin film by texturing meshed surfaces,” Appl. Phys. Lett., vol. 90, 091102-1-091102-3, 2007.

[30]. K. Tong, X. Liu, F. Zhao, D. Chen, and Q. Pei, “Efficient Light Extraction of Organic Light-Emitting Diodes on a Fully Solution-Processed Flexible Substrate, “Adv. Optical Mater., vol. 5, 1700307-1-1700307-8, 2017.

[31]. J.Y. Kim and K.C. Choi, “Improvement in outcoupling efficiency and image blur of organic light-emitting diodes by using imprinted microlens array,” J. Disp. Technol., vol. 7, 377–381, 2011.

[32]. S. Möller and S. R. Forrest, “Improved light out-coupling in organic light emitting diodes employing ordered microlens arrays,” J. Appl. Phys., vol. 91, 3324-3327, 2002.

[33]. F. Galeotti, W. Mróz, G. Scavia, and C. Botta, “Microlens arrays for light extraction enhancement in organic light-emitting diodes: A facile approach,” Org. Electron., vol. 14, 212-218, 2013.

[34]. J. P. Yang, Q. Y. Bao, Z. Q. Xu, Y. Q. Li, J. X. Tang, and S. Shen, “Light out-coupling enhancement of organic light-emitting devices with microlens array,” Appl. Phys. Lett., vol. 97, 223303-1-223303-3, 2010.

[35]. K. Saxena, D. S. Mehta, V. K. Rai, R. Srivastava, G. Chauhan, and M. N. kamalasanan, “Implementation of anti-reflection coating to enhance light out-coupling in organic light-emitting devices,” Journal of Luminescence, vol. 128, 525-530, 2008.

[36]. T. Tsuitsui, M. Yahiro, H. Yokogawa, K. Kawano, and Y. Yokoyama, “Doubling coupling-out efficiency in organic light-emitting devices using a thin silica aerogel layer,” Adv. Mater., vol. 13, 1149-1152, 2001.

[37]. T. Nakamura, N. Tsutsumi, N. Juni, and H. Fujii, “Thin-film waveguiding mode light extraction in organic electroluminescent device using high refractive index substrate,” J. Appl. Phys., vol. 97, 054505-1–054505-054506, 2005.

[38]. Y. Sun and S. R. Forrest, “Enhanced light out-coupling of organic light-emitting devices using embedded low-index grids,” Nat. Photonics, vol. 2, 483-487, 2008.

[39]. S. Forrest and Y. Sun, “Low index grids (LIG) to increase outcoupled light from top or transparent OLED,” US 20080265757 A1, Oct. 30, 2008.

[40]. M. Fujita, T. Ueno, T. Asano, S. Noda, H. Ohata, T. Tsuji, H. Nakada, and N. Shimoji, “Organic light-emitting diode with ITO/organic photonic crystal,” Electron. Lett., vol. 39, 1750-1752, 2003.

[41]. Y.-J. Lee, S. –H. Kim, G. –H. Kim, Y.-H. Lee, S. –H. Cho, Y. –W. Song, Y. –C. Kim, and Y. R. Do, “Far-field radiation of photonic crystal organic light-emitting diode,” Opt. Exp., vol. 13, 5864-5870, 2005.

[42]. K. Ishihara, F. Masayuki, I. Matsubara, T. Asano, S. Noda, H. Ohata, A. Hirasawa, H. Nakada, and N. Shimoji, “Organic light-emitting diodes with photonic crystals on glass substrate fabricated by nanoimprint lithography,” Appl. Phys. Lett., vol. 90, 111114-1-111114-3, 2007.

[43]. J. S. Lee, J. –H. Ko, J. Park, and J. W. Lee, “Simulation study on the effect of the emitter orientation and photonic crystals on the outcoupling efficiency of organic light emitting diodes,” J. Opt. Soc. Korea, vol. 18, 732-738, 2014.

[44]. M. Kumar, R. Jindal, and J. Joseph, “FDTD modeling based comparison of RIE based and sol-gel based PC- OLED devices,” J. Opt., vol. 41, 243-250, 2012.

[45]. Y. J. Lee, S. H. Kim, J. Huh, G. H. Kim, Y. H. Lee, S. Cho, H. Kim, and Y. R. Do, “A high-extraction-efficiency nanopatterned organic light-emitting diode,” Appl. Phys. Lett., vol. 82, 3779-3781, 2003.

[46]. S. Jeon, J. –W. Kang, H. –D. Park, J. –J. Kim, J. R. Youn, J. Shim, J. –H. Jeong, D. –G. Choi, K. –D. Kim, A. O. Altun, S. –H. Kim, and Y. –H. Lee, "Ultraviolet nanoimprinted polymer nanostructure for organic light emitting diode application," Appl. Phys. Lett., vol. 92, 223307-1–223307-3, 2008.

[47]. H. –Y. Lin, J. –H. Lee, M. –K. Wei, C. –C. Dai, C. –F. Wu, Y. –H. Ho, H. –Y. Lin, and T. –C. Wu, "Improvement of the outcoupling efficiency of an organic light-emitting device by attaching microstructured films," Opt. Commun., vol. 275, 464-469, 2007.

[48]. S. M. Jeong, F. Araoka, Y. Machida, Y. Takanishi, K. Ishikawa, H. Takezoe, S. Nishimura, and G. Suzaki, "Enhancement of Light Extraction from Organic Light-Emitting Diodes with Two-Dimensional Hexagonally Nanoimprinted Periodic Structures Using Sequential Surface Relief Grating," Jpn. J. Appl. Phys., vol. 47, 4566-4571 2008.

[49]. J. Frischeisen, Q. Niu, A. Abdellah, J.B. Kinzel, R. Gehlhaar, G. Scarpa, C. Adachi, P. Lugli, and W. Brütting, "Light extraction from surface plasmons and waveguide modes in an organic light-emitting layer by nanoimprinted gratings," Opt. Express, vol. 19, A7-A19, 2011.

[50]. J. Lee, N. Chopra, and F. So, "Cavity effects on light extraction in organic light emitting devices," Appl. Phys. Lett., vol. 92, 033303-1-033303-3, 2008.

[51]. N. Gupta, R. Grover, D. S. Mehta, and K. Saxena, "Efficiency enhancement in blue organic light emitting diodes with a composite hole transport layer based on poly(ethylenedioxythiophene): poly(styrenesulfonate) doped with TiO_2 nanoparticles," Displays, vol. 39, 104-108, 2015.

[52]. T. Yamasaki, K. Sumioka, and T. Tsutsui, "Organic light-emitting device with an ordered monolayer of silica microspheres as a scattering medium," Appl. Phys. Lett., vol. 76, 1243-1245, 2000.

[53]. J. J. Shiang, T. J. Faircloth, and A. R. Duggal, "Experimental demonstration of increased organic light emitting device output via volumetric light scattering," J. Appl. Phys., vol. 95, 2889-2895, 2004.

[54]. P. V. Kamat, "Meeting the Clean Energy Demand: Nanostructure Architectures for Solar Energy Conversion," J. Phys. Chem. C, vol. 111, 2834-2860, 2007.

[55]. B. Li, L. Wang, B. Kang, P. Wang, and Y. Qui, "Review of recent progress in solid-state dye-sensitized solar cells", Sol. Energy Mater Sol. Cells, vol. 90, 549-573, 2006.

[56]. V. P. -Koch, “Milestones of Solar Conversion and Photovoltaics,” in High-Efficient Low-Cost Photovoltaics, Springer Berlin Heidelberg, 2009.

[57]. D. M. Chapin, C. S. Fuller, and G. L. Pearson, “A New Silicon p-n Junction Photocell for Converting Solar Radiation into Electrical Power,” J. Appl. Phys., vol. 25, 676-677, 1954.

[58]. https://www.nrel.gov/pv/assets/images/efficiency-chart.png

[59]. M. A. Green, “Third Generation Photovoltaics: Ultra-high Conversion Efficiency at Low Cost,” Prog. Photovolt: Res. Appl., vol. 9, 123-135, 2001.

[60]. M. A. Green, “Third Generation Photovoltaics: Advanced Solar Energy Conversion,” Phys. Today, vol. 57, 71-72, 2004.

[61]. G. Conibeer, “Third generation photovoltaics,” Mater. Today, vol. 10, 42-50, 2007.

[62]. C. S. Solanki, “Solar Photovoltaics: Fundamentals, Technologies and Applications,” PHI Learning Private Limited, New Delhi, 2011.

[63]. http://rredc.nrel.gov/solar/spectra/am1.5/

[64]. H. Hoppe and N. S. Sariciftci, “Organic solar cells: An overview,” J. Mater. Res., vol. 19, 1924-1945, 2004.

[65]. C. W. Tang, “Two-layer organic photovoltaic cell,” Appl. Phys. Lett., vol. 48, 183-185, 1986.

[66]. V. S. Gevaerts, L. J. A. Koster, M. M. Wienk, and R. A. J. Janssen, “Discriminating between Bilayer and Bulk Heterojunction Polymer: Fullerene Solar Cells Using the External Quantum Efficiency,” ACS Appl. Mater. Interfaces, vol. 3, 3252-3255, 2011.

[67]. M. Hiramoto, H. Fujiwara, and M. Yokoyama, “Three-layered organic solar cell with a photoactive interlayer of codeposited pigments,” Appl. Phys. Lett., vol. 58, 1062-1064, 1991.

[68]. J. A. Bartlet, Z. M. Beiley, E. T. Hoke, W. R. Matekar, J. D. Douglas, B. A. Collins, J. R. Tumbleston, K. R. Graham, A. Amassian, H. Ade, J. M. J. Fréchet, M. F. Toney, and M. D. McGehee, “The importance of Fullerene Percolation in the Mixed Regions of Polymer-Fullerene Bulk Heterojunction Solar Cells,” Adv. Energy Mater., vol. 3, 364-374, 2013.

[69]. J. Gilot, I. Barbu, M. M. Wienk, and R. A. J. Janssen, “The use of ZnO as optical spacer in polymer solar cells: Theoretical and experimental study,” Appl. Phys. Lett., vol. 91, 113520-1-113520-3, 2007.

[70]. Z. Wang, E. Wang, L. Hou, F. Zhang, M. Andersson, and O. Inganäs, "Mixed solvents for reproducible photovoltaic bulk heterojunctions," J. Photonics Energy, vol. 1, 011122-1-011122-7, 2011.

[71]. G. H. Jung, K. Hong, W. J. Dong, S. Kim, and J. -L. Lee, "BCP/Ag/MoO_3 Transparent Cathodes for Organic Photovoltaics," Adv. Energy Mater., vol. 1, 1023-1028, 2011.

[72]. R. Chaudhary, K. Patel, R. K. Sinha, S.Kumar, and P. K. Tyagi, "Potential application of mono/bi-layer molybdenum disulfide (Mo_{S2}) sheet as an efficient transparent conducting electrode in silicon heterojunction solar cells," J. Appl. Phys., vol. 120, 013104-1- 013104-10, 2016.

[73]. Z. Yu, L. Li, Q. Zhang, W. Hu, and Q. Pei, "Silver Nanowire-Polymer Composite Electrodes for Efficient Polymer Solar Cells," Adv.Mater., vol. 23, 4453–4457, 2011.

[74]. Y. –C. Tseng, A. U. Mane, J. W. Elam, and S. B. Darling, "Ultrathin molybdenum oxide anode buffer layer for organic photovoltaic cells formed using atomic layer deposition," Sol. Energy Mater Sol. Cells, vol. 99, 235-239, 2012.

[75]. S. Albrecht, S. Schäfer, I. Lange, S. Yilmaz, I. Dumsch, S. Allard, U. Scherf, A. Hertwig, and D. Neher, "Light management in PCPDTBT:PC_{70}BM solar cells: A comparison of standard and inverted device structures," Org. Electron., vol. 13, 615-622, 2012.

[76]. J. Gilot, I. Barbu, M. M. Wienk, and R. A. J. Janssen, "The use of ZnO as optical spacer in polymer solar cells: Theoretical and experimental study," Appl. Phys. Lett., vol. 91, 113520-1-113520-3, 2007.

[77]. B. V. Andersson, D. M. Huang, A. J. Moulé, and O. Inganäs, "An optical spacer is no panacea for light collection in organic solar cells," Appl. Phys. Lett., vol. 94, 043302-1 (2009).

[78]. J. Zhao and M. A. Green, "Optimized Antireflection Coatings for High-Efficiency Silicon Solar Cells," IEEE Trans. Electron Devices, vol. 38, 1925-1934, 1991.

[79]. S. Joseph and J. Joseph, "Influence of periodic texture profile and parameters for enhanced light absorption in amorphous silicon ultra-thin solar cells," Appl. Opt., vol. 56, 5013-5022, 2017.

[80]. E. Yablonovitch and G. D. Cody, “Intensity Enhancement in Textured Optical Sheets for Solar Cells,” IEEE Trans. Electron Devices, vol. ED-29, 300-305, 1982.

[81]. H. W. Deckman, C. B. Roxlo, and E. Yablonovitch, “Maximum statistical increase of optical absorption in textured semiconductor films,” Opt. Lett., vol. 8, 491-493, 1983.

[82]. O. Guilatt, B. Apter, and U. Efron, “Light absorption enhancement in thin silicon film by embedded metallic nanoshells,” Opt. Lett., vol. 35, 1139-1141, 2010.

[83]. K. Forberich, G. Dennler, M. C. Scharber, K. Hingerl, T. Fromherz, and C. J. Brabec, “Performance improvement of organic solar cells with moth eye anti-reflection coating,” Thin Solid Films, vol. 516, 7167-7170, 2008.

[84]. C. Cocoyer, L. Rochaa, L. Sicot, B. Geffroy, R. de Bettignies, C. Sentein, C. F. Debuisschert, and P. Raimond, “Implementation of submicrometric periodic surface structures toward improvement of organic-solar-cell performances,” Appl. Phys. Lett., vol. 88, 133108-1-133108-3, 2006.

[85]. L. M. -Meskamp, Y. H. Kim, T. Roch, S. Hofmann, R. Scholz, S. Eckardt, K. Leo, and A. F. Lasagni, “Efficiency Enhancement of Organic Solar Cells by Fabricating Periodic Surface Textures using Direct Laser Interference Patterning,” Adv. Mater., vol. 24, 906-910, 2012.

[86]. K. Tvingstedt, S. D. Zilio, O. Inganäs, and M. Tormen, “Trapping light with micro lenses in thin film organic photovoltaic cells,” Opt. Express, vol. 16, 21608-21615, 2008.

[87]. S. D. Zilio, K. Tvingstedt, O. Inganäs, and M. Tormen, “Fabrication of a light trapping system for organic solar cells,” Microelectron. Eng., vol. 86, 1150-1154, 2009.

[88]. J. D. Myers, W. Cao, V. Cassidy, S. -H. Eom, R. Zhou, L. Yang, W. You and J. Xue, “A universal optical approach to enhancing efficiency of organic-based photovoltaic devices,” Energy Environ. Sci., vol. 5, 6900-6904, 2012.

[89]. J. Singh, N. Prasad, V. S. Nirwal, K. Gautam, K. R. Peta, and P. K. Bhatnagar, “Optical absorption and emission characterization of P3HT: graphene composite for its prospective photovoltaic application,” AIP Conf. Proc., vol. 1731, 050129-1-050129-3, 2016.

[90]. S. R. Forrest, “The Limits to Organic Photovoltaic Cell Efficiency,” Mater. Res. Bull., vol. 30, 28-32, 2005.

[91]. K. Tvingstedt, V. Andersson, F. Zhang, and O. Inganäs, “Folded reflective tandem polymer solar cell doubles efficiency,” Appl. Phys. Lett., vol. 91, 123514-1-123514-3, 2007.

[92]. Y. Zhou, F. Zhang, K. Tvingstedt, W. Tian, and O. Inganäs, “Multifolded polymer solar cells on flexible substrates,” Appl. Phys. Lett., vol. 93, 033302-1-033302-3, 2008.

[93]. B. V. Andersson, U. Wuerfel, and O. Inganäs, “Full day modelling of V-shaped organic solar cell,” Solar Energy, vol. 85, 1257-1263, 2011.

[94]. Y. Qin, Y. Chen, Y. Cui, S. Zhang, H. Yao, J. Huang, W. Li, Z. Zheng, and J. Hou, “Achieving 12.8% Efficiency by Simultaneously Improving Open Circuit Voltage and Short Circuit Current Density in Tandem Organic Solar Cells,” Adv. Mater., vol. 29, 1606340-1-1606340-7, 2017.

[95]. M. Niggemann, M. Glatthaar, A. Gombert, A. Hinsch, and V. Wittwer, “Diffraction gratings and buried nano-electrodes—architectures for organic solar cells,” Thin Solid Films, vol. 451-452, 619-623, 2004.

[96]. S. -I. Na, S. -S. Kim, J. Jo, S. -H. Oh, J. Kim, and D. -Y. Kim, “Efficient Polymer Solar Cells with Surface Relief Gratings Fabricated by Simple Soft Lithography,” Adv. Funct. Mater., vol. 18, 3956-3963, 2008.

[97]. C. Min, J. Li, G. Veronis, J. -Y. Lee, S. Fan, and P. Peumans, “Enhancement of optical absorption in thin-film organic solar cells through the excitation of plasmonic modes in metallic gratings,” Appl. Phys. Lett., vol. 96, 133302-1-133302-3, 2010.

[98]. K. Q. Le, A. Abass, B. Maes, P. Bienstman, and A. Alù, “Comparing plasmonic and dielectric gratings for absorption enhancement in thin-film organic solar cells,” Opt. Express, vol. 20, A39-A50, 2012.

[99]. F. X. Xie, W. C. H. Choy, C. C. D. Wang, W. E. I. Sha, and D. D. S. Fung, “Improving the efficiency of polymer solar cells by incorporating gold nanoparticles into all polymer layers,” Appl. Phys. Lett. 99, 153304-1-155304-3, 2011.

[100]. Y. A. Akimov, W. S. Koh, S. Y. Sian, and S. Ren, “Nanoparticle-enhanced thin film solar cells: Metallic or dielectric nanoparticles?,” Appl. Phys. Lett., vol. 96, 073111-1-073111-3, 2010.

[101]. N. Kalfagiannis, P. G. Karagiannidis, C. Pitsalidis, N. T. Panagiotopoulos, C. Gravalidis, S. Kassavetis, P. Patsalas, S. Logothetidis, “Plasmonic silver nanoparticles for improved organic solar cells,” Sol. Energy Mater Sol. Cells, vol. 104, 165-174, 2012.

[102]. W. Zhang, M. Saliba, S. D. Stranks, Y. Sun, X. Shi, U. Wiesner, and H. J. Snaith, “Enhancement of Perovskite-Based Solar Cells Employing Core-Shell Metal Nanoparticles,” Nano Lett., vol. 13, 4505−4510, 2013.

[103]. J. Singh, V. S. Nirwal, P. K. Bhatnagar, and K. R. Peta, “Effect of incorporation of silver nanoparticles in PEDOT:PSS layer on performance of organic solar cell,” AIP Conf. Proc., vol. 1953, 030251-1-030251-3, 2018.

[104]. H. -C. Liao, C. -S. Tsao, T. -H. Lin, M. -H. Jao, C. -M. Chuang, S. -Y. Chang, Y. -C. Huang, Y. -T. Shao, C. -Y. Chen, C. -J. Su, U. -S. Jeng, Y. -F. Chen, and W. -F. Su, “Nanoparticle-Tuned Self-Organization of a Bulk Heterojunction Hybrid Solar Cell with Enhanced Performance,” ACS Nano, vol. 6, 1657-1666, 2012.

[105]. J. Krantz, T. Stubhan, M. Richter, S. Spallek, I. Litzov, G. J. Matt, E. Spiecker, and C. J. Brabec, “Spray-Coated Silver Nanowires as Top Electrode Layer in Semitransparent P3HT:PCBM-Based Organic Solar Cell Devices,” Adv. Funct. Mater., vol. 23, 1711-1717, 2013.

[106]. P. Maisch, K. C. Tam, L. Lucera, H. –J. Egelhaaf, H. Scheiber, E. Maier, and C. J. Brabec, “Inkjet printed silver nanowire percolation networks as electrodes for highly efficient semitransparent organic solar cells,” Org. Electron., vol. 38, 139-143, 2016.

[107]. Y. Taff, B. Apter, E. A. Katz, and U. Efron, “Modeling plasmonic efficiency enhancement in organic photovoltaics,” Appl. Opt., vol. 54, 7957-7961, 2015.

[108]. D. -H. Ko, J. R. Tumbleston, L. Zhang, S. Williams, J. M. DeSimone, R. Lopez, and E. T. Samulski, “Photonic Crystal Geometry for Organic Solar Cells,” Nano Lett., vol. 9, 2742-2746, 2009.

[109]. A. Peer and R. Biswas, “Nanophotonic Organic Solar Cell Architecture for Advanced Light Trapping with Dual Photonic Crystals,” ACS Photonics, vol. 1, 840-847, 2014.

[110]. X. Zheng and L. Zhang, “Photonic nanostructures for solar energy conversion,” Energy Environ. Sci., vol. 9, 2511-2532, 2016.

[111]. C. P. Poole Jr. and F. J. Owens, “Introduction to Nanotechnology,” Wiley, New York, 2003.

[112]. C. F. Bohren and D. R. Huffman, “Absorption and Scattering of Light by Small Particles,” Wiley, New York, 1983.

[113]. P. Matheu, S. H. Lim, D. Derkacs, C. McPheeters, and E. T. Yu, “Metal and dielectric nanoparticle scattering for improved optical absorption in photovoltaic devices,” Appl. Phys. Lett., vol. 93, 113108-1-113108-3, 2008.

[114]. M. N. O. Sadiku, “Numerical techniques in Electromagnetics with Matlab,” Taylor and Francis Group, London, 2009.

[115]. W. Lee and F. L. Degertekin, “Rigorous Coupled-Wave Analysis of Multilayered Grating Structures,” J. Light. Tech., vol. 22, 2359-2363, 2004.

[116]. A. Ghatak and K. Thyagarajan, “Optical Electronics,” Cambridge University Press, UK, 2003.

[117]. G. Mie, “Beiträge zur Optik Trüber Median, Speziell Kolloidaler Metallosungen,” Annalen der Physik, vol. 330, 377-445, 1908.

[118]. K. S. Yee, “Numerical Solution of initial boundary-value problems involving Maxwell’s equations in isotropic media,” IEEE Trans. Ant. Prop., vol. AP-14, 302-307, 1966

[119]. A. Taflove and M. E. Brodwin, “Numerical solution of steady-state electromagnetic scattering problems using time dependent Maxwell’s equations,” IEEE Micro. Theo. Tech., vol. MTT-23, 623-630, 1975.

[120]. A. Taflove and K. R. Umashankar, “A hybrid moment method/finite-difference time-domain approach to electromagnetic coupling and aperture penetration into complex geometries,” IEEE Trans. Ant. Prop., vol. AP-30, 617-627, 1982.

[121]. A. Taflove and K. R. Umashankar, “The finite-difference time-domain method for numerical modeling of electromagnetic wave interactions,” Electromagnetics, vol. 10, 105-126, 1990.

[122]. M. Okoniewski, “Vector wave equation 2D-FDTD method for guided wave equation,” IEEE Micro. Guided Wave Lett., vol. 3, 307-309, 1993.

[123]. M. N. O. Sadiku, V. Bemmel, and S. Agbo, “Stability criteria for finite-difference time-domain algorithm,” Proc. IEEE Southeastcon, 48-50, 1990.

[124]. J. C. Olivier, “On the synthesis of exact free space absorbing boundary conditions for the finite-difference time-domain method,” IEEE Trans. Ant. Prog., vol. 40, 456-460, 1992.

[125]. C. J. Railton, E. M. Daniel, and J. P. McGeehan, “Use of second order absorbing boundary conditions for the termination of planar waveguides in the FDTD method,” Elect. Lett., vol. 29, 900-902,1993.

[126]. P. Y. Wang, S. Kozaki, M. Ohki, and T. Yabe, “Higher order formulation of absorbing boundary conditions for finite-difference time-domain method,” Elect. Lett., vol. 29, 2018-2019, 1993.

[127]. J. P. Berenger, “A perfectly matched layer for the absorption of electromagnetic waves,” J. Comp. Phys., vol. 114, 185-200, 1994.

[128]. D. S. Katz, E. T. Thiele, and A. Taflove, “Validation and extension to three dimensions of the Berenger PML absorbing boundary conditions for FDTD meshes,” IEEE Micro. Guided wave Lett., vol. 4, 268-270, 1994.

[129]. J. P. Berenger, “Perfectly matched layer for the FDTD solution of wave-structure interaction problems,” IEEE Trans. Ant. Prop., vol. 44, 110-117, 1996.

[130]. A. Taflove, Computational electrodynamics: The Finite Difference Time-Domain Method, MA: Artech House, Boston, 1995.

[131]. Lumerical FDTD Solutions 7.5, Inc., http://www.lumerical.com/tcad-products/fdtd.

[132]. RSoft RCAD, Fullwave and Solar Cell Utility Manual, https://optics.synopsys.com/rsoft/.

[133]. J. –W. Park, Md. H. Ullah, S. S. Park, and C. –S. Ha, “Organic electroluminescent devices using quantum-size silver nanoparticles,” J. Mater. Sci: Mater. Electron., vol. 18, S393–S397, 2007.

[134]. D. Liu, M. Fina, L. Ren, and S. S. Mao, “Enhanced luminance of organic light-emitting diodes with metal nanoparticle electron injection layer,” Appl Phys A, vol. 96, 353-356, 2009.

[135]. X. Ma, J. Benavides, C. R. Haughn, F. Xu, M. F. Doty, and S. G. Cloutier, “High polymer-LEDs enhancement by exciton–plasmon coupling using encapsulated metallic nanoparticles,” Org. Electron., vol. 14, 1916-1923, 2013.

[136]. H. Sung, J. Lee, K. Han, J. –K. Lee, J. Sung, D. Kim, M. Choi, and C. Kim, “Controlled positioning of metal nanoparticles in an organic light-emitting device for enhanced quantum efficiency,” Org. Electron., vol. 15, 491-499, 2014.

[137]. B. Riedel, Y. Shen, J. Hauss, M. Aichholz, X. Tang, U. Lemmer, and M. Gerken, “Tailored Highly Transparent Composite Hole-Injection Layer

Consisting of PEDOT:PSS and SiO_2 Nanoparticles for Efficient Polymer Light-Emitting Diodes," Adv. Mater., vol. 23, 740-745, 2011.

[138]. H. Lee, I. Park, J. Kwak, D. Y. Yoon, and C. Lee, "Improvement of electron injection in inverted bottom-emission blue phosphorescent organic light emitting diodes using zinc oxide nanoparticles," Appl. Phys. Lett., vol. 96, 153306-1-153306-3, 2010.

[139]. C. –J. Sun, Y. Wu, Z. Xu, B. Hu, J. Bai, J. –P. Wang, J. Shen, "Enhancement of quantum efficiency of organic light emitting devices by doping magnetic nanoparticles," Appl. Phys. Lett., vol. 90, 232110-1-232110-3, 2007.

[140]. A. N. Aleshina, A. D. Sokolovskayab, I. P. Shcherbakova, P. N. Brunkova, and V. P. Ulin, "Organic Light Emitting Diodes Based on Polyvinylcarbazole Films Doped with Polymer Nanoparticles," Phys. Solid State, vol. 55, 675-680, 2013.

[141]. F. Liu, B. S. Rao, and J. –M. Nunzi, "A dye functionalized silver–silica core–shell nanoparticle organic light emitting diode," Org. Electron., vol. 12, 1279-1284, 2011.

[142]. F. Liu and J. –M. Nunzi, "Phosphorescent organic light emitting diode efficiency enhancement using functionalized silver nanoparticles," Appl. Phys. Lett., vol. 99, 123302-1-122302-3, 2011.

[143]. T. Kim, H. Kang, S. Jeong, D. J. Kang, C. Lee, C. –H. Lee, M. –K. Seo, J. –Y. Lee, and B. J. Kim, "Au@Polymer Shell Core–Shell Nanoparticles for Simultaneously Enhancing Efficiency and Ambient Stability of Organic Optoelectronic Devices," Appl. Mater. Interfaces, vol. 6, 16956-16965, 2014.

[144]. H. –W. Chang, K. –C. Tien, M. –H. Hsu, Y. –H. Huang, M. –S. Lin, C. –H. Tsai, Y. –T. Tsai, C. –C. Wu, "Organic light-emitting devices integrated with internal scattering layers for enhancing optical out-coupling," J. Soc. Inf. Disp., vol. 19, 196-204, 2011.

[145]. H. -W. Chang, J. Lee, S. Hofmann, Y. H. Kim, L. M. Meskamp, B. Lussem, C. -C. Wu, K. Leo, and M.C. Gather, "Nano-particle based scattering layers for optical efficiency enhancement of organic light-emitting diodes and organic solar cells," J. Appl. Phys., vol. 113, 204502-1-204502-8, 2013.

[146]. C. –H. Shin, E. Y. Shin, M. –H. Kim, J. –H. Lee, and Y. Choi, "Nanoparticle scattering layer for improving light extraction efficiency of organic light emitting diodes," Opt. Express, vol. 23, A133-A139, 2015.

[147]. Y. J. Lee, S. H. Kim, J. Huh, G.H. Kim, Y. H. Lee, S. -H. Cho, Y. -C. Kim, and Y. R. Do, “A high-extraction-efficiency nanopatterned organic light-emitting diodes,” Appl. Phys. Lett., vol. 82, 3779–3781, 2003.

[148]. J. -H. Park, W. -S. Chu, M. -C. Oh, K. Lee, J. Moon, S. K. Park, H. Cho, and D. -H. Cho, “Outcoupling efficiency analysis of OLEDs fabricated on a Wrinkled substrate,” J. Disp. Technol., vol. 12, 801–807, 2016.

[149]. E. D. Palik, “Handbook of Optical Constants of Solids I,” Academic Press, San Diego, 1985.

[150]. W. C. H. Choy and H. H. Fong, “Comprehensive investigation of absolute optical properties of organic materials,” J. Phys. D: Appl. Phys., vol. 41, 1-7, 2008.

[151]. H. Kim and C. M. Gilmore, “Electrical, optical and structural properties of indium-tin oxide thin films for organic light-emitting devices,” J. Appl. Phys. 86, vol. 86, 6451-6461, 1999.

[152]. J. R. Nagel and M. A. Scarpulla, “Enhanced absorption in optically thin solar cells by scattering from embedded dielectric nanoparticles,” Opt. Express, vol. 18, A139–A146, 2010.

[153]. Lumerical MODE Solutions 7.10, Inc., https://www.lumerical.com/tcad-products/mode.

[154]. F. C. Krebs, “Fabrication and processing of polymer solar cells: A review of printing and coating techniques,” Sol. Energy Mater. Sol. Cells, vol. 93, 394–412, 2009.

[155]. P. E. Shaw, A. Ruseckas, and I. D. W. Samuel, “Exciton diffusion measurements in poly(3-hexylthiophene),” Adv. Mater., vol. 20, 3516–3520, 2008.

[156]. S. Li, Y. Le, W. Zhao, H. Yan, B. Lang, D. Liu, W. Li, H. Ade, and J. Hou, “A Wide Band Gap Polymer with a Deep Highest Occupied Molecular Orbital Level Enables 14.2% Efficiency in Polymer Solar Cells,” J. Am. Chem. Soc., vol. 140, 7159–7167, 2018.

[157]. L. Meng et al., “Organic and solution-processed tandem solar cells with 17.3% efficiency,” Science, vol. 361, 1094-1098, 2018.

[158]. H. Shen, P. Bienstman, and B. Maes, “Plasmonic absorption enhancement in organic solar cells with thin active layers,” J. Appl. Phys., vol. 106, 073109-1-073109-5, 2009.

[159]. H. C. Liao et al., “Nanoparticle-tuned self-organization of a bulk heterojunction hybrid solar cell with enhanced performance,” ACS Nano, vol. 6, 1657-1666, 2012.

[160]. M. T. Khan, A. Kaur, S. K. Dhawan, and S. Chand, “In-Situ growth of cadmium telluride nanocrystals in poly(3-hexylthiophene) matrix for photovoltaic application,” J. Appl. Phys., vol. 110, 044509-1-044509-7, 2011.

[161]. D. Q. Yun, W. Feng, H. C. Wu, and K. Yoshino, “Efficient conjugated polymer-ZnSe and -PbSe nanocrystals hybrid photovoltaic cells through full solar spectrum utilization, Sol. Energy Mater. Sol. Cells, vol. 93, 1208–1213, 2009.

[162]. S. H. Oh, S. J. Heo, J. S. Yang, H. J. Kim, “Effects of ZnO nanoparticles on P3HT:PCBM organic solar cells with DMF-modulated PEDOT:PSS buffer layers,” ACS Appl. Mater. Int., vol. 5, 11530–11534, 2013.

[163]. S. R. Gollu, R. Sharma, G. Srinivas, S. Kundu, and D. Gupta, “Incorporation of SiO_2 dielectric nanoparticles for performance enhancement in P3HT:PCBM inverted organic solar cells,” Org. Electron., vol. 24, 43-50, 2015.

[164]. P. Shao et al. “Facile embedding of SiO_2 nanoparticles in organic solar cells for performance improvement,” Org. Electron., vol. 50, 77-81, 2017.

[165]. K. N’Konou, L. Peres, and P. Torchio, “Optical absorption Modeling of Plasmonic Organic Solar Cells Embedding Silica-Coated Silver Nanospheres,” Plasmonics, vol. 13, 297-303, 2018.

[166]. M. S. Pereira, F. A. S. Lima, T. S. Riberio, M. R. da Silva, R. Q. Almeida, E. B. Barros, and I. F. Vasconcelos, “Application of Fe-doped SnO_2 nanoparticles in organic solar cells with enhanced stability,” Opt. Mater., vol. 64, 548-556, 2017.

[167]. W. Wang, Y. Hao, Y. Cui, X. Tian, Y. Zhang, H. Wang, F. Shi, B. Wei, and W. Huang, “High-efficiency, broad-band and wide-angle optical absorption in ultra-thin organic photovoltaic devices,” Opt. Express, vol. 22, A376-A385, 2014.

[168]. S. Y. Kim, “Simultaneous determination of refractive index, extinction coefficient, and void distribution of titanium dioxide thin film by optical methods,” Appl. Opt. vol. 35, 6703-6707, 1996.

[169]. P. T. B. Shaffer, “Refractive index, Dispersion, and Birefringence of Silicon Carbide Polytypes,” Appl. Opt., vol. 10, 1034-1036, 1971.

[170]. F. Moreno, B. García-Cámara, J. M. Saiz, and F. González, “Interaction of nanoparticles with substrates: effects on the dipolar behavior of the particles,” Opt. Express, vol. 16, 12487-12504, 2008.

[171]. C. Cho et al. “Random and V-groove texturing for efficient light trapping in organic photovoltaic cells,” Sol. Energy Mater. Sol. Cells 115, 36-41, 2013

[172]. H. Heidarzadeh, A. Rostami, S. Matloub, M. Dolatyari, and G. Rostami, “Analysis of the light trapping effect on the performance of silicon-based solar cells: absorption enhancement,” Appl. Opt., vol. 54, 3591-3601, 2015.

[173]. B. Cocilovo et al., “Effect of modular diffraction gratings on absorption in P3HT:PCBM layers,” Appl. Opt. 52, 1025-1034, 2013

[174]. J. R. Tumbleston, D. -H. Ko, E. T. Samulski, and R. Lopez, “Absorption and quasiguided mode analysis of organic solar cells with photonic crystal photoactive layers,” Opt. Express 17, 7670-7681, 2009.

[175]. H. Heidarzadeh, A. Rostami, M. Dolatyari, and G. Rostami, “Plasmon-enhanced performance of an ultrathin silicon solar cell using metal-semiconductor core-shell hemispherical nanoparticles and metallic back grating,” Appl. Opt., vol. 55, 1779-1785, 2016.

[176]. P. Sheng, A. N. Bloch, and R. S. Stepleman, “Wavelength-selective absorption enhancement in thin-film solar cells,” Appl. Phys. Lett., vol. 43, 579-581, 1983.

[177]. C. Min, J. Li, G. Veronis, J. –Y. Lee, S. Fan, and P. Peumans, “Enhancement of optical absorption in thin-film organic solar cells through the excitation of plasmonic modes in metallic gratings,” Appl. Phys. Lett., vol. 496, 133302-133302-3, 2010.

[178]. P. T. Dang, T. K. Nguyen, and K. Q. Le, “Revisited design optimization of metallic gratings for plasmonic light- trapping enhancement in thin organic solar cells,” Opt. Commun., vol. 382, 241- 245, 2017.

[179]. M. A. Sefunc, A. K. Okyay, and H. V. Demir, “Plasmonic backcontact grating for P3HT:PCBM organic solar cells enabling strong optical absorption increased in all polarizations,” Opt. Express, vol. 19, 14200-14209, 2011.

[180]. S. Lee, S. J. In, D. R. Mason, and N. park, “Incorporation of nanovoids into metallic gratings for broadband plasmonic organic solar cells,” Opt. Express, vol. 21, 4055-4060, 2013.

[181]. D. Barettin, A. D. Carlo, R. D. Angelis, M. Casalboni, and P. Prosposito, “Effect of dielectric Bragg grating nanostructuring on dye sensitized solar cells,” Opt. Express, vol. 20, A888-A897, 2012.

[182]. H. Shen and B. Maes, “Combined plasmonic gratings in organic solar cells,” Opt. Express, vol. 19, A1202-A1210, 2011.

[183]. Y. -S. Hsiao, S. Charan, F. –Y. Wu, F. –C. Chien, C. –W. Chu, P. Chen, and F. –C. Chen, “Improving the Light Trapping Efficiency of Plasmonic Polymer Solar Cells through Photon Management,” J. Phys. Chem. C, vol. 116, 20731-20737, 2012.

[184]. R. S. Kim, J. Zhu, J. H. Park, L. Li, Z. Yu, H. Shen, M. Xue, K. L. Wang, G. Park, T. J. Anderson, and Q. Pei, “E-beam deposited Ag-nanoparticles plasmonic organic solar cell and its absorption enhancement analysis using FDTD-based cylindrical nano-particle optical model,” Opt. Express, vol. 20, 12649-12657, 2012.

[185]. D. L. Wood and K. Nassau, “Refractive index of cubic zirconia stabilized with yttria,” Appl. Opt., vol. 16, 2978-2981, 1982.